Old Dominion University

ODU Digital Commons

Mathematics & Statistics Theses & Dissertations

Mathematics & Statistics

Spring 1999

A Numerical Solution of Low-Energy Neutron Boltzmann Equation

Martha Sue Clowdsley
Old Dominion University

Follow this and additional works at: https://digitalcommons.odu.edu/mathstat_etds

 Part of the Mathematics Commons

Recommended Citation

Clowdsley, Martha S.. "A Numerical Solution of Low-Energy Neutron Boltzmann Equation" (1999). Doctor of Philosophy (PhD), Dissertation, Mathematics & Statistics, Old Dominion University, DOI: 10.25777/4ssj-p747
https://digitalcommons.odu.edu/mathstat_etds/20

This Dissertation is brought to you for free and open access by the Mathematics & Statistics at ODU Digital Commons. It has been accepted for inclusion in Mathematics & Statistics Theses & Dissertations by an authorized administrator of ODU Digital Commons. For more information, please contact digitalcommons@odu.edu.

A NUMERICAL SOLUTION OF

THE LOW ENERGY NEUTRON BOLTZMANN EQUATION

by

Martha Sue Clowdsley
B.S. May 1990, University of Notre Dame
M.S. May 1995, Old Dominion University

A Dissertation Submitted to the Faculty of
Old Dominion University in Partial Fulfillment of the
Requirements for the Degree of

DOCTOR OF PHILOSOPHY

COMPUTATIONAL AND APPLIED MATHEMATICS

OLD DOMINION UNIVERSITY
May 1999

Approved by:

John H. Heinbockel (Director)

John W. Wilson (Member)

John Adam (Member)

Fang Hu (Member)

Reproduced with permission of the copyright owner. Further reproduction prohibited without permission.

ABSTRACT

A NUMERICAL SOLUTION OF THE LOW ENERGY NEUTRON BOLTZMANN EQUATION

Martha Sue Clowdsley
Old Dominion University, 1999
Director: Dr. John H. Heinbockel

A multigroup method using a straight ahead approximation is created to calculate low energy neutron fluence due to the elastic scattering of evaporation neutrons produced in interactions of high energy particles with target nuclei. This multigroup method is added to NASA Langley Research Center's HZETRN particle transport code. This new code is used to calculate the energy spectra of the neutron fluence in several different materials. The multigroup method is found to be an efficient way of calculating low energy neutron fluence in multiple atom materials as well as single atom materials. Comparisons to results produced by Monte Carlo methods show that the straight ahead multigroup method is accurate for larger depths but less accurate for small depths due to leakage at the boundary. For this reason, an improved multigroup method is created which propagates neutrons in two directions, forward and backward approximately accounting for the isotropic distribution of the evaporation source. This new multigroup method compares well with the Monte Carlo method at all depths. For this reason, the multigroup method is considered an accurate method which is highly computationally efficient for calculating low energy neutron fluence.

Reproduced with permission of the copyright owner. Further reproduction prohibited without permission.

ACKNOWLEDGMENTS

This research was funded by NASA research grant NCC1-42. I would like to thank John Wilson at NASA Langley Research Center for both suggesting the problem solved in this thesis and providing much needed assistance. I would also like to thank Francis Badavi and Robert Singleterry at NASA Langley Research Center for their advice and encouragement.

I would like to thank the faculty of Old Dominion University's math department. Specifically, I would like to thank John Adam and Fang Hu for their many comments and suggestions. Most of all, I would like to thank John Heinbockel for his advice and assistance and his never ending encouragement.

Finally, I would like to thank my brother Dan for his assistance creating several of the figures in this thesis and my parents Martin and Mary Ruth for their help editing this document and their unlimited moral support.

Reproduced with permission of the copyright owner. Further reproduction prohibited without permission.

TABLE OF CONTENTS

Reproduced with permission of the copyright owner. Further reproduction prohibited without permission.

Reproduced with permission of the copyright owner. Further reproduction prohibited without permission.

LIST OF TABLES

Reproduced with permission of the copyright owner. Further reproduction prohibited without permission.

LIST OF FIGURES

Reproduced with permission of the copyright owner. Further reproduction prohibited without permission.

Reproduced with permission of the copyright owner. Further reproduction prohibited without permission.

Reproduced with permission of the copyright owner. Further reproduction prohibited without permission.

CHAPTER I

INTRODUCTION

In addition to having many ill effects on human beings, radiation can damage electronic components and degrade material properties. For these reasons, radiation shielding is a primary concern of designers of manned and unmanned spacecraft and high altitude aircraft. In order to provide adequate shielding, a designer would need an estimate of the radiation field that a spacecraft or aircraft would encounter, a way of evaluating the transport of the particles making up the radiation field through the shielding material, and a way of evaluating the effects of a particular radiation field on a target material. This thesis is primarily concerned with particle transport. More specifically, it is concerned with the transport of low energy neutrons.

A Brief History of Radiation Research

Research into the negative effects of radiation on humans began shortly after x-rays were discovered in 1895. In the early 1900's, x-rays and gamma rays were being used mostly for medical applications and large sheets of lead or bricks were used as shields. Over time, a large amount of shielding data was developed for the much used x-rays and gamma rays. Most of this data was in the form of half-thicknesses or absorption coefficients for exponential factors. The half-thickness of a shield is the depth at which half of the incident particles will probably be

The model journal used is *Nuclear Science and Engineering.*

Reproduced with permission of the copyright owner. Further reproduction prohibited without permission.

absorbed. If absorption coefficients for exponential factors are used, then the probability that an incident particle will be absorbed by a depth, x, is $1 - e^{-\mu x}$ where μ is the absorption coefficient. More recent data has been developed mostly on a statistical basis. This data is mostly in the form of tables and graphs.

In 1932, the neutron was discovered. This discovery led to the development of nuclear weapons and nuclear reactors. The development of nuclear weapons led to much experimental and theoretical research in the 1950's and 1960's in the area of shielding against gamma-rays from nuclear weapon fallout.

The development of nuclear reactors led to research on neutron shielding. In the 1950's, necessary shield depths were approximated using absorption coefficients for exponential factors in the same way x-ray shields had been designed. Then researchers began using statistical methods, such as the Monte Carlo method[1,2] to predict the probable paths of each incident neutron through shielding material. These methods were fairly accurate but time consuming, and the necessary computer time could be very expensive. For these reasons, scientist began exploring other more deterministic, numerical methods of approximating the neutron transport. The Boltzmann transport equation was considered a good model of neutron transport, but it is difficult to solve. For this reason, scientists began making simplifying assumptions to the Boltzmann equation. The assumption could be made that the neutron fluence at position $\vec{r}$ moving in direction $\vec{\Omega}$ with energy E, $\phi(\vec{r}, \vec{\Omega}, E)$, is equivalent to $\overline{\phi(\vec{r}, \vec{\Omega})}e^{-\mu E}$ for some function $\overline{\phi(\vec{r}, \vec{\Omega})}$ and some constant μ. Note that the neutron fluence is the number of neutrons per unit area per unit energy per steradian and is measured in #

Reproduced with permission of the copyright owner. Further reproduction prohibited without permission.

particles/cm^2 Mev. Other simplifying assumptions involved limiting the geometry of the problem. One example of this would be the assumption that the fluence of particles is the same in all directions. Another would be that all particle transport is one dimensional. The Boltzmann equation could then be solved using a variety of methods: perturbation techniques[1], integral equations[3], finite difference approximations[2,4], Laplace transforms, method of moments[2], multigroup methods[1,2,4], P_n methods[1,2,4], and S_n methods[1,4]. These numerical methods lacked the accuracy of the Monte Carlo method, but they were faster and less expensive and it was usually easier to estimate their error.

Nuclear reactor designers can compensate for a lack in accuracy in the numerical solution of the Boltzmann equation by adding extra shielding. Space craft designers, on the other hand, have less freedom to add extra shielding and indeed the shield they design must also act as the outer shell of the space craft. An excellent history of space radiation research is contained in chapter 1 of the NASA reference publication, *Transport Methods and Interactions for Space Radiations*[5]. A summary of that history follows.

Space Radiation Research

Scientists first became concerned about damage due to space radiation in the late 1940's. In 1948, Freier, Lofgren, Ney, and Oppenhiemer published a paper stating that heavy ions in the galactic cosmic rays exist in the earth's atmosphere at high altitudes[6]. Speaking on this subject at the 1949 panel meeting, "Aero Medical Problems of Space Travel" at the School of Aviation Medicine, Wright Field, Ohio, C. F. Gell pointed out that space radiation could be life threatening

Reproduced with permission of the copyright owner. Further reproduction prohibited without permission.

and therefore, suggested that space radiation protection be further investigated[7]. Reason for this concern was verified in 1950 by H. J. Schaefer who produced data showing that while these galactic cosmic ray ions produced a dose of only 0.1 mR*/day at sea level, the dose at 70,000 ft was 15 mR/day[8].

The solar flare event of February 1956 sparked greater interest in space radiation protection. Solar flare radiation was discussed extensively at the Conference on Radiation Problems in Manned Space Flight organized by NASA in 1960[9]. Here it was suggested that short term exposure to galactic cosmic rays might not be dangerous, but that shielding must be designed to protect astronauts from solar flares.

NASA Langley Research Center began studying space radiation in 1958 and still continues this research. The importance of this area of research increased dramatically when the U.S. Supersonic Transport Program was begun. The Supersonic Transport, still in the design stages, will be a commercial aircraft which will fly at supersonic velocities and very high altitudes.

The first attempts to model the transport of space radiation through shielding material, like those modeling radiation transport in nuclear reactors, used Monte Carlo techniques. Much of the early work in space radiation shielding used the HETC, High-Energy Transport Code, created by Kinney, Coveyou, and Zerby. However, by the late 1960's, so many researchers were waiting to use the HETC code at Oak Ridge National Laboratory that NASA Langley Research

* The roentgen (abbreviation R) is defined as 2.58×10^{-4} Coulomb of separated charge (either positive or negative) per kilogram of air in the incremental volume where the primary photon interactions occur.

Reproduced with permission of the copyright owner. Further reproduction prohibited without permission.

Center began to develop its own code. This code PROPER-C also used Monte Carlo techniques. This code was improved by adding a data base of Bertini's data for intranuclear-cascade calculations and by making a high energy extrapolation. The new code was called PROPER-3C. PROPER-3C was faster than HETC because it used Bertini's data rather than calculating the intranuclear-cascade, yet because it used Monte Carlo techniques it still required large amounts of expensive computer time.

For this reason, by the mid 1970's, Langley researchers began working on more deterministic methods of calculating radiation transport. These methods used perturbation techniques to solve the one-dimensional Boltzmann transport equation. The first of these codes written at Langley applied only to transport of nucleons (neutrons and protons)[10,11]. This code was later improved to handle other light ions as well. The resulting code, called BRYNTRN, gave a good approximation to the radiation fields created in shielding material exposed to the high energy protons produced by a solar flare[5,12,13]. BRYNTRN stands for baryon transport.

After creating BRYNTRN, Langley researchers turned their attention to heavy ion transport theory. More long term missions, such as the space station and the mars mission, were being planned and work on the Supersonic Transport continued. For these reasons, long term galactic cosmic ray exposure became an important concern.

This research lead to the development of a new code which handles the transport of heavy ions[14–16]. This heavy ion code and the solar flare code,

Reproduced with permission of the copyright owner. Further reproduction prohibited without permission.

BRYNTRN, were put together into one large code call HZETRN[5,17,18]. HZETRN stands for high charge and energy transport. The user sets up HZETRN to run for either a galactic cosmic ray environment or one of several solar flare environments.

The heavy ion transport code in HZETRN is believed to be accurate for the broad energy spectrum found in the galactic cosmic ray. It is less effective, though, for mono-energetic laboratory beams. Researchers at Langley are currently working on a radiation transport code that will work for both laboratory conditions and space conditions[19–25].

A need for improvement in the way HZETRN calculates the transport of low energy neutrons has recently been recognized. In a 1994 Technical Memorandum[26], Judy Shinn et al. compared the neutron fluences in water exposed to the February 1956 solar flare calculated by the BRYNTRN program with the same fluences calculated by the LAHET program. The LAHET program (Los Alamos High-Energy Transport code) is a Monte Carlo routine made up of the HETC code and the MCNP code (Monte Carlo Neutron Photon code). In this comparison, the number of low energy neutrons produced by the BRYNTRN code was significantly smaller than that given by the Monte Carlo routine. It was assumed that BRYNTRN does not adequately model the scattering of low energy neutrons produced by evaporation.

One attempt to rectify this problem was made by Robert Singleterry, then at the University of Arizona[27]. He used an F_N method to solve the Boltzmann equation. This method had the advantage of taking into account the angular dependence of the neutron fluence, and it proved to be fairly accurate in an

Reproduced with permission of the copyright owner. Further reproduction prohibited without permission.

aluminum slab. It, however, was time consuming, and difficulty arose trying combine this method with the one dimensional transport methods already used in the HZETRN program.

For these reasons, it was suggested that a new approach that treats the low energy neutrons separately but still uses a one dimensional transport process should be attempted.

Objective of This Thesis

This thesis contains a description of a new method for calculating the transport of low energy neutrons due to evaporation. In this new method, the low energy neutrons produced by evaporation due to the collision of higher energy neutrons and other ions with the nuclei of target atoms are treated as sources in the one dimensional Boltzmann transport equation. The fluences of these higher energy particles have already been calculated by the HZETRN program. The Boltzmann transport equation with source terms is then solved separately for just low energy neutrons using a multigroup technique.

In this multigroup method, the entire energy spectrum is divided up into small energy groupings. The Boltzmann transport equation is then rewritten in terms of an integral fluence for each energy group. This changes the transport equation to a system of differential equations, one for each energy group. These differential equations are then solved for the integral fluences, and the neutron fluences are approximated from these integral fluences.

This multigroup method is added to the HZETRN program as a subroutine. Because this method also uses a straight ahead approximation, the low energy

Reproduced with permission of the copyright owner. Further reproduction prohibited without permission.

neutron fluences produced can easily be added to the neutron fluences produced by the main HZETRN program.

This new amended HZETRN program is run for a variety of radiation backgrounds and a variety of targets. The total neutron fluences produced are then compared to neutron fluences produced by other programs.

The possibility of further improving the low energy neutron calculations by including a backward and forward approximation is then investigated. These fluences are also compared to fluences produced by other programs.

Reproduced with permission of the copyright owner. Further reproduction prohibited without permission.

CHAPTER II

THEORY

Radiation damage is caused by the transfer of energy from high energy incident particles to the atoms of a target material. Dose or dose equivalence, for human targets, is the measure of this damage. In order to calculate the dose or dose equivalence, an estimate of the number, types, and energies of particles at each point in a target material is required. Estimating these quantities not only requires a count of the incident particles at the targets boundary but an understanding of the ways in which these particles can interact with and be transported through the target material.

Background

Consider a beam of high energy nucleons incident upon a slab of homogeneous material as in Figure 1.

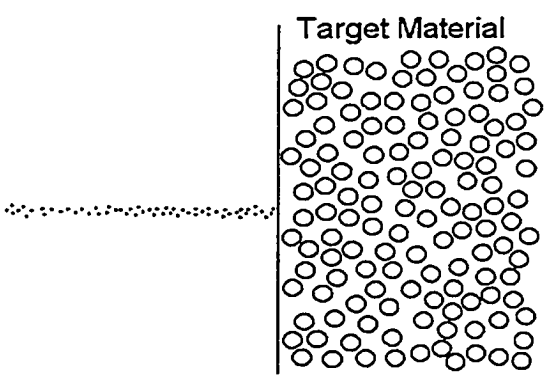

Fig. 1. Nucleons incident upon a target material.

Reproduced with permission of the copyright owner. Further reproduction prohibited without permission.

Two kinds of interactions can occur between the incident ions and nucleons and the atoms of the target material: electromagnetic interactions and nuclear collisions. By far the most common type of electromagnetic interactions are coulomb interactions. Coulomb interactions occur when a charged particle passes close enough to an atom to have an effect on it. When this occurs, one of two things happens; either the atom is left in an excited bound state, or the atom is ionized by ejecting an electron.

An atom is made up of a positively charged nucleus orbited by a number of negatively charged electrons. Together the nucleus and the electrons are neutrally charged. Ionization occurs when a positively charged particle pulls an electron away from the atom. The incident particle loses energy doing this, and the atom is left with a positive charge.

Nuclear collisions occur when the incident particle impacts the atom nucleus directly. The volume of the nucleus of an atom is small compared with the volume of the whole atom. For this reason, charged particles interact with many orbital electrons between nuclear reactions. In fact, for energies below 100 MeV, most protons will not have a nuclear collision before stopping. Neutrons, however, because of their neutral charge, interact with target atoms mostly through nuclear collisions.

Two types of nuclear collisions can occur: elastic collisions and non-elastic collisions. In an elastic collision, energy is transferred from the projectile to the nucleus by recoil of the nucleus. In this case, the nucleus is not left in an excited state. In a non-elastic collision, the impact excites the nucleus, and nucleons with

Reproduced with permission of the copyright owner. Further reproduction prohibited without permission.

energies almost as large as the original nucleon are immediately ejected in the same direction. Then the nucleus, still in an excited state, emits lower energy particles in all directions in order to return to its natural state. This process of isotropically expelling low energy particles is called evaporation.

Therefore, incident particles loose energy as they pass through the target material through electromagnetic interactions and nuclear collisions. These particles eventually loose all of their energy and come to a stop. Secondary particles, however, are also produced through nuclear collisions. These particles also move through the target material interacting with other target atoms. For this reason, the transport of these secondaries must also be modeled in order to estimate dose.

The Boltzmann Transport Equation

The Boltzmann transport equation

$$\begin{aligned}\vec{\Omega}\cdot\nabla\phi_j(\vec{x},E,\vec{\Omega}) - \frac{\partial}{\partial E}\left[S_j(E)\phi_j(\vec{x},E,\vec{\Omega})\right] + \sigma_j(E)\phi_j(\vec{x},E,\vec{\Omega}) \\ = \sum_{k\geq j}\int_E^\infty dE' \int d\vec{\Omega}' f_{jk}(E,E',\vec{\Omega},\vec{\Omega}')\phi_k(\vec{x},E',\vec{\Omega}') \\ + g_j(\vec{x},E,\vec{\Omega}) \qquad (2.1)\end{aligned}$$

accurately models the transport of incident particles and their secondaries.

In this equation, $\phi_j(\vec{x},E,\vec{\Omega})$ is the fluence of type j particles at position $\vec{x}$ with energy E and moving in direction $\vec{\Omega}$ per unit area per unit energy per steradian. For example, $\phi_1(\vec{x},E,\vec{\Omega})$ represents the number of neutrons, and $\phi_2(\vec{x},E,\vec{\Omega})$ represents the number of protons.

The term $\sigma_j(E)$ represents the macroscopic cross section of the particles of type j. The probability that a type j particle of energy E will have a collision in

Reproduced with permission of the copyright owner. Further reproduction prohibited without permission.

distance l is given by $\sigma_j(E)\ l$. This function has been evaluated experimentally.

The term $S_j(E)$ represents the stopping power or linear energy transfer of type j particles. A charged particle loses energy in discrete increments due to ionization. However, since the distance between ionizing events is small compared with the average path length and the energy loss per event is small, this energy loss is modeled as a continuous function and written as a derivative, $S_j(E) = -\frac{dE}{dl}$ which represents the energy loss per unit path length.

The term $f_{jk}(E, E', \vec{\Omega}, \vec{\Omega}')$ is the production cross section for type j fragment particles of energy E moving in direction $\vec{\Omega}$ due to a collision caused by a type k particle of energy E' from direction $\vec{\Omega}'$.

The term $g_j(\vec{x}, E, \vec{\Omega})$ is the number of type j particles produced at position $\vec{x}$, with energy E, and direction $\vec{\Omega}$ and represents a source term. The source term is often assumed to be zero when dealing with certain space applications.

Appendix A contains a complete derivation of the Boltzmann transport equation. However, a brief explanation of the terms in equation (2.1) is important toward understanding the equation. The first term $\vec{\Omega} \cdot \nabla\phi_j(\vec{x}, E, \vec{\Omega})$ is the rate of change in the number of particles with energy E with respect to distance traveled. The second term $-\frac{\partial}{\partial E}\left[S_j(E)\phi_j(\vec{x}, E, \vec{\Omega})\right]$ accounts for the rate at which type j particles with energy E is changing due to ionization. The third term $\sigma_j(E)\phi_j(\vec{x}, E, \vec{\Omega})$ gives the number of type j particles with energy E and direction $\vec{\Omega}$ at position $\vec{x}$ lost due to nuclear collisions. The term, $\sum_{k \geq j} \int_E^\infty dE' \int d\vec{\Omega}' f_{jk}(E, E', \vec{\Omega}, \vec{\Omega}')\phi_k(\vec{x}, E', \vec{\Omega}')$, accounts for the secondaries produced with energy E and direction $\vec{\Omega}$ by a nuclear collision at position

Reproduced with permission of the copyright owner. Further reproduction prohibited without permission.

$\vec{x}$. The final term $g_j(\vec{x}, E, \vec{\Omega})$ accounts for any sources of particles at position $\vec{x}$ having energy E and moving in direction $\vec{\Omega}$

A straight ahead approximation is often applied to the Boltzmann equation for high energy particles to make it easier to solve. When this approximation is used, it is assumed that all secondaries due to nuclear collisions move in the same direction as the primaries. This approximation is not true for the low energy reaction products which tend to be produced isotropically. Low energy charged particles have short ranges and the errors of straight ahead approximation are limited. The most serious errors are for low energy neutrons which are very penetrating in most materials. The transport of an isotropic neutron source will be addressed in this thesis.

The Boltzmann equation with the straight ahead approximation then becomes

$$\frac{\partial}{\partial x}\phi_j(x,E) - \frac{\partial}{\partial E}\left[S_j(E)\phi_j(x,E)\right] + \sigma_j(E)\phi_j(x,E) = \sum_{k\geq j}\int_E^\infty f_{jk}(E,E')\phi_k(x,E')dE' + g_j(x,E). \qquad (2.2)$$

This approximation is reasonably accurate for high energy nucleons and ions and is used in the HZETRN program.

Neutron Transport

Neutrons do not lose energy through ionization. Therefore, the stopping

Reproduced with permission of the copyright owner. Further reproduction prohibited without permission.

power for neutrons $S_1(E)$ is zero and the transport equation becomes

$$\begin{aligned}\vec{\Omega}\cdot\nabla\phi_1(\vec{x},E,\vec{\Omega})+\sigma_1(E)\phi_1(\vec{x},E,\vec{\Omega})\\ =\sum_{k\geq 1}\int_E^\infty dE'\int d\vec{\Omega}' f_{1k}(E,E',\vec{\Omega},\vec{\Omega}')\phi_k(\vec{x},E',\vec{\Omega}')\\ +g_1(\vec{x},E,\vec{\Omega})\end{aligned} \tag{2.3}$$

or

$$\begin{aligned}\frac{\partial}{\partial x}\phi_1(x,E)+\sigma_1(E)\phi_1(x,E)\\ =\sum_{k\geq 1}\int_E^\infty f_{1k}(E,E')\phi_k(x,E')dE'+g_1(x,E).\end{aligned} \tag{2.4}$$

if the straight ahead approximation is used. Assuming that there are no sources of neutrons, this equation becomes

$$\frac{\partial}{\partial x}\phi_1(x,E)+\sigma_1(E)\phi_1(x,E)=\sum_{k\geq 1}\int_E^\infty f_{1k}(E,E')\phi_k(x,E')dE'. \tag{2.5}$$

As previously stated, the perturbation methods used by the HZETRN program to solve the neutron transport equation, equation (2.5), have been accurate for high energy neutrons but are less accurate for low energy neutrons. At lower energies, below 20 MeV, the elastic scattering cross sections become large. This means that a low energy neutron is likely to have many elastic nuclear collisions over a short distance. The energy loss per collision depends on the target nucleus mass and is small for most nuclei except for hydrogen. These larger cross sections make equation (2.5) a much stiffer equation at low energies. For this reason, different methods are needed to calculate the scattering of low energy neutrons. It is, therefore, useful, to break the neutron Boltzmann equation into

Reproduced with permission of the copyright owner. Further reproduction prohibited without permission.

two equations, one that can be used to evaluate the low energy neutron fluence and another that can be used to calculate the higher energy neutron fluence.

Let the neutron fluence be divided into two groups, those created by evaporation $\phi_{1e}(x, E)$ and those created by direct cascading effects $\phi_{1d}(x, E)$ so that the following equation holds.

$$\phi_1(x, E) = \phi_{1d}(x, E) + \phi_{1e}(x, E). \tag{2.6}$$

Note that most of the low energy neutrons will have been created by evaporation and most of the higher energy neutrons will have come from direct cascading so that $\phi_{1e}(x, E) >> \phi_{1d}(x, E)$ for energies below 15 Mev and $\phi_{1d}(x, E) >> \phi_{1e}(x, E)$ for higher energies. The corresponding interaction term $f_{1k}(E, E')$ can be separated into three terms

$$f_{1k}(E, E') = f_{1ke}(E, E') + f_{1kd}(E, E') + f_{1kel}(E, E')\delta_{1k} \tag{2.7}$$

representing the evaporation, direct knockout, and elastic scattering respectively. Typical values for the first two terms are shown in Figure 2. The third elastic scattering term will be treated in detail.

Reproduced with permission of the copyright owner. Further reproduction prohibited without permission.

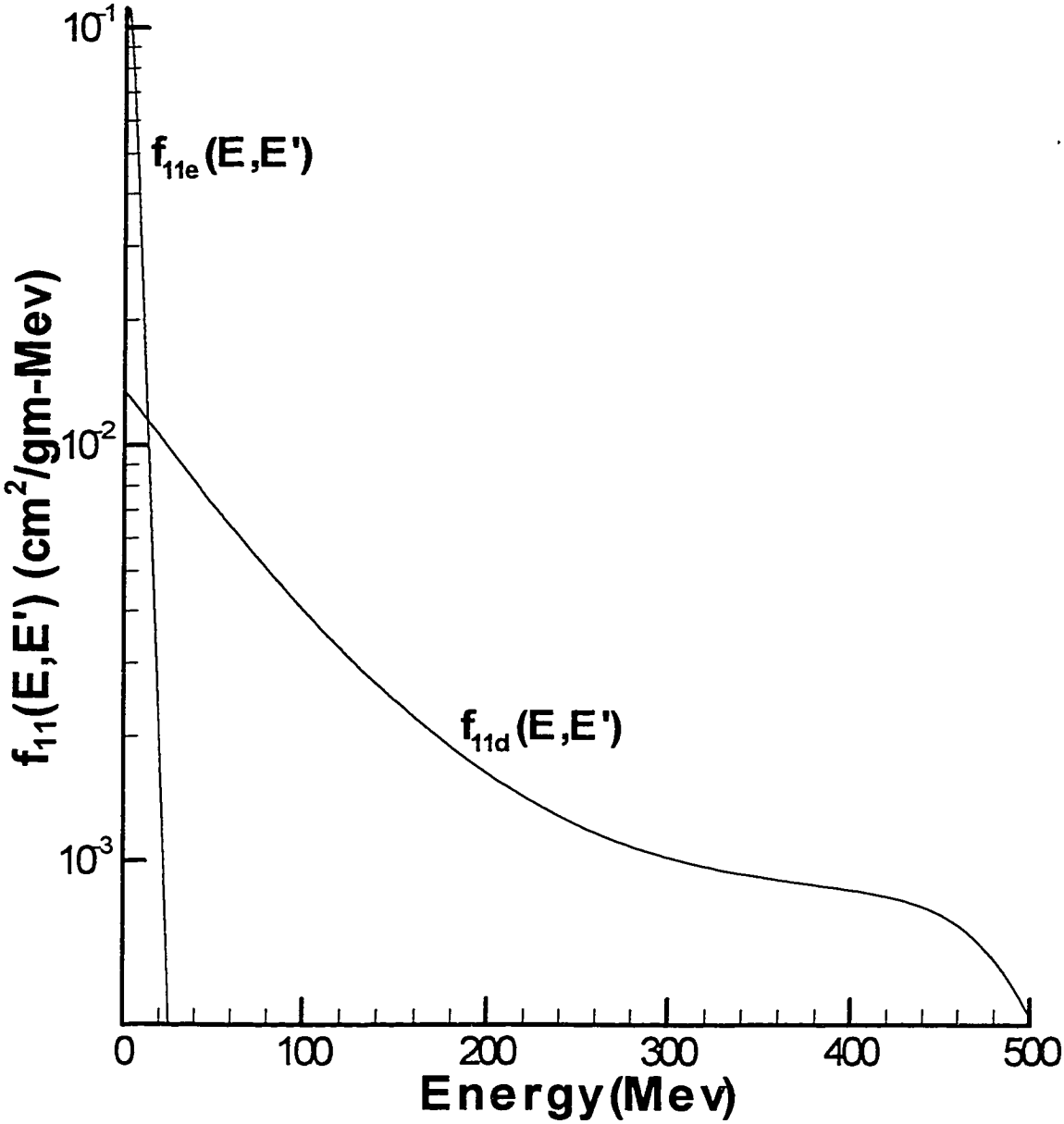

Fig. 2. Evaporation and direct cascade production cross sections for neutrons produced as a result of a nuclear collision between a neutron with energy 500 Mev and an aluminum atom.

Reproduced with permission of the copyright owner. Further reproduction prohibited without permission.

Substituting equations (2.6) and (2.7) into equation (2.5) gives the following equation

$$\frac{\partial}{\partial x}\left[\phi_{1d}(x,E)+\phi_{1e}(x,E)\right]+\sigma_1(E)\left[\phi_{1d}(x,E)+\phi_{1e}(x,E)\right]$$
$$=\int_E^\infty f_{11}(E,E')\left[\phi_{1d}(x,E')+\phi_{1e}(x,E')\right]dE'$$
$$+\sum_{k>1}\int_E^\infty f_{1k}(E,E')\phi_k(x,E')dE'. \tag{2.8}$$

where

$$f_{11}(E,E')=f_{11e}(E,E')+f_{11d}(E,E')+f_{11el}(E,E') \tag{2.9}$$

and

$$f_{1k}(E,E')=f_{1ke}(E,E')+f_{1kd}(E,E') \tag{2.10}$$

for $k>1$. At higher energies E, where $f_{11e}(E,E')$ is close to zero, equation (2.8) can be approximated by the equation

$$\frac{\partial}{\partial x}\phi_{1d}(x,E)+\sigma_1(E)\phi_{1d}(x,E)$$
$$=\int_E^\infty f_{11d}(E,E')\phi_{1d}(x,E')dE'$$
$$+\int_E^\infty f_{11el}(E,E')\phi_{1d}(x,E')dE'$$
$$+\sum_{k>1}\int_E^\infty f_{1kd}(E,E')\phi_k(x,E')dE'. \tag{2.11}$$

This equation is equivalent to (2.5) for higher energies, because $\phi_1(x,E)\approx\phi_{1d}(x,E)$ for higher energies. The HZETRN code was modified to return solutions to equation (2.11). The choice of boundary condition is simplified since neutrons are not present in space radiations.

At lower energies, where $\phi_{1d}(x,E)$ is small, and since the reactive processes at low energies have small cross sections in spacecraft materials. equation (2.8)

Reproduced with permission of the copyright owner. Further reproduction prohibited without permission.

can be approximated by the equation

$$\begin{aligned}
&\frac{\partial}{\partial x}\phi_{1e}(x,E)+\sigma_1(E)\phi_{1e}(x,E)\\
&\quad=\int_E^\infty f_{11el}(E,E')\phi_{1e}(x,E')dE'\\
&\quad+\int_E^\infty f_{11e}(E,E')\phi_{1d}(x,E')dE'\\
&\quad+\sum_{k>1}\int_E^\infty f_{1ke}(E,E')\phi_k(x,E')dE'. \qquad (2.12)
\end{aligned}$$

Note that $\phi_{1d}(x,E)$ is included in the third term because the integration in this term is from E to ∞. Therefore, the number of low energy neutrons produced by evaporation is dependent upon the number of higher energy direct cascade neutrons. Equation (2.12) is the equation for which a new method of solving is required because HZETRN underestimates the lower energy fluences. In this equation, however, $\phi_{1d}(x,E)$, the fluence of direct cascade neutrons, and $\phi_k(x,E)$ for $k > 1$, the fluence of other ions, are known functions. The perturbation methods used in the HZETRN program accurately calculate them except at the lowest energies where elastic scattering dominates but the solution is small. Note that $\phi_{1d}(x,E)$ is calculated from equation (2.11) and is not dependent upon $\phi_{1e}(x,E)$. The fluence of other types of particles, $\phi_k(x,E)$ for $k > 1$, is calculated from equation (2.2) and is only dependent upon heavier ions and not the neutron fluence.

Also note that equations (2.11) and (2.12) are only approximations, because $\phi_{1d}(x,E)$ is small but not exactly zero for low energies and $\phi_{1e}(x,E)$ is small but not exactly zero for larger energies. The error introduced by using these equations, however, will be small.

Reproduced with permission of the copyright owner. Further reproduction prohibited without permission.

The HZETRN program also contains a subroutine ELSPEC which will calculate the scattering function, $f_{jkel}(E, E')$, for all j and all k values at energies E, E'. The third and fourth terms of equation (2.12) can be calculated from the appropriate evaporation terms of equation (2.7). If these two terms are viewed as a source term, then equation (2.12) becomes

$$\frac{\partial}{\partial x}\phi_{1e}(x,E)+\sigma_1(E)\phi_{1e}(x,E)=\int_E^\infty f_{11el}(E,E')\phi_{1e}(x,E')dE'+g(x,E) \quad (2.13)$$

where

$$g(x,E)=\int_E^\infty f_{11e}(E,E')\phi_{1d}(x,E')dE'+\sum_{k>1}\int_E^\infty f_{1ke}(E,E')\phi_k(x,E')dE'. \quad (2.14)$$

In fact, the HZETRN program does calculate this source term and stores it in an array called $NSORCF(i,k,l)$.

Equation (2.13), then, is the low energy neutron equation which must be solved. However, because the remainder of this thesis deals only with the transport of low energy neutrons, equation (2.13) will henceforth be written in the form

$$\frac{\partial\phi(x,E)}{\partial x}+\sigma(E)\phi(x,E)=\int_E^\infty f(E,E')\phi(x,E')dE'+g(x,E) \quad (2.15)$$

where $\phi(x,E)=\phi_{1e}(x,E)$ refers to the fluence of low energy neutrons only and $f(E,E')=f_{11el}(E,E')$ is the neutron elastic scattering function. Also, because these low energy neutrons transport primarily through a process of elastic scattering in which the energy loss depends on the target nucleus and is kinematically limited by E/α so that the integral in equation (2.15) is bounded thus producing

Reproduced with permission of the copyright owner. Further reproduction prohibited without permission.

the equation

$$\frac{\partial \phi(x,E)}{\partial x} + \sigma(E)\phi(x,E) = \int_{E}^{E/\alpha} f(E,E')\phi(x,E')dE' + g(x,E) \qquad (2.16)$$

where

$$\alpha = \left(\frac{A_T - 1}{A_T + 1}\right)^2 \qquad (2.17)$$

is less than one and determined by the atomic weight A_T of the target material.

Reproduced with permission of the copyright owner. Further reproduction prohibited without permission.

CHAPTER III

THE MULTIGROUP METHOD FOR SINGLE ATOM MATERIALS

The one-dimensional low energy neutron transport equation for a single atom target material was given as follows

$$\frac{\partial\phi(x,E)}{\partial x}+\sigma(E)\phi(x,E)=\int_{E}^{E/\alpha}f(E,E')\phi(x,E')dE'+g(x,E). \qquad (2.16)$$

Currently this equation cannot be solved directly, however approximate solutions have been found. Shultis and Faw[2], Duderstadt and Hamilton[4], and Bell and Glasstone[1] have all suggested using a multigroup technique to calculate the neutron fluences in a nuclear reactor. This method is also useful for space radiation.

The Multigroup Method

First, the energy interval $[E_{min}, E_{max}]$, where E_{min} is the smallest energy for which fluences are needed and E_{max} is the largest energy for which fluences are not assumed to be zero, must by divided into N subintervals $[E_i, E_{i+1}]$, $i = 1, 2, ..., N$, where $E_1 = E_{min}$ and $E_{N+1} = E_{max}$. Integrating each term of the equation from E_i to E_{i+1}, for each i, changes equation (2.16) into a system of N differential equations.

The *ith* differential equation is found by letting

$$\Phi_i(x)=\int_{E_i}^{E_{i+1}}\phi(x,E)dE \qquad (3.1)$$

Reproduced with permission of the copyright owner. Further reproduction prohibited without permission.

and

$$b_i(x) = \int_{E_i}^{E_{i+1}} g(x,E)dE. \tag{3.2}$$

Then, by interchanging the order of integration and differentiation, the first term becomes

$$\int_{E_i}^{E_{i+1}} \frac{\partial}{\partial x}\phi(x,E)dE = \frac{d}{dx}\Phi_i(x). \tag{3.3}$$

For the second term the mean value theorem for integrals[28] is used,

$$\int_{E_i}^{E_{i+1}} \sigma(E)\phi(x,E)dE = \sigma(E_i^*)\int_{E_i}^{E_{i+1}} \phi(x,E)dE \tag{3.4}$$

where $E_i^* = E_i + \theta_i^*(E_{i+1} - E_i)$ for some value of θ_i^*, $0 \leq \theta_i^* \leq 1$, to obtain the approximation

$$\int_{E_i}^{E_{i+1}} \sigma(E)\phi(x,E)dE = \sigma(E_i^*)\Phi_i(x). \tag{3.5}$$

Note that because the value of θ_i^* is unknown, an approximate value must be chosen. Ways in which this value can be chosen are discussed in Chapter IV.

In order to write the third term,

$$I = \int_{E_i}^{E_{i+1}} \int_{E}^{E/\alpha} f(E,E')\phi(x,E')dE'dE, \tag{3.6}$$

in terms of $\Phi_i(x)$, the order of integration must be interchanged. This can happen in several ways depending on the size of the interval $[E_i, E_{i+1}]$ as explored in Appendix B.

If $E_{i+1} = E_i/\alpha$, the integration in (3.6) is over the shaded area illustrated in Figure 3.

Reproduced with permission of the copyright owner. Further reproduction prohibited without permission.

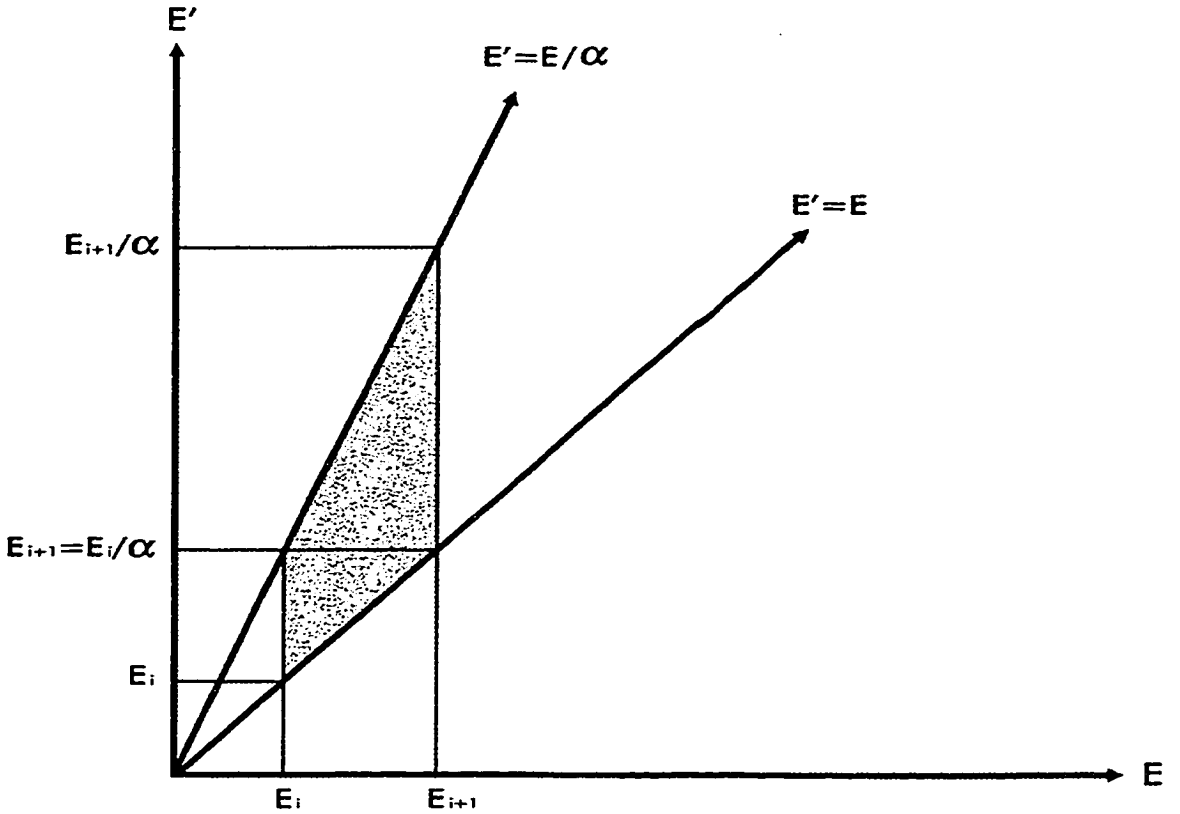

Fig. 3. Area of integration when $E_{i+1} = E_i/\alpha$.

Interchanging the order of integration in equation (2.16) produces

$$I = \int_{E_i}^{E_{i+1}} \int_{E_i}^{E'} f(E, E')\phi(x, E')dEdE' + \int_{E_{i+1}}^{E_{i+1}/\alpha} \int_{\alpha E'}^{E_{i+1}} f(E, E')\phi(x, E')dEdE'. \tag{3.7}$$

This choice for E_{i+1} involves less computation and will require fewer approximations. Therefore, the energy grid must be set up so that $E_{i+1} = \frac{E_i}{\alpha}$ for $i = 1, 2, ..., N$. Note that equation (3.7) is derived more completely and other energy grids are explored in Appendix B. Then, by once again using a mean value theorem, the third term can be rewritten

$$\left[\int_{E_i}^{E_i^*} f(E, E_i^*)dE\right] \Phi_i(x) + \left[\int_{\alpha E_i^*}^{E_{i+1}} f(E, E_{i+1}^*)dE\right] \Phi_{i+1}(x), \tag{3.8}$$

Reproduced with permission of the copyright owner. Further reproduction prohibited without permission.

where $E_i^* = E_i + \theta_i^*(E_{i+1} - E_i)$ for some θ_i^* such that $0 \leq \theta_i^* \leq 1$. Note that the same θ_i^* is used here as was used when $\int_{E_i}^{E_{i+1}} \sigma(E)\phi(x,E)dE$ was calculated.

An integration over the *ith* energy interval $[E_i, E_{i+1}]$ produces the *ith* equation

$$\frac{d\Phi_i(x)}{dx} + \sigma(E_i^*)\Phi_i(x) = \left[\int_{E_i}^{E_i^*} f(E, E_i^*)dE\right] \Phi_i(x) + \left[\int_{\alpha E_i^*}^{E_{i+1}} f(E, E_{i+1}^*)dE\right] \Phi_{i+1}(x) + b_i(x), \quad (3.9)$$

which is a first order linear differential equation for $i = 1, 2, ..., N$.

By letting,

$$a_{i,i} = \int_{E_i}^{E_i^*} f(E, E_i^*)dE - \sigma(E_i^*) \quad (3.10)$$

and

$$a_{i,i+1} = \int_{\alpha E_i^*}^{E_{i+1}} f(E, E_{i+1}^*)dE, \quad (3.11)$$

the equations given by (3.9) can be written as the following system of ordinary differential equations.

$$\begin{aligned}
\frac{d\Phi_1(x)}{dx} &= a_{1,1}\Phi_1(x) + a_{1,2}\Phi_2(x) + b_1(x) \\
\frac{d\Phi_2(x)}{dx} &= a_{2,2}\Phi_2(x) + a_{2,3}\Phi_3(x) + b_2(x) \\
&\vdots \\
\frac{d\Phi_i(x)}{dx} &= a_{i,i}\Phi_i(x) + a_{i,i+1}\Phi_{i+1}(x) + b_i(x) \\
&\vdots \\
\frac{d\Phi_N(x)}{dx} &= a_{N,N}\Phi_N(x) + b_N(x). \quad (3.12)
\end{aligned}$$

Note that Φ_{N+1} does not appear in the Nth equation because $\phi(x,E)$ is small for $E > E_{N+1}$. Also, each differential equation is subject to the initial condition

Reproduced with permission of the copyright owner. Further reproduction prohibited without permission.

$\Phi_i(0)$ specified at $x = 0$. The equation (3.12) can also be written in the form

$$\frac{d\vec{y}}{dx} = A\vec{y} + \vec{b} \tag{3.13}$$

where

$$\vec{y} = col(\Phi_1, \Phi_2, ..., \Phi_N), \tag{3.14}$$

$$\vec{b} = col(b_1, b_2, ..., b_N), \tag{3.15}$$

and A is the upper triangular matrix

$$A = \begin{bmatrix} a_{1,1} & a_{1,2} & 0 & 0 & 0 & \cdots & 0 \\ & a_{2,2} & a_{2,3} & 0 & 0 & & \\ & & a_{3,3} & a_{3,4} & 0 & & \vdots \\ & & & \ddots & \ddots & & \\ & & & & a_{N-2,N-2} & a_{N-2,N-1} & 0 \\ & & & & & a_{N-1,N-1} & a_{N-1,N} \\ & & & & & & a_{N,N} \end{bmatrix} \tag{3.16}$$

From this system of differential equations, each value of Φ_i can be calculated. Then the low energy neutron fluence at each energy E_i, $i = 1, 2, ..., N$ can be approximated using the equation

$$\phi(x, E_i) = \frac{\Phi_i(x)}{E_{i+1} - E_i} = \frac{1}{E_{i+1} - E_i} \int_{E_i}^{E_{i+1}} \phi(x, E) dE \tag{3.17}$$

as it represents the average fluence over the energy interval $[E_i, E_{i+1}]$. Linear interpolation can then be used to find this fluence at any other energy in the interval $[E_1, E_{N+1}]$ if values of ϕ over some other energy grid are required. For example, the HZETRN energy grid is not the same as the $E_{i+1} = E_i/\alpha$ energy grid and so interpolation is required to add contributions.

Reproduced with permission of the copyright owner. Further reproduction prohibited without permission.

A Numerical Solution

In order to solve the system of differential equations (3.12) given in the previous section, the Nth equation

$$\frac{d\Phi_N(x)}{dx} = a_{N,N}\Phi_N(x) + b_N(x) \tag{3.18}$$

must be solved first. This equation can be solved analytically giving the exact solution

$$\Phi_N(x) = e^{a_{N,N}x}\Phi_N(0) + e^{a_{N,N}x}\int_0^x b_N(s)e^{-a_{N,N}s}ds. \tag{3.19}$$

Once $\Phi_N(x)$ has been calculated, the equation for $\Phi_{N-1}(x)$ can be solved. Then $\Phi_{N-1}(x)$ can be used to solve the equation for $\Phi_{N-2}(x)$. This method can be repeated until $\Phi_i(x)$ is known for all values of the index i. The general equation for $\Phi_i(x)$ is

$$\Phi_i(x) = e^{a_{i,i}x}\Phi_i(0) + e^{a_{i,i}x}\int_0^x [a_{i,i+1}\Phi_{i+1}(s) + b_i(s)]e^{-a_{i,i}s}ds \tag{3.20}$$

for $i = 1, 2, ..., N-1$.

In (3.19) and (3.20), $\Phi_i(x)$ is calculated in terms of $\Phi_i(0)$ for each i. From these equations, it is possible to derive the following equations for $\Phi_N(x+\Delta x)$ in terms of $\Phi_N(x)$,

$$\Phi_N(x+\Delta x) = e^{a_{N,N}\Delta x}\Phi_N(x) + e^{a_{N,N}(x+\Delta x)}\int_x^{x+\Delta x} b_N(s)e^{-a_{N,N}s}ds \tag{3.21}$$

and for $\Phi_i(x+\Delta x)$ in terms of $\Phi_i(x)$,

$$\Phi_i(x+\Delta x) = e^{a_{i,i}\Delta x}\Phi_i(x) + e^{a_{i,i}(x+\Delta x)}\int_x^{x+\Delta x} [a_{i,i+1}\Phi_{i+1}(s) + b_i(s)]e^{-a_{i,i}s}ds \tag{3.22}$$

Reproduced with permission of the copyright owner. Further reproduction prohibited without permission.

for $i = 1, 2, ..., N-1$. These new equations can then be used in a marching technique in which Φ_i is calculated at each new depth, $x + \Delta x$, from the previous smaller depth, x, thus saving computation time.

The integrals in equations (3.21) and (3.22) can be approximated using the trapezoid rule

$$\int_x^{x+\Delta x} b_N(s) e^{-a_{N,N}s} ds \approx \frac{1}{2}\Delta x \left[b_N(x) e^{-a_{N,N}x} + b_N(x+\Delta x) e^{-a_{N,N}(x+\Delta x)} \right] \tag{3.23}$$

and

$$\begin{aligned} \int_x^{x+\Delta x} & [a_{i,i+1}\Phi_{i+1}(s) + b_i(s)] e^{-a_{i,i}s} ds \\ & \approx \frac{1}{2}\Delta x \big\{ [a_{i,i+1}\Phi_{i+1}(x) + b_i(x)] e^{-a_{i,i}x} \\ & \quad + [a_{i,i+1}\Phi_{i+1}(x+\Delta x) + b_i(x+\Delta x)] e^{-a_{i,i}(x+\Delta x)} \big\}. \end{aligned} \tag{3.24}$$

Then equations (3.19) and (3.20) will have the forms

$$\Phi_N(x+\Delta x) \approx e^{a_{N,N}\Delta x} \left[\Phi_N(x) + \frac{1}{2}\Delta x b_N(x) \right] + \frac{1}{2}\Delta x b_N(x+\Delta x) \tag{3.25}$$

and

$$\begin{aligned} \Phi_i(x+\Delta x) \approx & e^{a_{i,i}\Delta x} \left[\Phi_i(x) + \frac{1}{2}\Delta x (a_{i,i+1}\Phi_{i+1}(x) + b_i(x)) \right] \\ & + \frac{1}{2}\Delta x (a_{i,i+1}\Phi_{i+1}(x+\Delta x) + b_i(x+\Delta x)) \end{aligned} \tag{3.26}$$

for $i = 1, 2, ..., N-1$.

The Marching Procedure

A general procedure can now be outlined for finding the low energy neutron spectrum at any given depth in a homogeneous slab. First, an energy grid is

Reproduced with permission of the copyright owner. Further reproduction prohibited without permission.

defined by letting E_1 be the smallest energy for which neutron fluences are needed and $E_{i+1} = E_i/\alpha$ for $i \geq 1$. Then a point E_{N+1} on this energy grid is chosen to be the maximum energy. The number of neutrons with energy larger than E_{N+1} produced by evaporation is assumed to be small compared to the number of neutrons with the same energy produced by direct cascading. Physical data supports a value of E_{N+1} between 20 Mev and 60 Mev.

Once the energy grid has been created, $\Phi_i(0)$ is calculated for all i using equation (3.1).

$$\Phi_i(0) = \int_{E_i}^{E_{i+1}} \phi(0, E) dE. \tag{3.27}$$

Note that for a single layer of target material the fluence due to evaporation at the boundary $\phi(0, E)$ is zero for all energies because no nuclear collisions have occurred yet. Therefore, for a single layer of material, $\Phi_i(0) = 0$ for all i.

Next, a suitable step size, Δx, must be chosen for marching through the depths of the target material. Recall, that there is an error on the order of $(\Delta x)^2$ associated with the trapezoid rule used. Also, note that the total number of steps needed, M, is the quotient of the total depth and Δx. Choosing $\Delta x = 0.1\ gm/cm^2$ gives an error on the order of 0.01 $particles/cm^2$ without requiring an unnecessarily large number of calculations. The choice of step size is discussed in more detail in Chapter 4.

Beginning at the largest energy, $\Phi_N(\Delta x)$ is calculated using equation (3.25) by letting $x = 0$,

$$\Phi_N(\Delta x) \approx e^{a_{N,N}\Delta x}\left[\Phi_N(0) + \frac{1}{2}\Delta x b_N(0)\right] + \frac{1}{2}\Delta x b_N(\Delta x). \tag{3.28}$$

Reproduced with permission of the copyright owner. Further reproduction prohibited without permission.

Then equation (3.25) can be used to calculate $\Phi_N(j\cdot\Delta x)$ by letting $x=(j-1)\cdot\Delta x$ for $j=2,3,4,...,M$,

$$\Phi_N(j\cdot x+\Delta x)\approx e^{a_{N,N}\Delta x}\left[\Phi_N((j-1)\cdot\Delta x)+\frac{1}{2}\Delta x b_N((j-1)\cdot\Delta x)\right] + \frac{1}{2}\Delta x b_N(j\cdot\Delta x). \tag{3.29}$$

This process can be repeated to calculate $\Phi_{N-1}(j\cdot\Delta x)$ for $j=1,2,3,...,M$ using equation (3.26). In the same way, Φ_{N-2}, Φ_{N-3}, Φ_{N-4},...,Φ_2, and Φ_1 can be calculated for each multiple of Δx using the equations

$$\Phi_i(\Delta x)\approx e^{a_{i,i}\Delta x}\left[\Phi_i(0)+\frac{1}{2}\Delta x(a_{i,i+1}\Phi_{i+1}(0)+b_i(0))\right] + \frac{1}{2}\Delta x(a_{i,i+1}\Phi_{i+1}(\Delta x)+b_i(\Delta x)) \tag{3.30}$$

and

$$\Phi_i(j\cdot\Delta x)\approx e^{a_{i,i}\Delta x}\left[\Phi_i((j-1)\cdot\Delta x) + \frac{1}{2}\Delta x(a_{i,i+1}\Phi_{i+1}((j-1)\cdot\Delta x)+b_i((j-1)\cdot\Delta x))\right] + \frac{1}{2}\Delta x(a_{i,i+1}\Phi_{i+1}(j\cdot\Delta x)+b_i(j\cdot\Delta x)) \tag{3.31}$$

for $j=2,3,4,...,M$.

Once $\Phi_i(j\cdot\Delta x)$ is known for $i=1,2,3,...,N$ and $j=1,2,3,...,M$, the fluences $\phi(j\cdot\Delta x, E_i)$ can be calculated for all values of i and j using equation (3.17). If ϕ is needed at some other depth or energy, linear interpolation can be used. In this way, the number of low energy neutron particles created by evaporation with any energy can be calculated at any depth.

Reproduced with permission of the copyright owner. Further reproduction prohibited without permission.

CHAPTER IV

A TEST PROBLEM

As a first check, the multigroup method described in Chapter III was applied to a test problem. A numerical solution to the Boltzmann transport equation,

$$\frac{\partial\phi(x,E)}{\partial x}+\sigma(E)\phi(x,E)=\int_{E}^{E/\alpha}f(E,E')\phi(x,E')dE'+g(x,E), \qquad (2.16)$$

was still needed, but in this test problem, both the scattering function $f(E,E')$ and source term $g(x,E)$ were approximated by analytical functions:

$$f(E,E')=\frac{\sigma(E')\tau e^{-\tau(E'-E)}}{1-e^{(1-\alpha)\tau E'}} \qquad (4.1)$$

and

$$g(x,E)=g(E)=KEe^{-E/T} \qquad (4.2)$$

where τ, K, and T are constants. Note that the source term $g(E)$ is in fact dependent on the depth in the material. This dependence, however is small when compared to the dependence on energy, E, and was assumed constant for this test case.

An approximation for the cross section, $\sigma(E)$, was also used,

$$\sigma(E)=\begin{cases} X, & E>E_* \text{ Mev} \\ \frac{X}{(E/E_*)^{1/2}}, & E<E_* \text{ Mev} \end{cases} \qquad (4.3)$$

where E_* is the constant 0.001 Mev and

$$X=\frac{\text{ave. cross section (barns)} \times \text{density (gm/cm}^3) \times 6.023(10)^{23}\text{(particles/mole)}}{\text{Atomic weight (gm/mole)}} \qquad (4.4)$$

Reproduced with permission of the copyright owner. Further reproduction prohibited without permission.

The Maxwellian averages of cross sections for various material can be found in the *Guidebook for the ENDF/B-V Nuclear Data Files*[29]. This reference also contains plots of the cross sections versus energy for various materials. Equation (4.3) was created by curve fitting these plots.

The Multigroup Solution

Multigroup solutions were found for three different materials: lithium, aluminum, and lead. The atomic weights, nuclear cross sections, and densities for these materials are listed in Table 1.

TABLE 1

Parameter Values for Selected Elements

Element	Symbol	A_T	Cross Section barns*	Density gm/cm^3	α
Lithium	Li	7	1.050	.534	.563
Aluminum	Al	27	1.348	2.7	.862
Lead	Pb	207	11.194	11.342	.981
* Maxwellian averages (elastic)					

The constants used in equations (4.1) and (4.2) to calculate the scattering function and the source term were $\tau = 0.4$, $K = 1$, and $T = 1$. Note that K should is related to the flux of high energy particles and could be on the order of 1 for cosmic background or on the order of 10^7. However, changing the value of K does not change the shape of the source function, $g(E)$. Therefore, for the sake of convenience, the value $K = 1$ was chosen for this test problem.

As a first step, an energy grid was set up such that $E_0 = 0.1$ Mev and $E_{i+1} = \frac{E_i}{\alpha}$ for $i = 1, ..., N$, where N was the smallest integer such that $\frac{E_0}{\alpha^N} \geq 30$

Reproduced with permission of the copyright owner. Further reproduction prohibited without permission.

Mev. Note that this meant that the number of grid points required was dependent on the atomic weight of the material with more points (finer grid) needed for heavy materials. This is shown in Table 2.

TABLE 2

Energy Partition Size N

Element	α	N	$0.1/\alpha^N$
Lithium	0.563	10	31.53
Aluminum	0.862	39	32.75
Lead	0.981	298	30.38

The spatial step size $\Delta x = 0.1\ gm/cm^2$ was also chosen.

Then $\Phi_i(x) = \int_{E_i}^{E_{i+1}} \phi(x,E)dE$ was calculated using equations (3.29) and (3.31),

$$\Phi_N(j\cdot x+\Delta x) \approx e^{a_{N,N}\Delta x}\left[\Phi_N((j-1)\cdot\Delta x)+b_N((j-1)\cdot\Delta x)\right]+b_N(j\cdot\Delta x). \quad (3.29)$$

for $i = N$ and $j = 1, 2, 3, ...$ and

$$\Phi_i(j\cdot\Delta x) \approx e^{a_{i,i}\Delta x}\left[\Phi_i((j-1)\cdot\Delta x) + a_{i,i+1}\Phi_{i+1}((j-1)\cdot\Delta x) + b_i(x)\right]$$
$$+ a_{i,i+1}\Phi_{i+1}(j\cdot\Delta x) + b_i(j\cdot\Delta x). \quad (3.31)$$

for $i = 1, 2, 3, ..., N-1$ and $j = 1, 2, 3, ...,$ with

$$a_{i,i} = \int_{E_i}^{E_i^*} f(E, E_i^*)dE - \sigma(E_i^*), \quad (3.10)$$

$$a_{i,i+1} = \int_{\alpha E_i^*}^{E_{i+1}} f(E, E_{i+1}^*)dE, \quad (3.11)$$

Reproduced with permission of the copyright owner. Further reproduction prohibited without permission.

and

$$b_i(x) = \int_{E_i}^{E_{i+1}} g(E)dE \tag{3.2}$$

where $E_i^* = E_i + \theta_i^{(1)}(E_{i+1} - E_i)$ and $E_{i+1}^* = E - i + 1 + \theta_i^{(2)}(E_{i+2} - E_{i+1})$ for some $\theta_i^{(1)}$ and $\theta_i^{(2)}$ such that $0 \leq \theta_i^{(1)} \leq 1$ and $0 \leq \theta_i^{(2)} \leq 1$. Here $\theta_i^{(1)}$ and $\theta_i^{(2)}$ were initially chosen to be 0.5 for all energies and all target materials. In this test case $b_i(x)$ was evaluated analytically to obtain

$$b_i = KT(E_i e^{-E_i/T} - E_{i+1}e^{-E_{i+1}/T}) + KT^2(e^{-E_i/T} - e^{-E_{i+1}/T}). \tag{4.5}$$

Note that b_i was not a function of x because $g(E)$ was not a function of x. Also, $\int_{E_i}^{E_i^*} f(E, E_i^*)dE$ and $\int_{\alpha E_i^*}^{E_{i+1}} f(E, E_i^*)dE$ were calculated exactly giving

$$\int_{E_i}^{E_i^*} f(E, E_i^*)dE = \frac{\sigma(E_i^*)e^{-\tau E_i^*}(e^{\tau E_i} - e^{\tau E_i^*})}{1 - e^{(1-\alpha)\tau E_i^*}} \tag{4.6}$$

and

$$\int_{\alpha E_i^*}^{E_{i+1}} f(E, E_i^*)dE = \frac{\sigma(E_i^*)e^{-\tau E_i^*}(e^{\tau E_{i+1}} - e^{\tau \alpha E_i^*})}{1 - e^{(1-\alpha)\tau E_i^*}}. \tag{4.7}$$

The fluence $\phi(x, E_i)$ for energy grid point E_i, was then approximated from $\Phi_i(x)$ using the equation,

$$\phi(x, E_i) = \frac{\Phi_i(x)}{E_{i+1} - E_i} \tag{4.8}$$

and fluences at other energies or depths were found by interpolating.

The fluences for each of the shield materials were plotted and compared to a numerical method and a recursive method. The values of $\theta_i^{(1)}$ and $\theta_i^{(2)}$ which were used in the mean value theorem were then altered to make the fluences calculated by the multigroup method more closely match those calculated by the

Reproduced with permission of the copyright owner. Further reproduction prohibited without permission.

numerical method. It was found that the choice of $\theta_i^{(1)}$ and $\theta_i^{(2)}$ had little effect on the fluences at smaller depths. However, at larger depths these choices had some effect on the fluences found in the heavier materials aluminum and lead. The following values were chosen

$$\theta_i^{(1)} = \begin{cases} 0.93 + 0.0030485(E_i - 3.037829) - \delta, & E_i > 3.037829 \\ 0.93 + 0.2490258(E_i - 3.037829) - \delta, & 0.5079704 < E_i < 3.037829 \\ 0.30 - 0.3937829(E_i - 0.5079704) - \delta, & E_i < 0.5079704 \end{cases} \tag{4.9}$$

where

$$\delta = 0.4680656(A_T{}^{-0.94888853}) \tag{4.10}$$

and

$$\theta_i^{(2)} = \begin{cases} 0.90 + 0.004355(E_{i+1} - 3.037829), & E_{i+1} > 3.037829 \\ 0.90 + 0.249026(E_{i+1} - 3.037829), & 0.5079704 < E_{i+1} < 3.037829 \\ 0.27 - 0.255920(E_{i+} - 0.5079704), & E_{i+1} < 0.5079704. \end{cases} \tag{4.11}$$

thus, $\theta_i^{(1)}$ and $\theta_i^{(2)}$ are dependent on energy and the atomic weight of the target material. The new fluences calculated by the multigroup method using these values of $\theta_i^{(1)}$ and $\theta_i^{(2)}$ are plotted along with the results of the numerical and recursive methods and are shown in Figures $4-6$ in the Comparisons of Results section.

A Numerical Solution

Since the scattering function, $f(E, E')$, was an analytic function and the source term, $g(x, E)$, was analytic function independent of depth x, it was possible to find another numerical solution for the test problem. This one used a modified predictor-corrector method.

Reproduced with permission of the copyright owner. Further reproduction prohibited without permission.

The spatial grid was set up so that $x_0 = 0$ and $x_i = i \cdot \Delta x$ for $i = 1, 2, 3, ...$ and the energy grid was set up so that $E_0 = 0$ Mev and $E_j = j \cdot \Delta E$ for $j = 1, 2, 3, ...$ The Δx and ΔE were chosen to assure convergence. Next, $\phi(x_i, E_j)$ was defined by

$$\phi(x_i, E_j) = u_{i,j} \tag{4.12}$$

where

$$u_{1,j} = \Delta x K E_j e^{-E_j/T} \tag{4.13}$$

for $j = 1, 2, 3, ...$ and $u_{i,j}$ was calculated in the following manner for $i = 2, 3, 4, ...$ and $j = 1, 2, 3, ...$

The quantity $v_{i,j}$ was defined by the following equation,

$$v_{i,j} = \int_{E_j}^{E_j/\alpha} \frac{\sigma(E')\tau e^{-\tau(E'-E_j)}}{1 - e^{-(1-\alpha)\tau E'}} \phi(x_i, E') dE' \tag{4.14}$$

and for each i, j value, $v_{i,j}$ was evaluated using Simpson's 1/3 rule.

Then the first step of a predictor-corrector method for solving equation (2.16) was given by

$$f_{i,j} = v_{i,j} + E_j e^{-E_j} - \sigma(E_j) u_{i,j} \tag{4.15}$$

and

$$u_{i+1,j} = \begin{cases} u_{i,j} + \Delta x f_{i,j}, & j = 0 \\ \frac{1}{2}(u_{i,j-1} + u_{i,j+1}) + \Delta x f_{i,j}, & j > 0 \end{cases} \tag{4.16}$$

for $i = 1, 3, 5, 7, ...$ and $j = 0, 1, 2, 3, ...$

The second step was given by

$$f_{i+1,j} = v_{i+1,j} + E_j e^{-E_j} - \sigma(E) u_{i+1,j} \tag{4.17}$$

Reproduced with permission of the copyright owner. Further reproduction prohibited without permission.

and

$$u_{i+2,j} = u_{i,j} + 2\Delta x f_{i+1,j} \tag{4.18}$$

for $i = 1, 3, 5, 7, ...$ and $j = 0, 1, 2, 3, ...$

The first step is an adaptation of the Fredrichs method[30], and the second is a second order central difference method.

After the two steps were each repeated one hundred times the following is added to the second step[31]

$$f_{i+2,j} = v_{i+2,j} + E_j e^{-E_j} - \sigma(E) u_{i+2,j} \tag{4.19}$$

and

$$u_{i+2,j} = \frac{1}{2}(u_{i+2,j} + ui + 1, j) + \Delta x f_{3,j} \tag{4.20}$$

for $i = 1, 3, 5, 7, ...$ and $j = 0, 1, 2, 3, ...$

Note that for heavy shielding materials, materials for which α is close to one, a very small ΔE is required for convergence of this numerical procedure.

The resulting neutron fluences were plotted in Figures $4 - 6$ in the Comparisons of Results section as a check against the multigroup method.

A Recursive Solution

An attempt was also made to find a recursive solution to equation (2.16) for the test problem. In this case, a solution of the form

$$\phi(x, E) = \sum_{n=1}^{\infty} \phi_n(E) f_n(x) \tag{4.21}$$

was sought.

Reproduced with permission of the copyright owner. Further reproduction prohibited without permission.

The function $\phi(x,E)$ was substituted into equation (2.16) to create the equation

$$\frac{\partial}{\partial x}\left[\sum_{n=1}^{\infty}\phi_n(E)f_n(x)\right]+\sigma(E)\sum_{n=1}^{\infty}\phi_n(E)f_n(x) = \int_E^{E/\alpha} f(E,E')\sum_{n=1}^{\infty}\phi_n(E')f_n(x)dE' + g(x,E) \tag{4.22}$$

or equivalently,

$$\sum_{n=1}^{\infty}\phi_n(E)\left[\frac{\partial}{\partial x}f_n(x)+\sigma(E)f_n(x)\right] = \sum_{n=1}^{\infty}\left[\int_E^{E/\alpha} f(E,E')\phi_n(E')dE'\right]f_n(x)+g(x,E). \tag{4.23}$$

Using the assumptions that the nuclear cross section, $\sigma(E)=\sigma$, is constant, which is approximately true in a restricted range for $E > 0.001$ Mev, and that the source term, $g(x,E)=g(E)$, is independent of depth, x, it can be seen that equation (4.23) is satisfied if the following equations are satisfied,

$$\phi_1(E) = g(E), \tag{4.24}$$

$$\phi_{n+1}(E) = \int_E^{E/\alpha} f(E,E')\phi_n(E')dE', \tag{4.25}$$

$$\frac{df_1(x)}{dx}+\sigma f_1(x) = 1, \tag{4.26}$$

and

$$\frac{df_{n+1}(x)}{dx}+\sigma f_{n+1}(x) = f_n(x), \tag{4.27}$$

where equations (4.25) and (4.27) hold for $n = 1,2,3,....$

Note that the initial condition

$$f_n(0) = 0 \tag{4.28}$$

Reproduced with permission of the copyright owner. Further reproduction prohibited without permission.

also holds because the low energy neutron fluence due to evaporation is 0 at depth $x = 0$,

$$\phi(0, E) = 0. \tag{4.29}$$

The differential equations (4.26) and (4.27) can be solved exactly to produce the following recursive relations,

$$f_1(x) = \frac{1}{\sigma}(1 - e^{-\sigma x}) \tag{4.30}$$

and

$$f_n(x) = \int_0^x f_{n-1}(u) e^{-\sigma(x-u)} du \tag{4.31}$$

for $n = 2, 3, 4, ...$

Note that the solution has a simple physical interpretation. The $\phi_1(E) f_1(x)$ term is the uncollided neutrons of the distributed source $g(E)$. The $\phi_2(E)$ is the first collision redistribution of energy and $f_2(x)$ their corresponding survival probability.

Equations (4.24), (4.25), (4.30), and (4.31) were used to create approximate solutions of the form

$$\phi(x, E) = \sum_{n=1}^{N} \phi_n(E) f_n(x). \tag{4.32}$$

These functions were plotted as a function of energy, E, for various depths. These plots showed that the functions converged quickly for depths less than or equal to one but did not converge for larger depths.

These approximate neutron fluences for depths less than or equal to one produced by equation (4.32), with N=6, are plotted in Figures $4 - 6$ in the next section and were also used as a check against the multigroup method.

Reproduced with permission of the copyright owner. Further reproduction prohibited without permission.

Comparisons of Results

The low energy neutron fluences obtained using the three methods previously described are plotted in Figures $4 - 6$ below. The fluences are plotted against energy at a number of depths; 0.1 g/cm^2, 0.5 g/cm^2, 1.0 g/cm^2, 5.0 g/cm^2, 10.0 g/cm^2, 50.0 g/cm^2, and 100.0 g/cm^2; for each of the three materials; lithium, aluminum, and lead.

Reproduced with permission of the copyright owner. Further reproduction prohibited without permission.

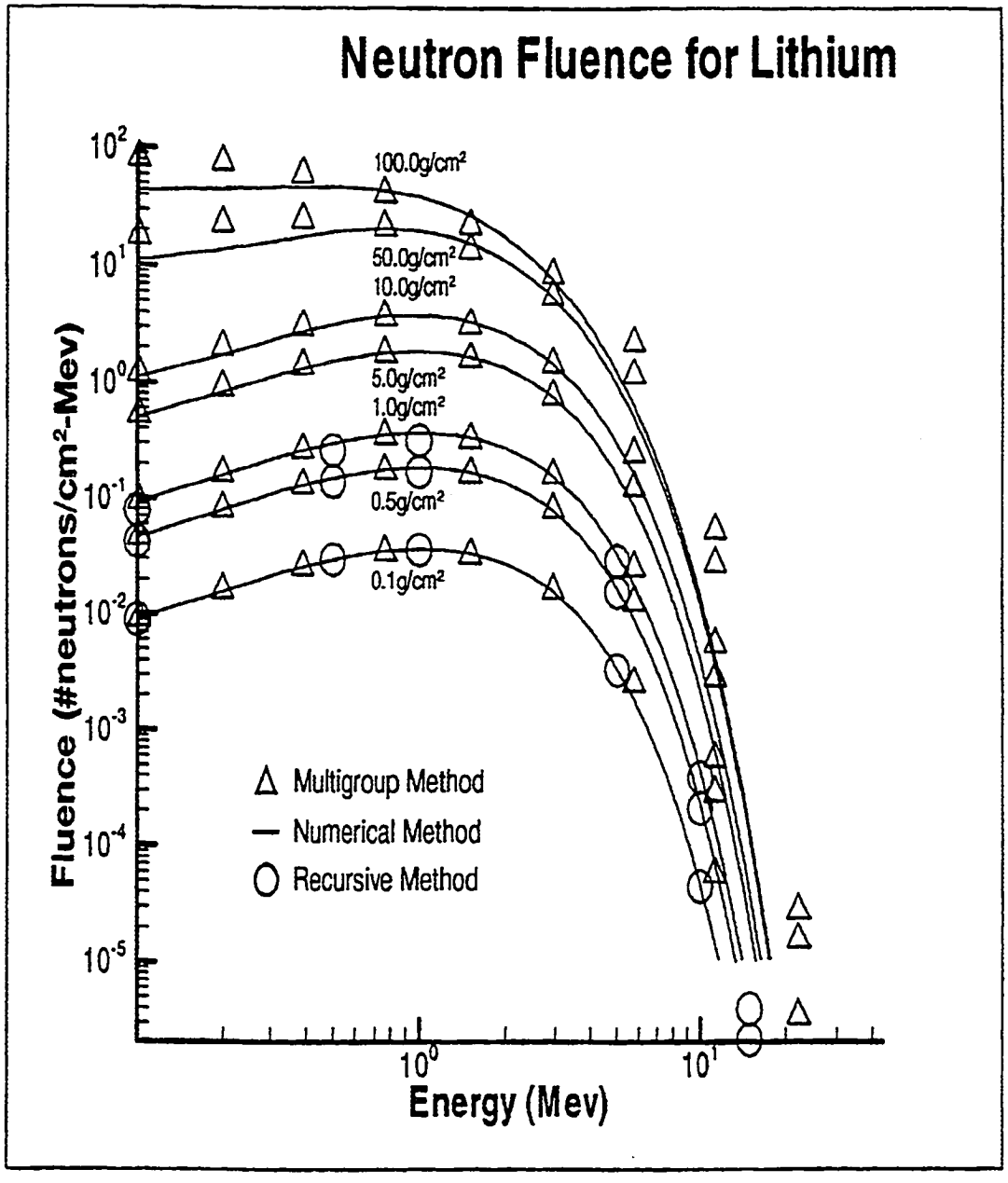

Fig. 4. Test problem solutions - energy spectra of evaporation neutron fluence in lithium.

Reproduced with permission of the copyright owner. Further reproduction prohibited without permission.

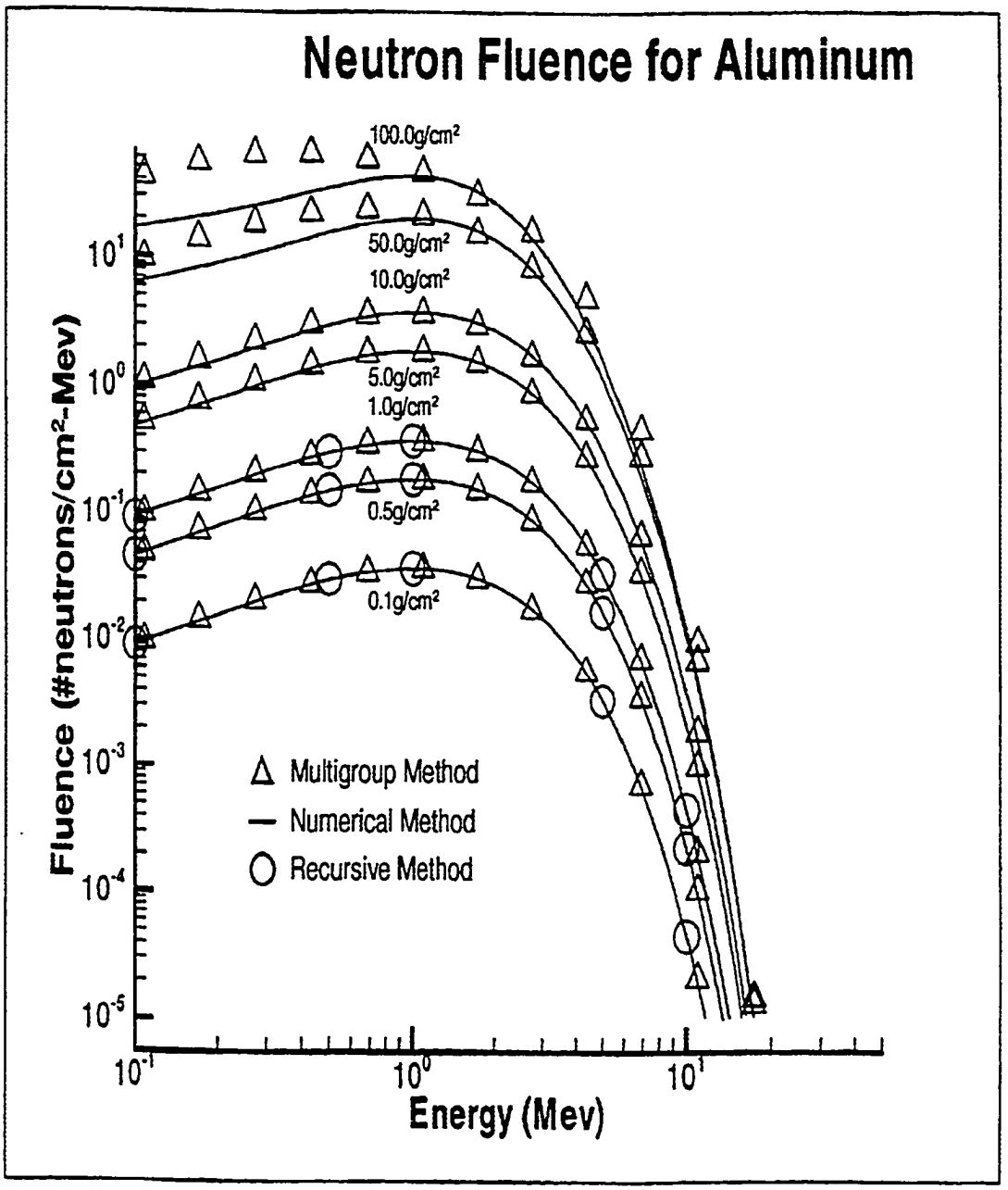

Fig. 5. Test problem solutions - energy spectra of evaporation neutron fluence in aluminum.

Reproduced with permission of the copyright owner. Further reproduction prohibited without permission.

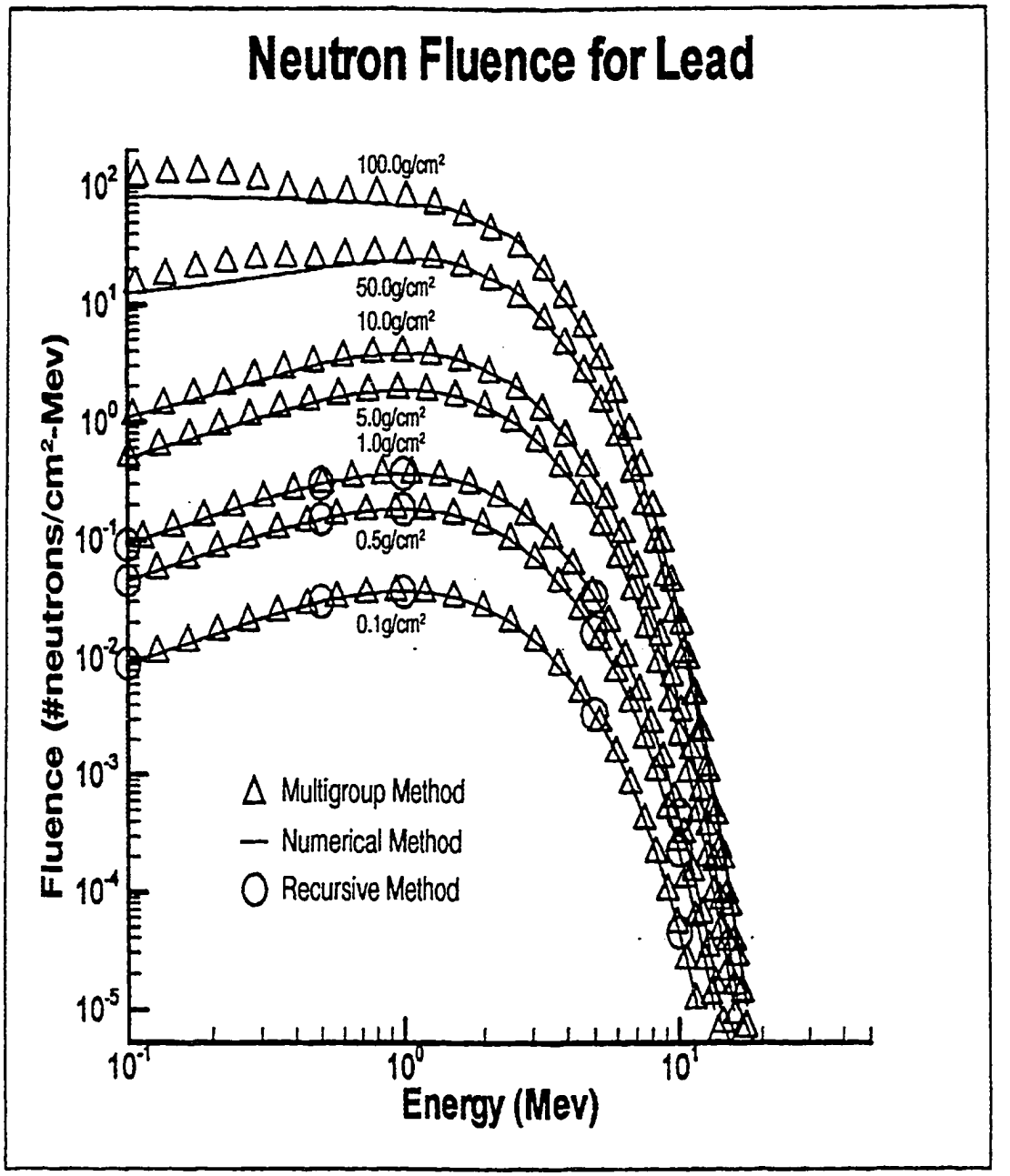

Fig. 6. Test problem solutions - energy spectra of evaporation neutron fluence in lead.

The graphs show a remarkably good agreement between the three methods. This proves that the multigroup method described in Chapter III is a reasonable method for the solution to this type of problem.

Reproduced with permission of the copyright owner. Further reproduction prohibited without permission.

The multigroup method also has several advantages over the other methods described in this chapter. First, it is fast computationally. The numerical method used a large amount of computer time, while the multigroup method ran in seconds. Second, it works for larger depths. The recursive method was limited to depths less than or equal to one g/cm^2. Lastly, the multigroup method is more versatile than either of the other two methods. The numerical method and the recursive method described in this chapter could be applied to this test problem only because the source term, $g(x, E) = g(E)$, was only dependent on energy, E. The multigroup method has no such limitations, nor does the multigroup method require that the cross sections, $\sigma(E)$, be constant or that the scattering function, $f(E, E')$, and the source term, $g(x, E)$, be rather simple analytical functions. For these reasons, the multigroup method was deemed an ideal method for use in trying to solve the more complicated problem described in the next chapter.

Reproduced with permission of the copyright owner. Further reproduction prohibited without permission.

CHAPTER V

INCORPORATING THE MULTIGROUP METHOD INTO THE HZETRN PROGRAM

Having proven to be very accurate on the test problem, the multigroup method described in Chapter III was then applied to a more realistic problem. In this case, it was desired to calculate the low energy neutron spectrum at various depths in an aluminum shield. To accomplish this a solution to equation (2.16) using more realistic values for both the scattering function $f(E, E')$ and the source term $g(x, E)$ as evaluated by the HZETRN program was needed. This was accomplished by adding the multigroup method to the HZETRN program in a subroutine called NPRP which stands for neutron propagation.

The HZETRN Program

Before running the HZETRN program, the background radiation must be specified. Models of radiation fields for several solar particle events (SPEs), February 1956, November 1960, and August 1972, are available. In the case of SPEs, the shield is bombarded by large numbers of low to high energy protons. As these protons interact with the atoms of the shield material, more protons and other light ions and neutrons are produced. It is also possible to set the program up to model galactic cosmic rays. In this case, the shield is bombarded with a variety of heavy ions in addition to protons and light ions, and the transport

Reproduced with permission of the copyright owner. Further reproduction prohibited without permission.

process produces more heavy and light ions and protons and neutrons. These eventually become the source term for the low energy neutron equation.

As an example, the SPE of February 23, 1956 was chosen as input data.

The HZETRN program is set up to calculate radiation transport in two slabs of material. The program models the transport of ions incident upon an outer slab of material called the shield. These transport calculations are then continued through an inner slab of material called the target.

In the main part of the program, the depths, $x(k)$ for $k = 1, 2, ..., 10$ for the shield and $y(l)$ for $l = 1, 2, ..., 10$ for the target, and the energies, $en(i)$ for values $i = 1, 2, ..., 30$, at which the low energy neutron source term will be calculated are input. These depths are also the depths at which the particle fluences are found. Then the shielding material is defined by inputting its atomic weight, charge, and density.

The program then sets up an energy grid, $etf(ie)$ for $ie = 1, 2, ..., 30$, based on an equal log spacing of the proton range. Then for each depth, $x(k)$ for $k = 1, 2, .., 9$ the subroutine PRPGT is called to propagate the fluence from $x(k)$ to $x(k+1)$. These fluences are calculated at every energy $etf(ie)$ for $ie = 1, 2, ..., 30$ and stored in the $ff(ie, j, k, l)$ array for $ie = 1, 2, ..., 30$; $j = 1, 2, ..., 6$; and $l = 1$. Here, the index j gives the type of ion being transported, ${}_0^1N$ (neutron), ${}_1^1H$ (proton), ${}_1^2D$ (deuteron), ${}_1^3T$ (triton), ${}_2^3He$ (helion), and ${}_2^4He$ (helium) for solar flares, and the index l gives the depth into the shield and is 1 for no target.

These fluences are then used in a subroutine called SOURCEF to calculate the source term for the low energy neutron transport equation. This source term

Reproduced with permission of the copyright owner. Further reproduction prohibited without permission.

corresponds to the number of neutrons per unit depth of energy $en(i)$ that are produced through evaporation when the particles stored in $ff(ie, j, k, l)$ collide with atomic nuclei. This source term is stored discretely in the $NSORF(i, k, l)$ array for $i = 1, 2, ..., 30$, $k = 1, 2, ..., 10$, and $l = 1$. $NSORF(i, k, 1)$ is the source term $g(x, E)$ needed in equation (2.16) at $x = x(k)$ and $E = en(i)$.

If allowed to continue, the program proceeds to define the target material, calculate the ion transport through the target, and evaluate the low energy neutron source terms for the target in much the same way. The fluences are then used to calculate estimated dose values for various shield-target geometries.

For this problem, however, the call statement for the multigroup subroutine, NPRP, was inserted right after the source term for the shield was calculated. Then the HZETRN program was terminated.

Description of The Multigroup Subroutine NPRP

When the main program calls the multigroup subroutine NPRP, the source term array $NSORCF(i, k, l)$, as well as the depths $x(k)$ and $y(l)$ and both the energy grid for the source term $en(i)$ and the energy grid for the fluences $etf(ie)$ are sent to the subroutine. The atomic weight, charge, and density of the shielding material are stored in a common block and are, therefore, also available to the subroutine.

Subroutine NPRP follows the method laid out in Chapter III. First, α is calculated from the atomic weight of the shield material. Then, yet another energy grid is created. This energy grid, stored in the $ena(ii)$ array for $ii = 1, 2, 3, ..., N$ is set up so that $ena(ii + 1) = ena(ii)/\alpha$ and N is chosen so that

Reproduced with permission of the copyright owner. Further reproduction prohibited without permission.

$ena(N) \geq 30$ MeV and $ena(N-1) < 30$ MeV.

Next, a step size for marching through the depths of the material is chosen. Here, care must be taken that each depth in the $x(k)$ array is a multiple of the chosen step size. In Chapter III, a step size of $\Delta x = 0.1\ gm/cm^2$ was suggested. 0.1 gm/cm^2 is adequate here, as well, so long as the depths in the $x(k)$ array are all multiples of 0.1 gm/cm^2. In the NPRP subroutine this step size is called *del*.

Once the step size has been defined, the maximum number of steps is calculated. This is the number of steps needed to get from $x(1)$ to $x(10)$ and is given by the equation $IMAX = INT\left(\frac{x(10)-x(1)}{del}\right)$.

Next, subroutine AMATRX is called to calculate $a_{ii,ii}$ and $a_{ii,ii+1}$ for values $ii = 1, 2, 3, ..., N$. These values are calculated as described in Chapter III,

$$a_{ii,ii} = \int_{E_{ii}}^{E_{ii}^*} f(E, E_{ii}^*)dE - \sigma(E_{ii}^*) \tag{5.1}$$

and

$$a_{ii,ii+1} = \int_{\alpha E_{ii}^*}^{E_{ii+1}} f(E, E_{ii}^*)dE. \tag{5.2}$$

The scattering function, $f(E, E')$, and the nuclear cross sections, $\sigma(E)$, however, are more complicated analytic functions than used in the test problem in chapter 3. Instead, the HZETRN program contains a subroutine, ELSPEC, that will calculate either the scattering function, $f_s(E, E')$, or the integral scattering function, $\int_{\alpha E'}^{E} f_s(\overline{E}, E')d\overline{E}$. Note, this scattering function, $f_s(E, E')$, is not the same as the scattering function described in chapter 2, but $f(E, E') = \sigma(E')f_s(E, E')$ is the scattering function described in chapter 2. The HZETRN program also contains a subfunction ELSEC which will calculate the elastic nuclear cross sec-

Reproduced with permission of the copyright owner. Further reproduction prohibited without permission.

tion $\sigma(E)$ for any energy E. Thus, the AMATRX subroutine calculates $a_{ii,ii}$ and $a_{ii,ii+1}$ using the equations

$$a_{ii,ii} = \sigma(E^*_{ii})\left[\int_{\alpha E^*_{ii}}^{E^*_{ii}} f_s(E, E^*_{ii})dE - \int_{\alpha E^*_{ii}}^{E_{ii}} f_s(E, E^*_{ii})dE\right] - \sigma(E_{ii}) \qquad (5.3)$$

and

$$a_{ii,ii+1} = \sigma(E^*_{ii}) \int_{\alpha E^*_{ii}}^{E_{ii+1}} f_s(E, E^*_{ii})dE, \qquad (5.4)$$

where $\int_{\alpha E^*_{ii}}^{E^*_{ii}} f_s(E, E^*_{ii})dE$, $\int_{\alpha E^*_{ii}}^{E_{ii}} f_s(E, E^*_{ii})dE$, and $\int_{\alpha E^*_{ii}}^{E_{ii+1}} \sigma(E^*_{ii}) f_s(E, E^*_{ii})dE$ are calculated by making calls to the ELSPEC subroutine, and $\sigma(E^*_{ii})$ and $\sigma(E_{ii})$ are calculated by the subfunction ELSEC. Once calculated, these values are stored in the $A(ii, ii)$ array.

Once the $A(ii, ii)$ array has been set up, the NPRP subroutine calls subroutine EINTERP to interpolate the source term values stored in the $NSORCF(i, k, l)$ array to the $ena(ii)$ energy grid. This subroutine uses linear interpolation. The interpolated source term values are stored in the $XNEW(ii, k, l)$ array, where $XNEW(ii, k, l)$ is the source term at energy $ena(ii)$ and depth $x(k)$ into the shield and $y(l)$ into the target.

After the source terms have been interpolated to the new energy grid, the NPRP subroutine calls subroutine INTX to calculate the integral of the source term from $ena(ii)$ to $ena(ii + 1)$ for $ii = 1, 2, 3, ..., N - 1$. The trapezoid rule is used to calculate these integrals. The new integrated source terms are stored in the array, $B(ii, k, l)$, where $B(ii, k, l)$ is the integral of the source term at $x(k)$ and $y(l)$ from $ena(ii)$ to $ena(ii + 1)$. Note that this is the $b_i(x)$ term given by equation (3.2) in Chapter III.

Reproduced with permission of the copyright owner. Further reproduction prohibited without permission.

Next, a new array called $YBAR(ii, icount)$ is initialized so that

$$YBAR(N, icount) = 0 \tag{5.5}$$

for $icount = 1, 2, 3, ..., imax$. This new array will contain the integral fluences, called $\Phi_i(x)$ in Chapter III. $YBAR(ii, icount)$ is the integral of the neutron fluence from energy $ena(ii)$ to energy $ena(ii+1)$ at depth $x = icount*del$. Therefore, $YBAR(N, icount)$ is the integral of the neutron fluence at the largest energy at depth $x = icount * del$. Recall, that the fluence of evaporation neutrons is small enough to be approximated by zero for energies greater than 30 Mev. For this reason, the integral fluence at energy $ena(N)$ is set to zero.

The marching process is begun at the next highest energy $ena(N-1)$ and continues downward to $ena(1)$.

At each of these energies, the depth and the depth counter are initially set to zero, $dep = 0$ and $icount = 0$. Then, the integral fluence is calculated at zero depth. For the shield material, this value is zero, because there can be no evaporation neutrons before any collisions have occurred. Therefore,

$$YBAR(ii, 0) = 0. \tag{5.6}$$

A second marching process, this one through the depths of the material, is, then, begun. At each step, the depth, *dep*, is increased by *del*, and the depth counter, *icount*, is increased by one.

At each depth, the subroutine BINT is called to interpolate the integral of the source term stored in the $B(ii, k, l)$ to the current depth. This new value is stored in the $BB(ii, icount)$ array. This subroutine also uses linear interpolation.

Reproduced with permission of the copyright owner. Further reproduction prohibited without permission.

Next $YBAR(ii, icount)$, the integral fluence at the current energy $ena(ii)$ and the current depth *dep*, is calculated from the integral fluence at the previous depth, $(icount-1)del$ and the integral fluences at the previous energy, ena(ii+1). If $icount = 1$, equation (3.30) from Chapter III is used

$$\Phi_i(\Delta x) \approx e^{a_{i,i}\Delta x}\left[\Phi_i(0)+a_{i,i+1}\Phi_{i+1}(0)+b_i(0)\right]+a_{i,i+1}\Phi_{i+1}(\Delta x)+b_i(\Delta x) \quad (3.30)$$

or in terms of the variable names used in the NPRP subroutine

$$\begin{aligned} YBAR(ii,1) =& e^{A(ii,ii)del}\left[YBAR(ii,0) + A(ii,ii+1)YBAR(ii+1,0) + BB(ii,0)\right] \\ &+ A(ii,ii+1)YBAR(ii+1,1) + BB(ii,1). \end{aligned} \quad (5.7)$$

Otherwise, equation (3.31) is used

$$\begin{aligned} \Phi_i(j\cdot\Delta x) \approx& e^{a_{i,i}\Delta x}\left[\Phi_i((j-1)\cdot\Delta x) + a_{i,i+1}\Phi_{i+1}((j-1)\cdot\Delta x) + b_i((j-1)\cdot\Delta x)\right] \\ &+ a_{i,i+1}\Phi_{i+1}(j\cdot\Delta x) + b_i(j\cdot\Delta x). \end{aligned} \quad (3.31)$$

or

$$\begin{aligned} YBAR(ii,icount) =& e^{A(ii,ii)del}\left[YBAR(ii,icount-1)\right. \\ &+ A(ii,ii+1)YBAR(ii+1,icount-1) \\ &\left.+ BB(ii,icount-1)\right] \\ &+ A(ii,ii+1)YBAR(ii+1,icount) \\ &+ BB(ii,icount). \end{aligned} \quad (5.8)$$

Once the integral fluence has been calculated, the NPRP subroutine checks to see if the current depth, *dep*, is one of the depths at which neutron fluences

Reproduced with permission of the copyright owner. Further reproduction prohibited without permission.

are needed, $x(k)$ for $k = 1, 2, 3, ..., 10$. If it is, the neutron fluence is calculated from the integral fluence by dividing the integral fluence by the difference in the energy grid, $ena(ii+1) - ena(ii)$. This fluence is stored in the $PHI(ii, k, l)$ array, where $PHI(ii, k, l)$ is the neutron fluence at energy $ena(ii)$ and depth $x(k)$ in the shield and $y(l)$ in the target.

Next, the NPRP subroutine goes on to the next depth and repeats this process. Once the maximum depth, $x(10)$, is reached, the program goes on to the next energy, one step lower on the energy grid than the one just finished, and starts again at depth $dep = 0$.

Once this process has been repeated for every energy, the NPRP subroutine interpolates the neutron fluences stored in the $PHI(ii, k, l)$ array back to the $etf(ie)$ energy grid provided by the main program. The new fluences are stored in the $fneu(ie, k, l)$ array, where $fneu(ie, k, l)$ is the low energy neutron fluence at energy $etf(ie)$ and depth $x(k)$ into the shield and $y(l)$ into the target. Once again, linear interpolation is used.

These low energy neutron fluences are then returned to the main program where they can be added to the other neutron fluences stored in $ff(ie, 1, k, l)$.

Results

The low energy neutron fluences created by the scattering of evaporation neutrons as calculated by the NPRP subroutine are plotted in Figure 7. Here, fluence is plotted against energy for nine depths, 0.1 gm/cm^2, 0.3 gm/cm^2, 1 gm/cm^2, 3 gm/cm^2, 5 gm/cm^2, 10 gm/cm^2, 20 gm/cm^2, 30 gm/cm^2, 50 gm/cm^2, and 100 gm/cm^2. Note that the fluence increases with depth. Also, note that the

Reproduced with permission of the copyright owner. Further reproduction prohibited without permission.

fluence at depth zero is zero and cannot be shown on a *log* plot.

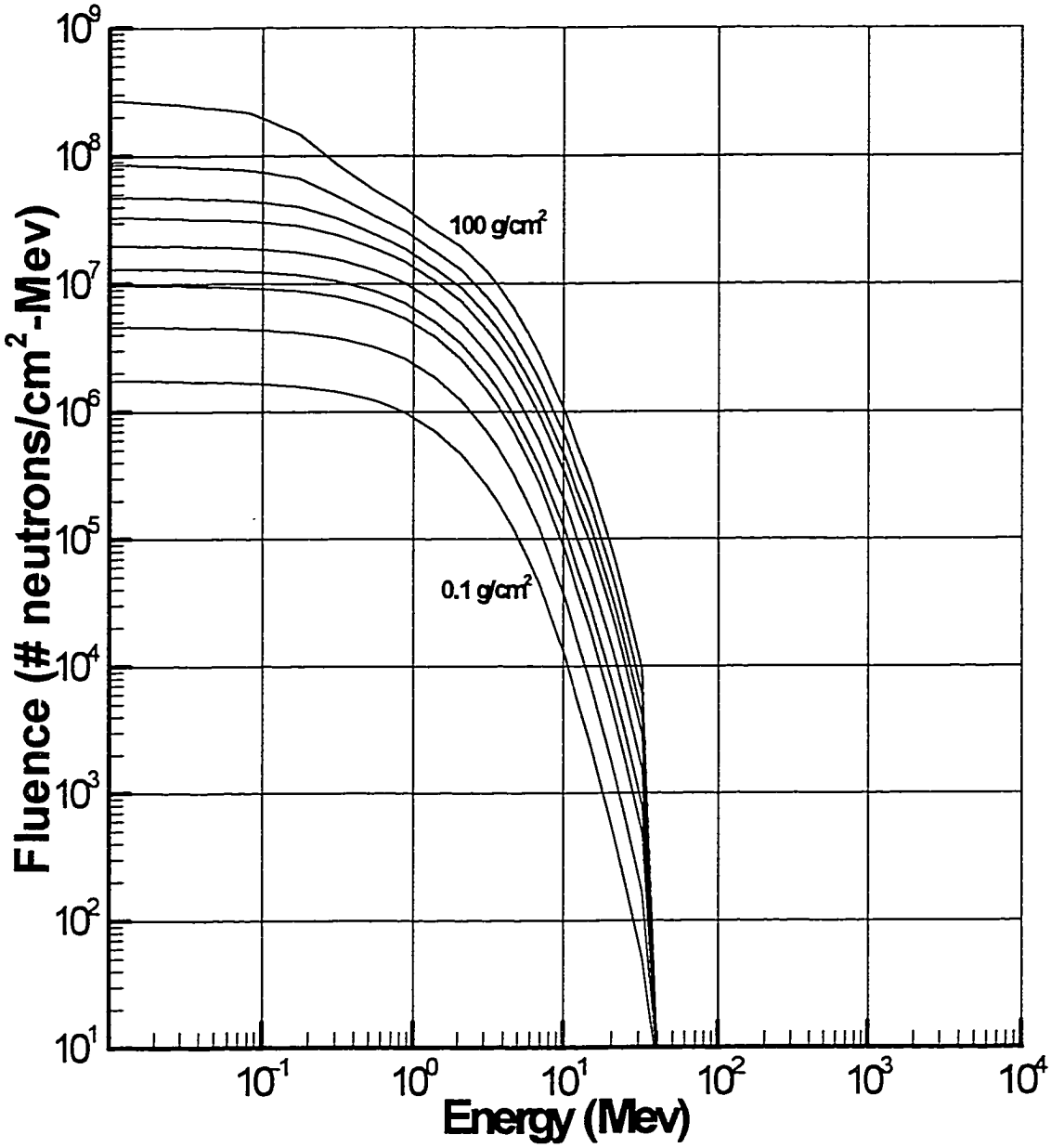

Fig. 7. Low energy neutron fluences due to scattering of evaporation neutrons in an aluminum shield exposed to the February 23, 1956 solar particle event.

Note that the shape of this graph is similar to that of Figure 5.

Figure 8 shows these fluences added to the neutron fluences produced by the

Reproduced with permission of the copyright owner. Further reproduction prohibited without permission.

HZETRN program. In other words, this plot shows the total neutron fluence.

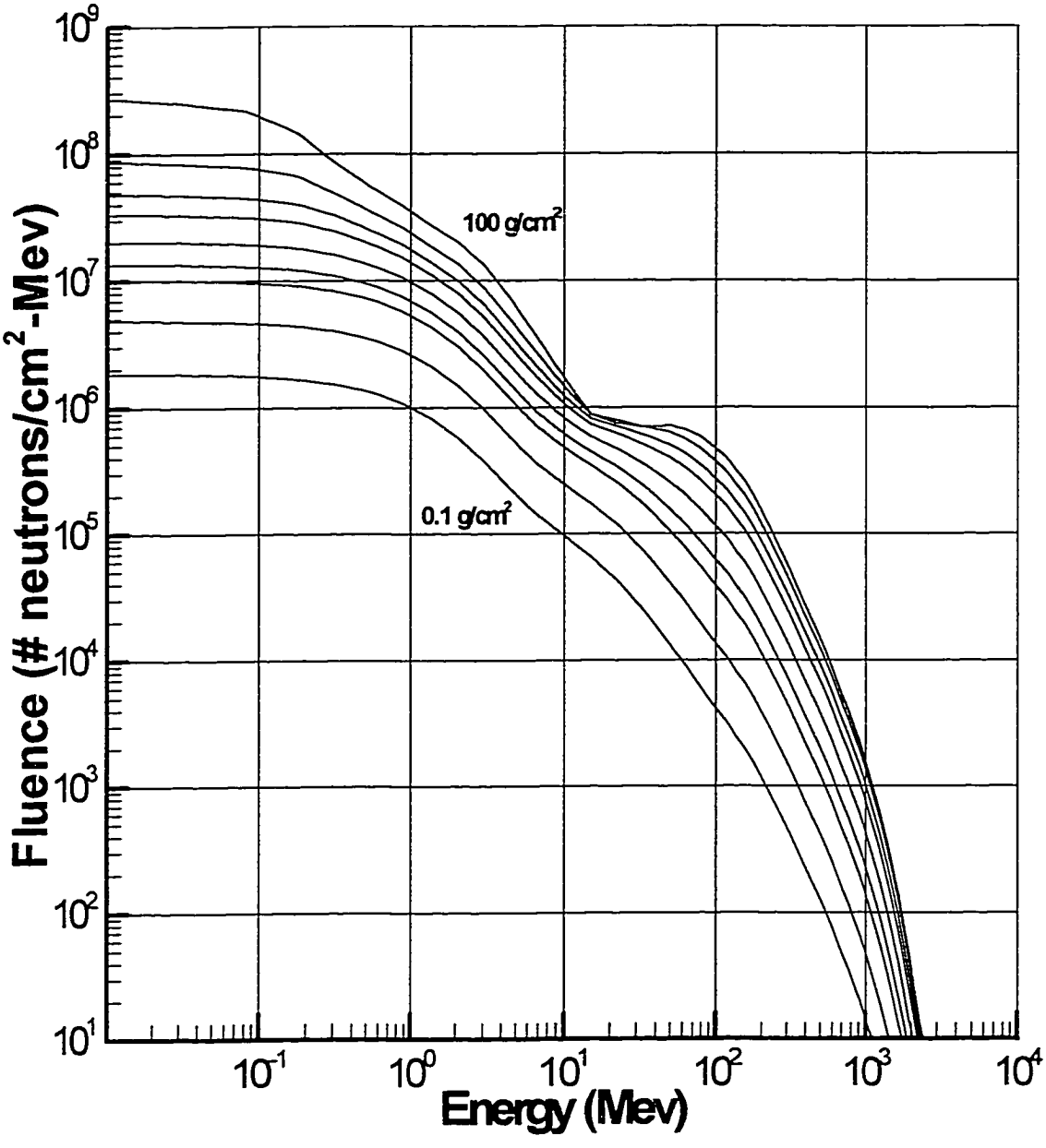

Fig. 8. Total neutron fluences in an aluminum shield exposed to the February 23, 1956 solar particle event.

Figures 9—11 show comparisons of the total neutron fluence calculated by the HZETRN program with the multigroup subroutine with the total neutron fluence

Reproduced with permission of the copyright owner. Further reproduction prohibited without permission.

calculated by the HZETRN program without transporting evaporation neutrons and the total neutron fluence calculated by the HZETRN program with the evaporation neutrons transported using the same perturbation methods used on the higher energy neutrons. These comparisons are made at depths of 1 gm/cm^2, 10 gm/cm^2, and 100 gm/cm^2 respectively.

Reproduced with permission of the copyright owner. Further reproduction prohibited without permission.

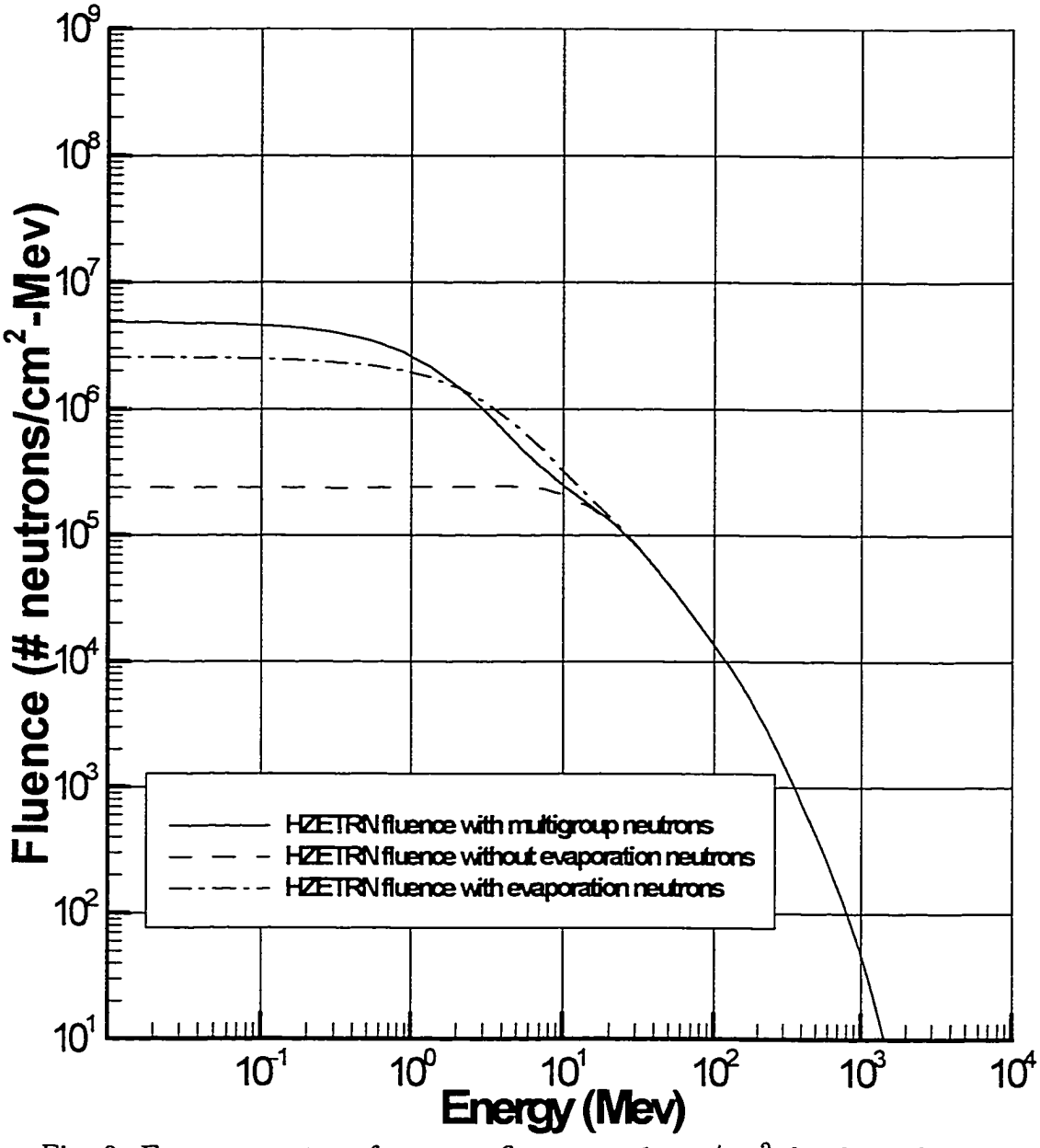

Fig. 9. Energy spectra of neutron fluence at 1 gm/cm^2 depth in aluminum exposed to the February 23, 1956 solar energetic particle event.

Reproduced with permission of the copyright owner. Further reproduction prohibited without permission.

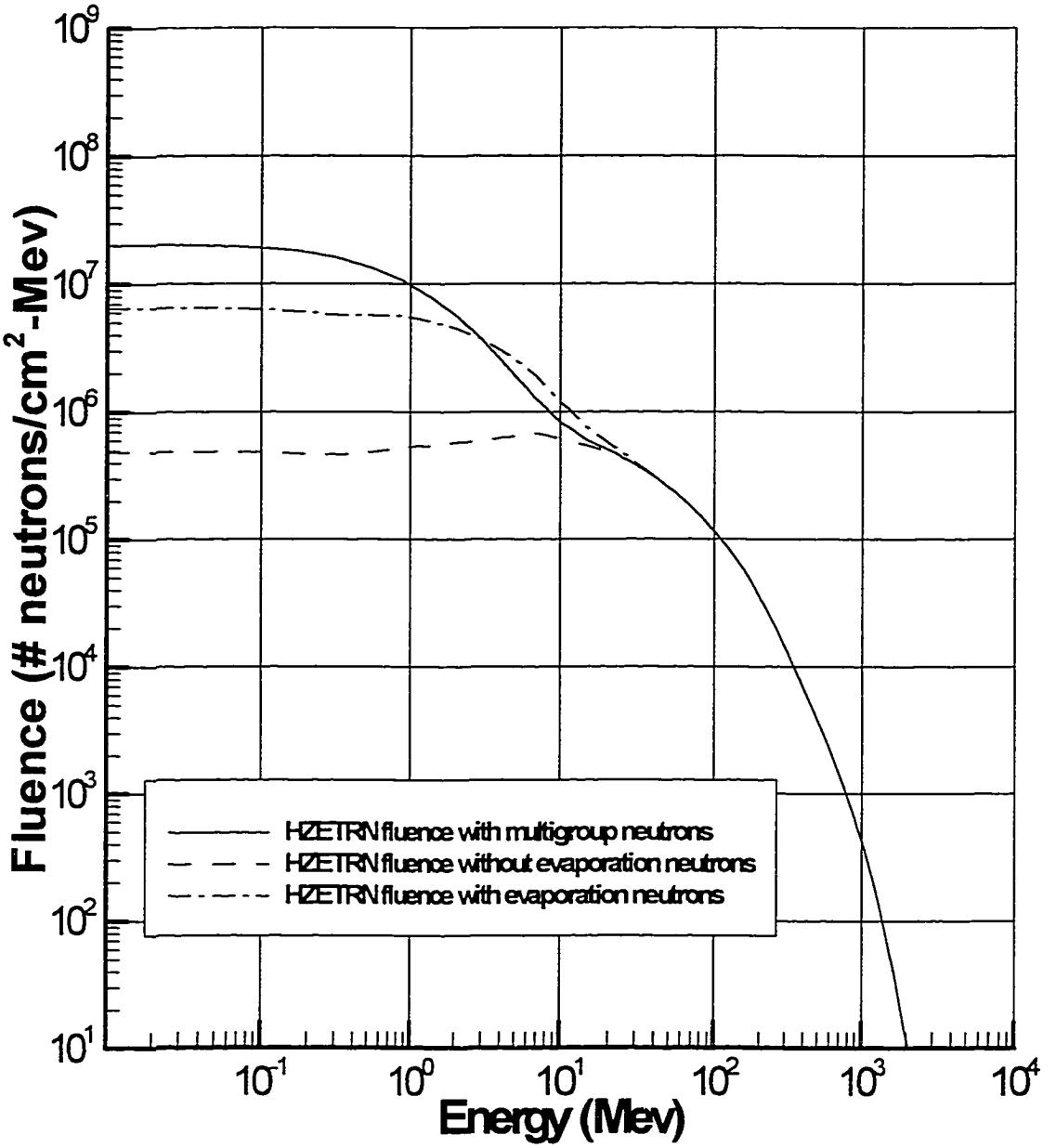

Fig. 10. Energy spectra of neutron fluence at 10 gm/cm^2 depth in aluminum exposed to the February 23, 1956 solar energetic particle event.

Reproduced with permission of the copyright owner. Further reproduction prohibited without permission.

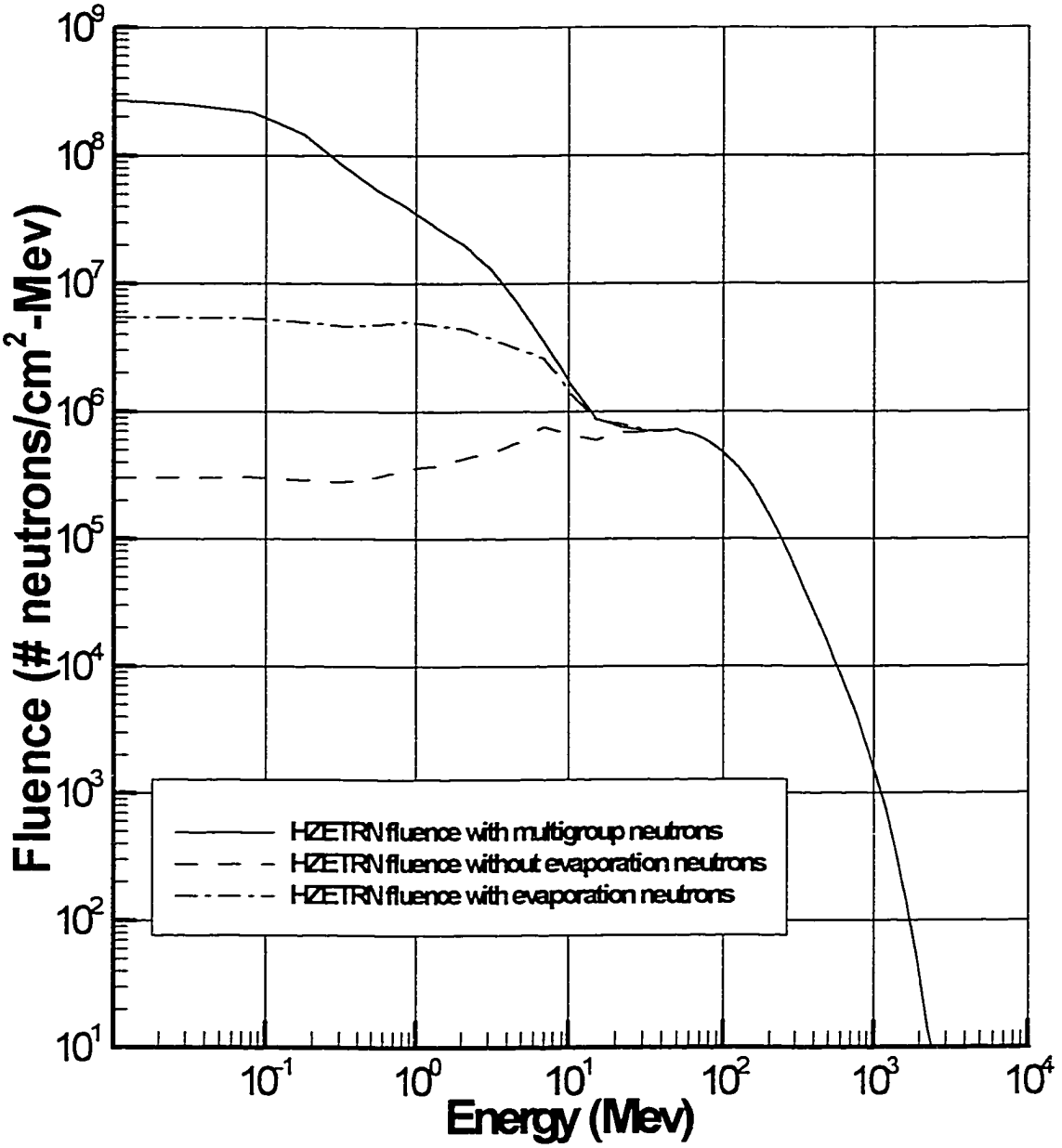

Fig. 11. Energy spectra of neutron fluence at 100 gm/cm^2 depth in aluminum exposed to the February 23, 1956 solar energetic particle event.

In all three cases, the total low energy neutron fluence calculated by the HZETRN program with the multigroup subroutine, NPRP, is larger than the total low energy neutron fluence calculated either of the other two ways. This indicates that

Reproduced with permission of the copyright owner. Further reproduction prohibited without permission.

the rescattering terms of the original HZETRN code were inaccurate representing a net loss of neutrons.

Reproduced with permission of the copyright owner. Further reproduction prohibited without permission.

CHAPTER VI

THE MULTIGROUP METHOD FOR MULTIPLE ATOM TARGET MATERIALS

The low energy neutron transport equation derived in Chapter II

$$\frac{\partial\phi(x,E)}{\partial x}+\sigma(E)\phi(x,E)=\int_{E}^{E/\alpha}f(E,E')\phi(x,E')dE'+g(x,E) \qquad (2.16)$$

must be altered when used to model transport in a material containing more than one type of atom such as CO_2 or water. A separate scattering function $f_\beta(E,E')$ must be calculated for each atom in the target material. For example, if the target is CO_2, then $f_C(E,E')$ will represent the number of scattered neutrons with energy E produced when a neutron with energy E' collides with the nucleus of a carbon atom, and $f_O(E,E')$ will represent the number of scattered neutrons with energy E produced when a neutron with energy E' collides with the nucleus of an oxygen atom. The low energy neutron transport equation then becomes

$$\frac{\partial\phi(x,E)}{\partial x}+\sigma(E)\phi(x,E)=\sum_{\beta}\int_{E}^{E/\alpha_\beta}f_\beta(E,E')\phi(x,E')dE'+g(x,E) \qquad (6.1)$$

where α_β is the α for atom type β given by equation (2.17).

Derivation of Multigroup Method for Multiple Atom Materials

The method described in Chapter III for solving equation (2.16) must also be altered for use with composite materials. For single atom materials, the multigroup energy grid is set up so that $E_{i+1}=E_i/\alpha$ for $i=1,2,3,...,N-1$ where

Reproduced with permission of the copyright owner. Further reproduction prohibited without permission.

α is dependent on the atomic weight of the material. For multiple atom materials, on the other hand, each different atom has a different atomic weight and, therefore, a different α. However, one energy grid must still be chosen in order to solve equation (6.1). Using a smaller energy grid will lead to smaller errors (see Appendix B). For this reason, the α for the heaviest atom in the target material should be used to create the energy grid. Recall that

$$\alpha = \left(\frac{A_T - 1}{A_T + 1}\right)^2 \tag{2.17}$$

where A_T is the atomic weight. Taking the derivative of α with respect to atomic weight, A_T, produces the equation

$$\frac{d\alpha}{dA_T} = \frac{4(A_T - 1)}{(A_T + 1)^3} \geq 0. \tag{6.2}$$

Recall that $A_T \geq 1$. This shows that α is a non-decreasing function of A_T. Therefore, α is maximized when A_T is maximized.

For this reason, a first step to solving equation (6.1) must be to sort the atoms of the target material putting them in order from heaviest to lightest and numbering them so that α_1 is the α for the heaviest atom, α_2 corresponds to the next heaviest atom, and so on. The energy grid can then be set up so that $E_{i+1} = E_i/\alpha_1$ for $i = 1, 2, 3, ..., N - 1$.

Next, each term of equation (6.1) is integrated from E_i to E_{i+1} as described in Chapter III. In fact, the first, second, and last term of equation (6.1) are integrated in exactly the same way as Chapter III,

$$\int_{E_i}^{E_{i+1}} \frac{\partial}{\partial x}\phi(x, E)dE = \frac{\partial}{\partial x}\Phi_i(x), \tag{3.3}$$

Reproduced with permission of the copyright owner. Further reproduction prohibited without permission.

$$\int_{E_i}^{E_{i+1}} \sigma(E)\phi(x,E)dE = \sigma(E_i^*)\Phi_i(x), \tag{3.4}$$

and

$$b_i(x) = \int_{E_i}^{E_{i+1}} g(x,E)dE. \tag{3.2}$$

The third term, however, is different. First, put the third term in the form

$$\sum_{\beta} \int_{E}^{E/\alpha_\beta} f_\beta(E,E')\phi(x,E')dE' = \int_{E}^{E/\alpha_1} f_1(E,E')\phi(x,E')dE' + \sum_{\beta>1} \int_{E}^{E/\alpha_\beta} f_\beta(E,E')\phi(x,E')dE'. \tag{6.3}$$

Now, $\int_{E_i}^{E_{i+1}} \int_{E}^{E/\alpha_1} f_1(E,E')\phi(x,E')dE'dE$ can be rewritten in the form

$$\left[\int_{E_i}^{E_i^*} f(E,E_i^*)dE\right] \Phi_i(x) + \left[\int_{\alpha_1 E_i^*}^{E_{i+1}} f(E,E_i^*)dE\right] \Phi_{i+1}(x), \tag{3.8}$$

as described in Chapter III.

Next, $\int_{E_i}^{E_{i+1}} \int_{E}^{E/\alpha_\beta} f_\beta(E,E')\phi(x,E')dE'dE$ must be calculated for each $\beta >$ 1. Here, $E_{i+1} < E_i/\alpha_\beta$. This situation is described in Appendix B and the

Reproduced with permission of the copyright owner. Further reproduction prohibited without permission.

relationship

$$
\begin{aligned}
&\int_{E_i}^{E_{i+1}} \int_{E}^{E/\alpha_\beta} f_\beta(E,E')\phi(x,E')dE'dE \\
&\qquad = \left[\int_{E_i}^{E_i^{(1)}} f_\beta(E,E_i^{(1)})dE\right]\Phi_i(x) \\
&\qquad + \sum_{m=i+1}^{j-1}\left[\int_{E_i}^{E_{i+1}} f_\beta(E,E_m^{(1)})dE\right]\Phi_m(x) \\
&\qquad + \left\{\eta_1^*\left[\int_{E_i}^{E_{i+1}} f_\beta(E,E_j^{(2)})\phi(x,E')dE\right]\right. \\
&\qquad\quad \left. + \eta_2^*\left[\int_{\alpha E_j^{(3)}}^{E_{i+1}} f_\beta(E,E_j^{(3)})\phi(x,E')dE\right]\right\}\Phi_j(x) \\
&\qquad + \sum_{m=j+1}^{k-1}\left[\int_{\alpha E_m^{(1)}}^{E_{i+1}} f_\beta(E,E_m^{(1)})dE\right]\Phi_m(x) \\
&\qquad + \eta_3^*\left[\int_{\alpha E_j^{(4)}}^{E_{i+1}} f_\beta(E,E_j^{(4)})\phi(x,E')dE\right]\Phi_k(x) \qquad (6.4)
\end{aligned}
$$

is derived. Here, j is such that E_j is the largest point on the energy grid that is less than E_i/α_β, and k is such that E_k is the largest point on the energy grid that is less than E_{i+1}/α_β. See Appendix B for unknown variables. Note that equation (6.4) will be truncated so that the largest index n appearing on the integral fluence, $\Phi_n(x)$ will be N, because the fluence $\phi(x,E)$ is assumed to be zero for energies larger than E_N.

Also, note that the hydrogen atom is a special case. The atomic weight of hydrogen is 1. This means that α for hydrogen is zero and E/α is infinite.

Reproduced with permission of the copyright owner. Further reproduction prohibited without permission.

Therefore, for hydrogen

$$\int_{E_i}^{E_{i+1}} \int_{E}^{\infty} f_H(E,E')\phi(x,E')dE'dE$$
$$= \left[\int_{E_i}^{E_i^{(1)}} f_H(E,E_i^{(1)})dE\right]\Phi_i(x)$$
$$+ \sum_{m=i+1}^{N}\left[\int_{E_i}^{E_{i+1}} f_H(E,E_m^{(1)})dE\right]\Phi_m(x). \tag{6.5}$$

.

Next, let,

$$a_{i,i} = \sum_{\beta}\int_{E_i}^{E_i^*} f_\beta(E,E_i^*)dE - \sigma(E_i^*) \tag{6.6}$$

and

$$a_{i,i+1} = \int_{\alpha_1 E_i^*}^{E_{i+1}} f_1(E,E_i^*)dE + \sum_{\beta>1}\int_{E_i}^{E_{i+1}} f_\beta(E,E_m^{(1)})dE \tag{6.7}$$

and

$$a_{i,i+n} = \sum_{\beta>1} C_{\beta,i+n} \tag{6.8}$$

for $n = 2,3,4,...,N-i$ where $C_{\beta,i+n}$ is the coefficient of $\Phi_{i+n}(x)$ given by equation (6.4) or equation (6.5). As in Chapter III, the low energy neutron transport equation, then, becomes sequence of N differential equations. However, for multiple atom materials the *ith* equation is given by

$$\frac{d\Phi_i(x)}{dx} = \sum_{n=i}^{N} a_{i,n}\Phi_n(x) + b_i(x) \tag{6.9}$$

for $i = 1,2,3,...,N$. In matrix form this equation is written

$$\frac{d\vec{y}}{dx} = A\vec{y} + \vec{b} \tag{3.13}$$

Reproduced with permission of the copyright owner. Further reproduction prohibited without permission.

where now A has the upper triangular form

$$A = \begin{bmatrix} a_{1,1} & a_{1,2} & a_{1,3} & a_{1,4} & a_{1,5} & \cdots & a_{1,N} \\ & a_{2,2} & a_{2,3} & a_{2,4} & a_{2,5} & & \\ & & a_{3,3} & a_{3,4} & a_{3,5} & & \vdots \\ & & & \ddots & \ddots & & \\ & & & & & a_{N-2,N-2} & a_{N-2,N-1} & a_{N-2,N} \\ & & & & & & a_{N-1,N-1} & a_{N-1,N} \\ & & & & & & & a_{N,N} \end{bmatrix} \tag{6.10}$$

These N equations can be solved by starting at the highest energy, E_N, and solving the Nth equation first. Then, $\Phi_N(x)$ can be used to calculate $\Phi_{N-1}(x)$ and $\Phi_N(x)$ and $\Phi_{N-1}(x)$ can be used to calculate $\Phi_{N-2}(x)$ and so on. In a manner similar to Chapter III, the following equation for $\Phi_i(x)$ can be derived.

$$\begin{aligned} \Phi_i(j \cdot \Delta x) = e^{a_{i,i}\Delta x}\Big[\Phi_i((j-1)\cdot\Delta x) \\ + \frac{1}{2}\Delta x \sum_{n=1}^{N-1-i} a_{i,i+n}\Phi_{i+n}((j-1)\cdot\Delta x) + \frac{1}{2}\Delta x b_i((j-1)\cdot\Delta x)\Big] \\ + \frac{1}{2}\Delta x \sum_{n=1}^{N-1-i} a_{i,i+n}\Phi_{i+n}(j\cdot\Delta x) + \frac{1}{2}\Delta x b_i(j\cdot\Delta x) \end{aligned} \tag{6.11}$$

for $i = 1, 2, 3, ..., N-1$ and $j = 1, 2, 3, ..., M$.

Neutron Fluences in Multiple Atom Materials

In order to actually calculate the low energy neutron fluence in a multiple atom target material, the equations derived in the previous section were added to the HZETRN program. First, a subroutine called SORT was created to sort the atoms in terms of atomic weight. A call to this subroutine was added to the beginning of the NPRP subroutine. Next, subroutine AMATRX was altered to calculate $a_{i,j}$ for $i = 1, 2, 3, ..., N$ and $j = i, i+1, i+2, ..., N$ using equations (6.6), (6.7), and (6.8). Then, the NPRP subroutine was altered to calculate the integral fluence, $\Phi_i(x)$ or $YBAR(i,k,l)$, using equation (6.11).

Reproduced with permission of the copyright owner. Further reproduction prohibited without permission.

Once the program was altered, the HZETRN program was run for a target of water, H_2O. Note that this is an important target because human tissue is mostly water and often modeled as water. Once again, the February 1956 SPE was used.

The total neutron fluence, evaporation neutrons and direct cascade neutrons, is plotted against energy in Figures $12-14$ for depths of 1 gm/cm^2, 10 gm/cm^2, and 30 gm/cm^2, respectively. These fluences are plotted with neutron fluences produced by the LAHET Monte Carlo code[26] . The neutron fluences calculated by the original HZETRN program are also plotted.

Reproduced with permission of the copyright owner. Further reproduction prohibited without permission.

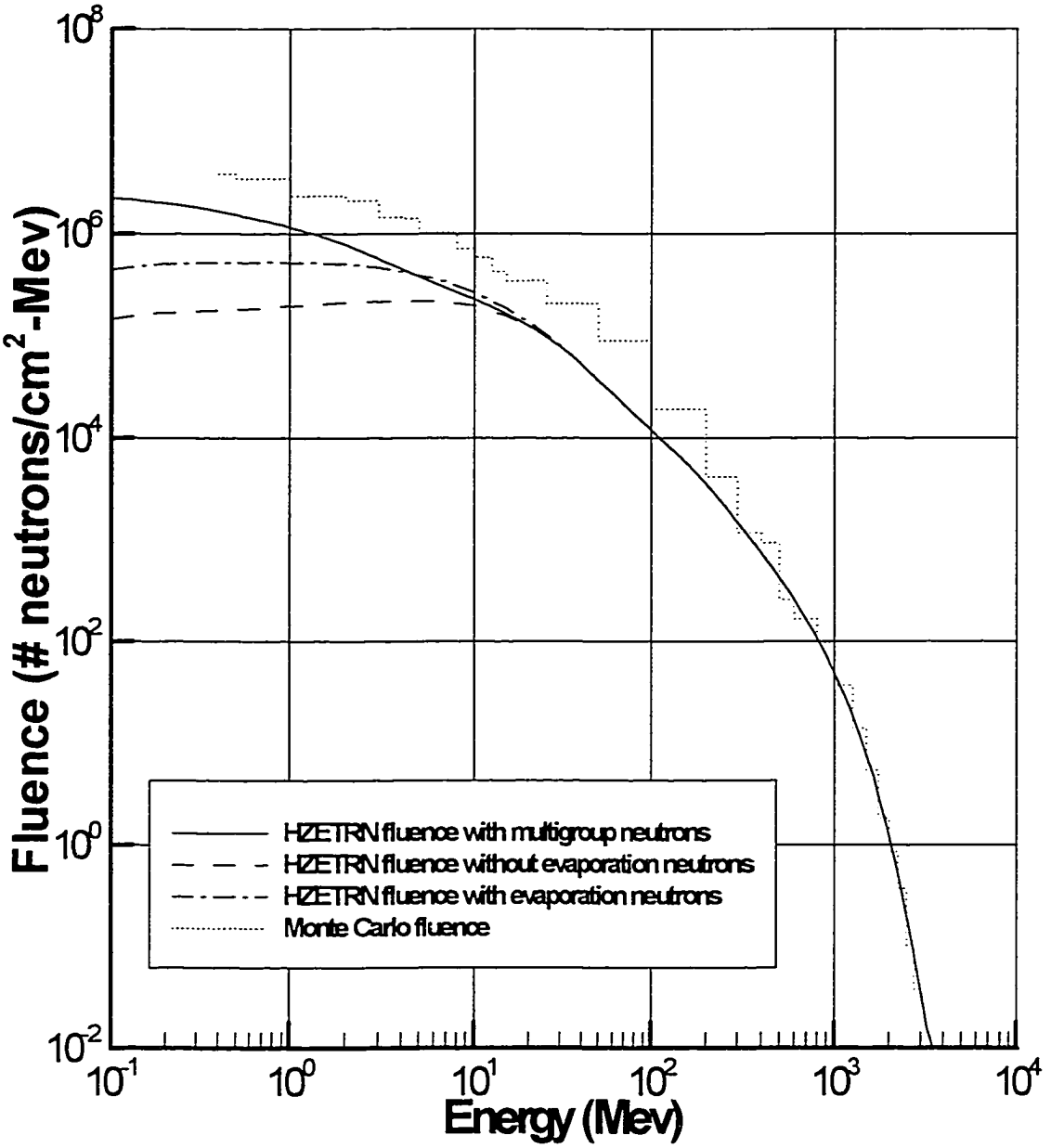

Fig. 12. Energy spectra of neutron fluence at 1 gm/cm^2 depth in water exposed to the February 23, 1956 solar energetic particle event.

Reproduced with permission of the copyright owner. Further reproduction prohibited without permission.

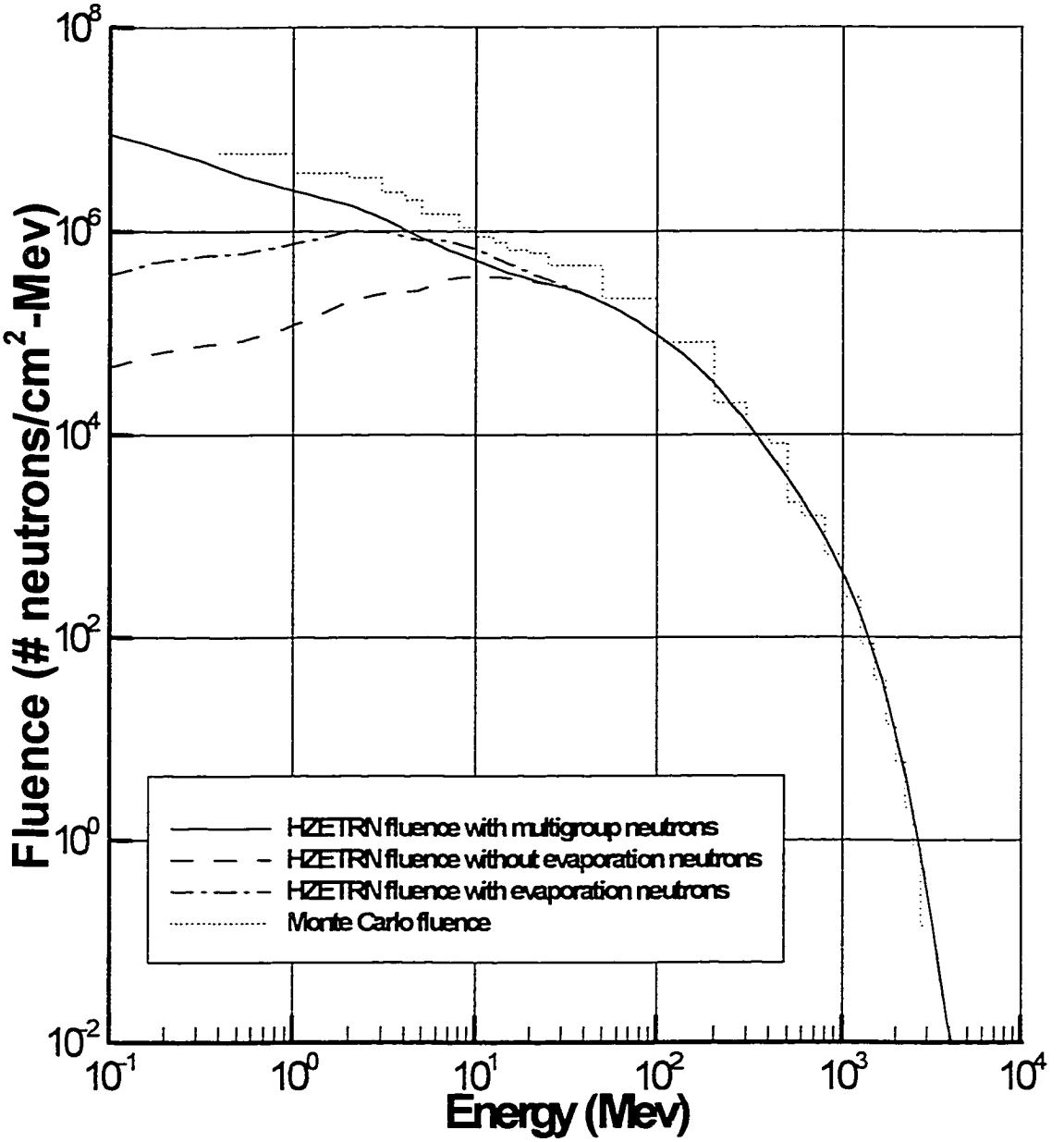

Fig. 13. Energy spectra of neutron fluence at 10 gm/cm^2 depth in water exposed to the February 23, 1956 solar energetic particle event.

Reproduced with permission of the copyright owner. Further reproduction prohibited without permission.

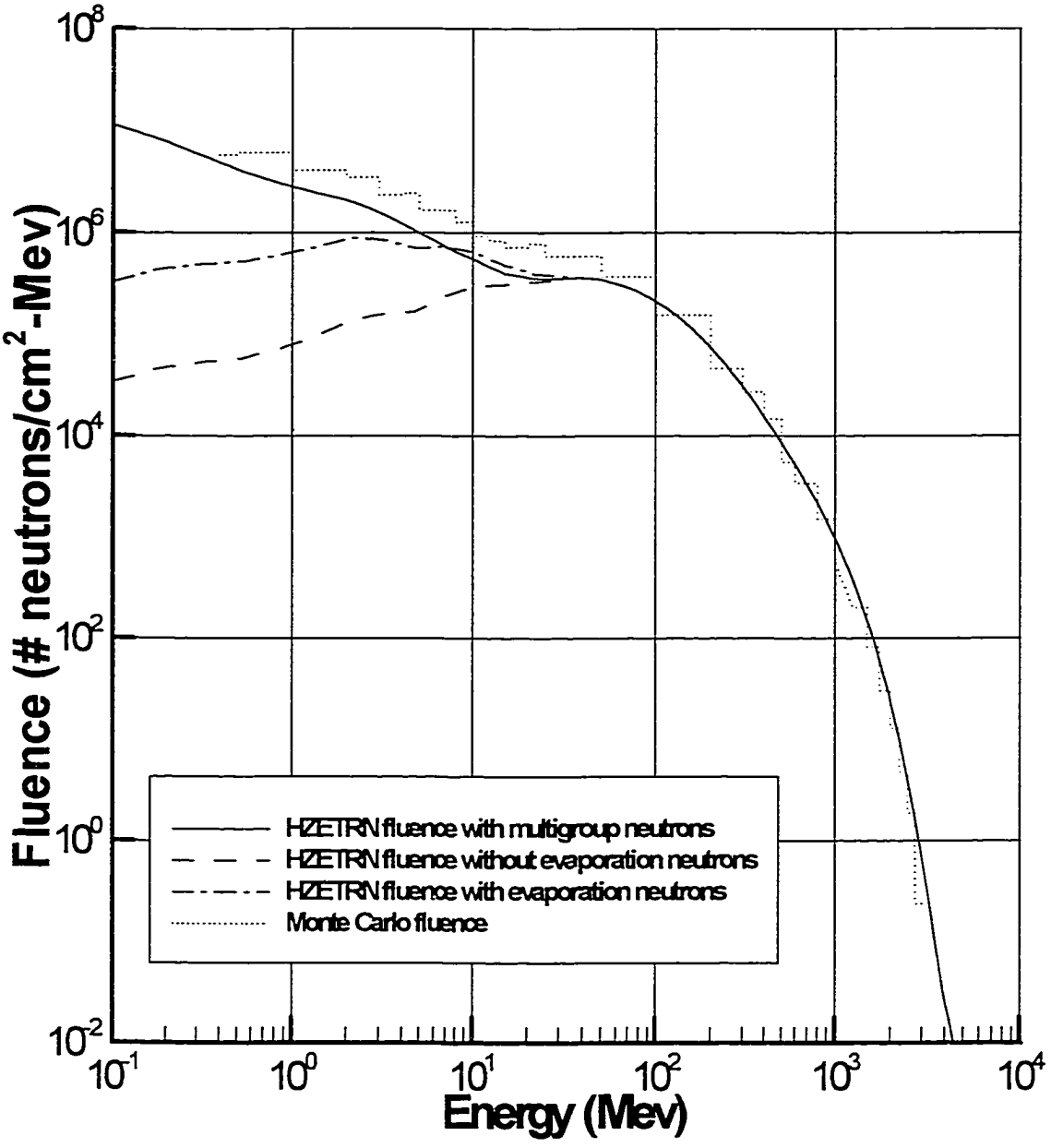

Fig. 14. Energy spectra of neutron fluence at 30 gm/cm^2 depth in water exposed to the February 23, 1956 solar energetic particle event.

These plots show that the low energy neutron fluences produced by the HZETRN program with the NPRP multigroup subroutine are much closer to those predicted by the Monte Carlo method. This is especially true at the deeper

Reproduced with permission of the copyright owner. Further reproduction prohibited without permission.

depths of penetration. This comparison confirms that the multigroup method is an improved predictor of the scattering of evaporation neutrons.

Figures 12 – 14 also show that while the results produced by the HZETRN program with the NPRP subroutine are close to those produced by the Monte Carlo method, much closer than those produced by the old HZETRN method, these fluences are still too low. Several hypotheses can be made as to the reason for this. First, there is some error in the perturbation methods used by the HZETRN program to produce the source terms needed for the multigroup method. Figures 12 – 14, however, show a good agreement between HZETRN and the Monte Carlo method at larger energies, so these errors must be assumed to be small. There are also some errors produced in the multigroup method when numerical integrations are performed, but the test problem in Chapter IV showed that these errors are small.

The nuclear cross sections used are believed to be a larger source of error. First, only the elastic cross sections were used in the multigroup subroutine. The elastic cross sections are much larger than the non-elastic cross sections at low energies. Non-elastic cascading does occur, however, and the multigroup method would be more accurate if both types of cross section were used.

Also, the nuclear cross sections used by the HZETRN program are interpolated from a large data base that was developed experimentally. Researchers at NASA Langley Research Center have some questions about its accuracy and are currently planning to update it.

Reproduced with permission of the copyright owner. Further reproduction prohibited without permission.

Transport in Two Directions

Another observation can be made from Figures 12 – 14. That is that the HZETRN program with the NPRP subroutine appears to be more accurate at larger depths. This is counterintuitive since any error produced by the numerical integration would build up as the program marches through the depths.

The fact that the multigroup method is less accurate for smaller depths is a result of the straight ahead approximation made to the Boltzmann transport equation when the method was derived. It was assumed that all secondaries produced by nuclear collisions would move in the same direction as the primary ion, proton, or neutron that caused the collision. For secondaries that are charged particles or high energy neutrons, this is an accurate assumption, most secondary particles do move in the same direction as the primaries. Low energy neutrons produced by evaporation, however, move in all directions. These neutrons make up the source term used in the multigroup method. Therefore, the multigroup method fails to account for the "leakage" at the boundary of low energy neutrons that have been transported back from deeper depths in the slab.

For this reason, a more accurate method would solve the full neutron transport equation, not the one dimensional equation produced when the straight ahead approximation is used. Solving the full neutron transport equation would, however, be inefficient in terms of computer time and incompatible with the HZETRN program. Therefore, this was not attempted. Instead, the one dimensional multigroup method was improved by making the assumption that half the source neutrons move in the forward direction and half the source neutrons move

Reproduced with permission of the copyright owner. Further reproduction prohibited without permission.

in the backward direction. Such an approximation is known to be consistent with diffusion theory.

The NPRP subroutine was altered so that the low energy neutron fluences $\phi_f(x, E)$ were calculated for all energies and all depths in the way described in Chapter V except that only half the source term was used. The process was then repeated using the other half of the source terms except this time instead of marching forward through the depths of the material, the program started at the largest depth and marched backward through the depths. The fluences produced by this backward propagation $\phi_b(x, E)$ were then added to the fluences from the forward propagation,

$$\phi(x, E) = \phi_f(x, E) + \phi_b(x_{max} - x, E). \tag{6.12}$$

In order to model an infinite slab, a large depth must be chosen. A depth of 100 gm/cm^2 was used for aluminum and water.

Some thought was given to how the initial fluence $\phi_b(0, E)$ should be calculated for the backward propagation. As already stated, for a single slab exposed to space radiation, $\phi_f(0, E) = 0$ for forward propagation. If an infinite slab is being modeled and the maximum depth is large enough, then $\phi_0(0, E) = 0$ is an accurate approximation. Another possibility is to use a mirror boundary condition where $\phi_b(0, E) = \phi_f(x_{max}, E)$. This models a slab with a second identical slab placed concurrently at its maximum depth. Both slabs are exposed to the same radiation field.

This new two direction multigroup method was applied to the 100 gm/cm^2

Reproduced with permission of the copyright owner. Further reproduction prohibited without permission.

slab of water. Both values of $\phi_b(0, E)$ were attempted and there was only a very small difference in the total neutron fluences produced with the two different boundary conditions. Figures $15 - 17$ show the total neutron fluences produced when this new two direction multigroup method is used for depths of 1 gm/cm^2, 10 gm/cm^2, and 30 gm/cm^2.

Reproduced with permission of the copyright owner. Further reproduction prohibited without permission.

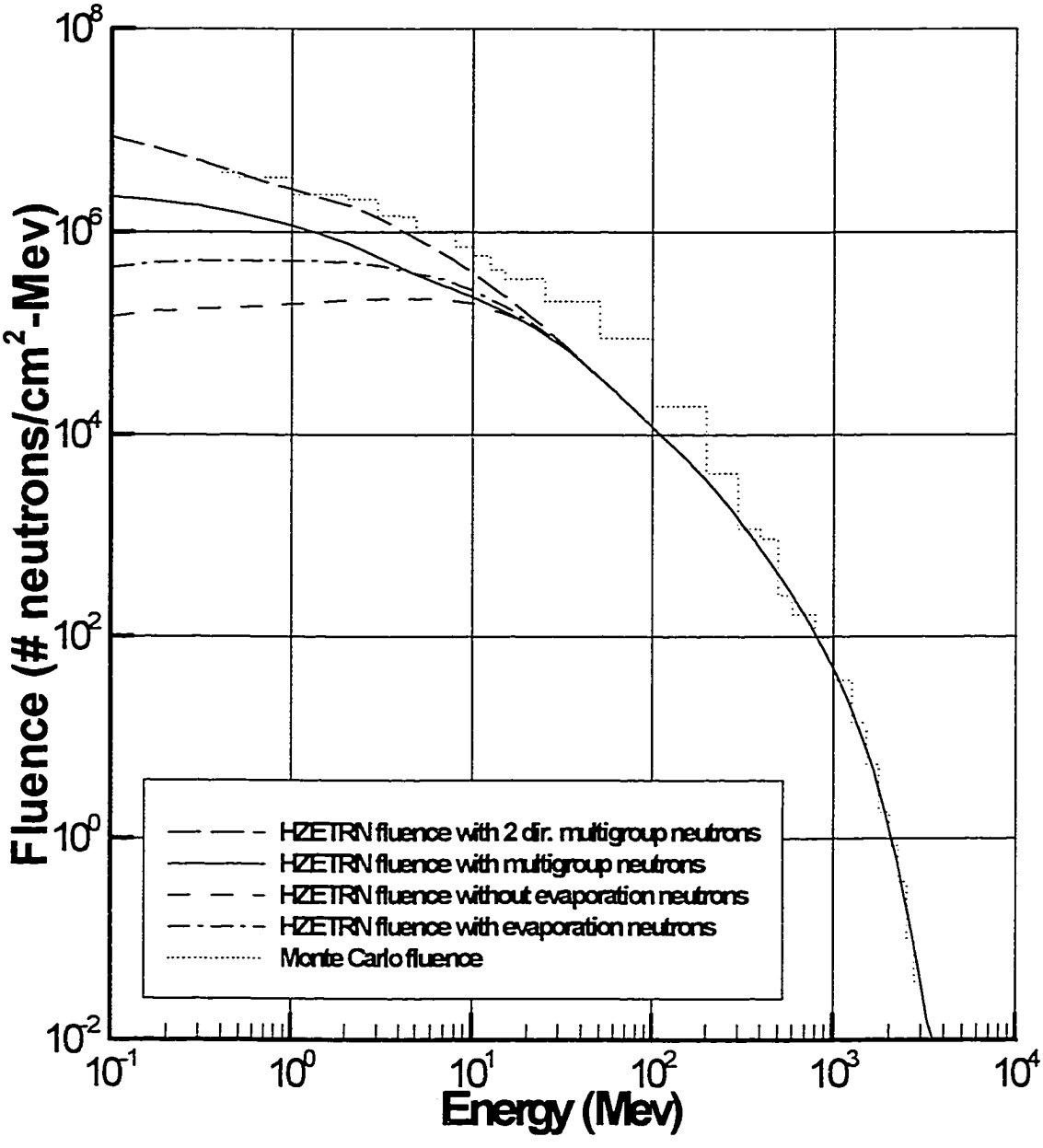

Fig. 15. Energy spectra of neutron fluence at 1 gm/cm^2 depth in water exposed to the February 23, 1956 solar energetic particle event calculated with the two direction multigroup method.

Reproduced with permission of the copyright owner. Further reproduction prohibited without permission.

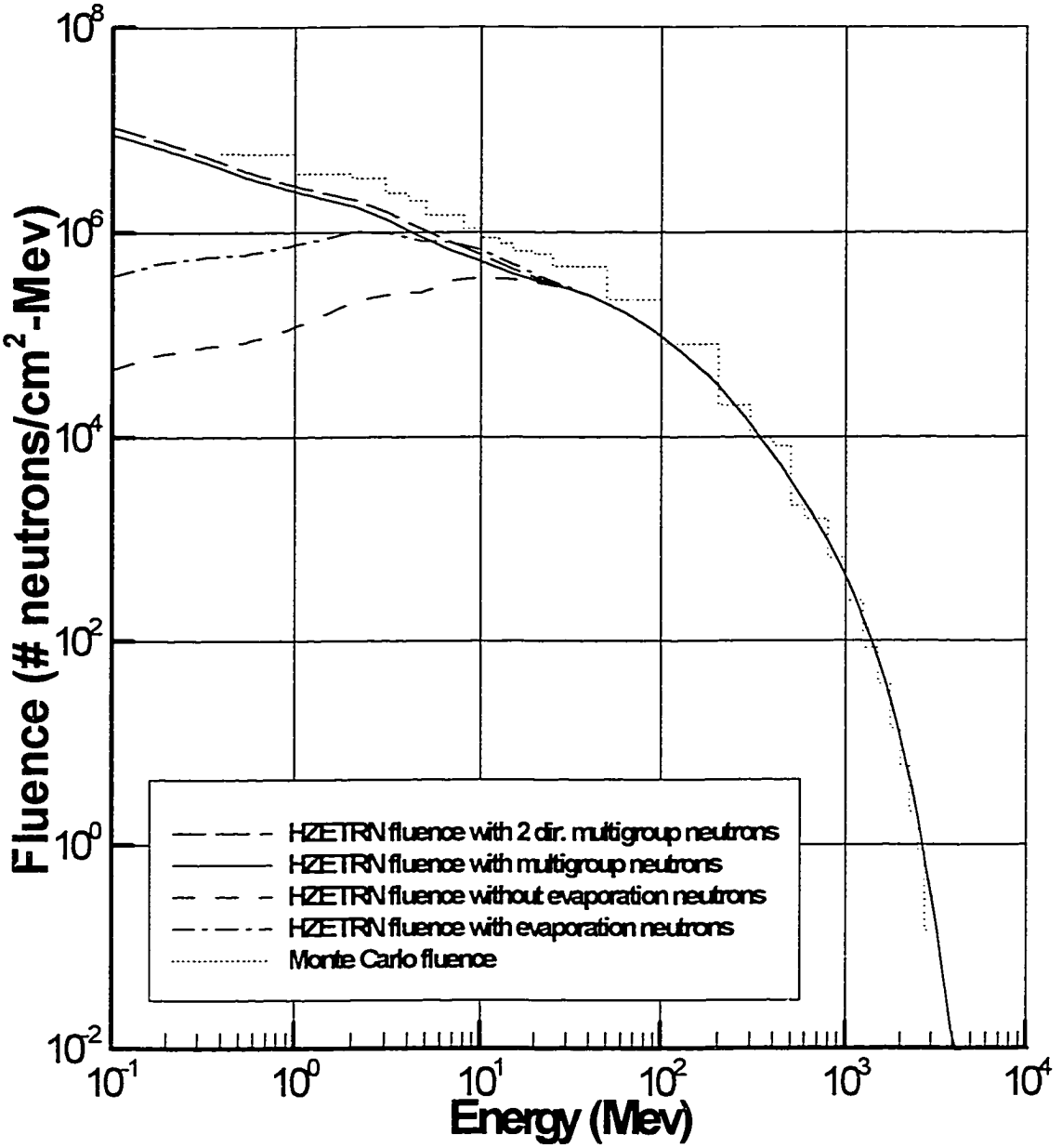

Fig. 16. Energy spectra of neutron fluence at 10 gm/cm^2 depth in water exposed to the February 23, 1956 solar energetic particle event calculated with the two direction multigroup method.

Reproduced with permission of the copyright owner. Further reproduction prohibited without permission.

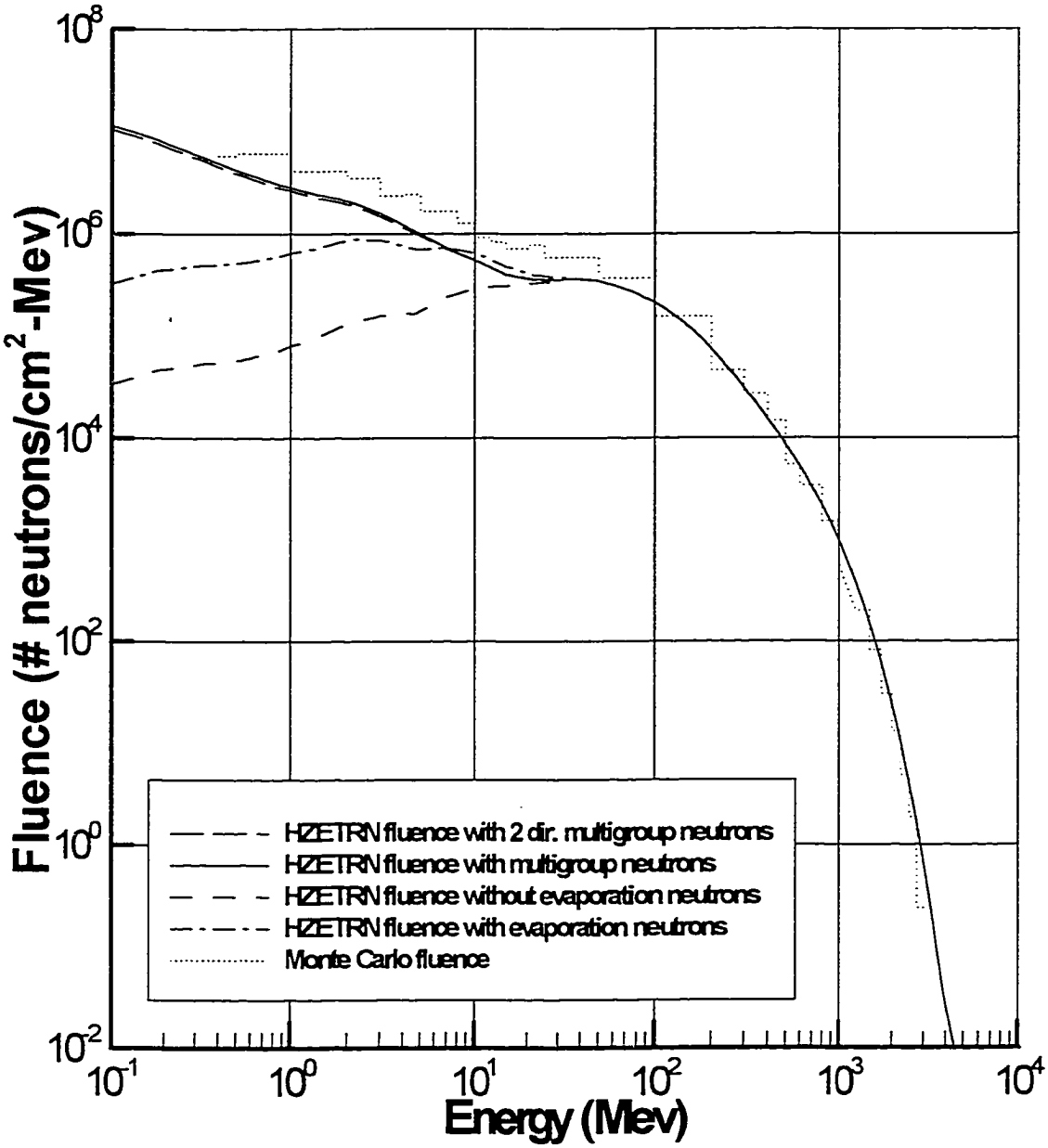

Fig. 17. Energy spectra of neutron fluence at 30 gm/cm^2 depth in water exposed to the February 23, 1956 solar energetic particle event calculated with the two direction multigroup method.

Figure 15 shows that the new two direction multigroup method greatly improves the low energy neutron fluence predictions at small depths. Figures 16

Reproduced with permission of the copyright owner. Further reproduction prohibited without permission.

and 17 show that switching to this new subroutine has a much smaller effect on the low energy neutron calculations at larger depths. This is because the build up of high energy neutrons reaches a maximum at some depth past which it declines. Since the low energy neutrons are in near equilibrium with their source, they maximize near the source maximum without regard to direction.

Neutron Transport in Two Materials

As previously stated in Chapter V, the HZETRN program is set up to calculate radiation transport through two materials, the first called the shield and the second referred to as the target. The HZETRN program calculates the radiation fluence at a number of depths in the shield. These depths are input at the beginning of the program and are stored in the $x(k)$ array. Then, for each of these shield depths, the HZETRN program calculates the radiation fluence at a number of target depths which were also input at the beginning of the program. The target depths are stored in the $y(l)$ array. The fluences are stored in the $ff(i,j,k,l)$ array, where $ff(i,j,k,l)$ is the fluence of type j particles with energy $etf(i)$ at shield depth $x(k)$ and target depth $y(l)$. Note that the $f(i,j,k,l)$ array is used instead of the $ff(i,j,k,l)$ array if galactic cosmic ray radiation is being transported instead of solar flare radiation. The program uses these fluences to make dose calculations.

For example, in order to calculate the radiation dose absorbed by an astronaut's liver, a ray tracing method uses 512 different evenly spaced rays, each of them pointing toward the center of the astronaut's liver. Each of these rays is considered a path along which particles can travel to the astronaut's liver. The

Reproduced with permission of the copyright owner. Further reproduction prohibited without permission.

amount of shield each ray passes through can be evaluated. The amount of human tissue each ray passes through to get to the liver can also be evaluated. Recall that human tissue is modeled as water. The HZETRN program calculates the particle fluence at each of the 512 needed (shield depth, target depth) pairs. It does this by interpolating over the fluences, $ff(i,j,k,l)$, that it has already calculated at the at shield and target depths given at the beginning of the program. The total number of each type of particle absorbed by the astronauts liver as a function of energy can then be calculated by integrating over these 512 fluences coming from different directions.

In order to be compatible with the main HZETRN program, the NPRP subroutine must also calculate fluences at the shield and target depths given at the beginning of the main program. It is easy to set up the older one direction NPRP subroutine to work this way. First, the HZETRN program is changed so that it calls the NPRP subroutine twice, once after the source terms for the shield are calculated and again after the source terms for all of the shield/target combinations are calculated. An integer variable called $NLAY$ tells the subroutine which layer to propagate through, $NLAY = 1$ for the shield and $NLAY = 2$ for the target. If $NLAY = 1$, the NPRP subroutine calculates the low energy neutron fluence for each of the shield depths $x(k)$ for $k = 1, 2, 3, ..., 10$ in exactly the way described in Chapter V. If $NLAY = 2$, the steps described in Chapter V are repeated ten times, once for each shield depth. This means that the NPRP subroutine starts with the first shield depth, usually set to be zero, and calculates the neutron fluence at each target depth in the way described in Chapter V. Then it

Reproduced with permission of the copyright owner. Further reproduction prohibited without permission.

starts over with the second shield depth and again calculates the fluence at each target depth. This process is repeated until the neutron fluence is calculated for every target depth for the largest shield depth. There is, however, one major difference in the way neutron fluences are calculated for the target. When the neutron fluences are calculated in the shield the initial condition is assumed to be zero, $\phi(0, E) = 0$. When calculating neutron fluences in the target, on the other hand, the initial fluence is equivalent to the fluence at the shield depth which was calculated the first time the NPRP subroutine was called. Note that this fluence must be interpolated to the new energy grid because the multigroup energy grid is dependent on the material. Once again, linear interpolation is used.

Setting up the two direction version of NPRP to work for a shield/target combination is more difficult. This subroutine cannot be set up to calculate fluences at all shield depth/target depth combinations. Instead, the user must choose one maximum shield depth $xmax$ and one maximum target depth $ymax$. Then the subroutine can be used to calculate the energy spectrum of the low energy neutron fluence at any depth in the shield or any depth in the target with a shield of $xmax$ gm/cm^2 in front of it. The program will propagate half the source neutrons through the shield material to the maximum shield depth and through the target material to the maximum target depth. It will then propagate the other half of the source term back through the target and back through the shield. In this case, when the NPRP subroutine is called the first time, after the source terms for the shield have been calculated, the neutron fluences for the forward propagation of half of the source term through the shield are calculated

Reproduced with permission of the copyright owner. Further reproduction prohibited without permission.

and stored in a common block. The atomic weights and atomic charges and the density for the shield are renamed and also stored in a common block along with the energy grid for the shield. All of these variables will be reassigned for the target material. The second time subroutine NPRP is called, the neutron fluences for the forward propagation of half of the source term through the target are calculated. Then, the neutron fluences for the backward propagation of the other half of the source term back through the target are calculated. Then, the energy grid is reset to the energy grid for the shield material and the neutron fluences for the backward propagation of the second half of the source term through the shield are calculated. Lastly, the forward propagation fluences and the backward propagation fluences are added together.

Both the one direction version of the code and the two direction version of the code were run for a shield of 100 gm/cm^2 and a target of 100 gm/cm^2 exposed to the solar flare environment of February 23, 1956. As a final check of the multigroup method, the results were compared to neutron fluences calculated with MCNPX Monte Carlo code[32]. These Monte Carlo fluences were prepared by Dr. Robert Singleterry at NASA Langley Research Center. The neutron fluences produced are graphed in Figures $18 - 23$.

Reproduced with permission of the copyright owner. Further reproduction prohibited without permission.

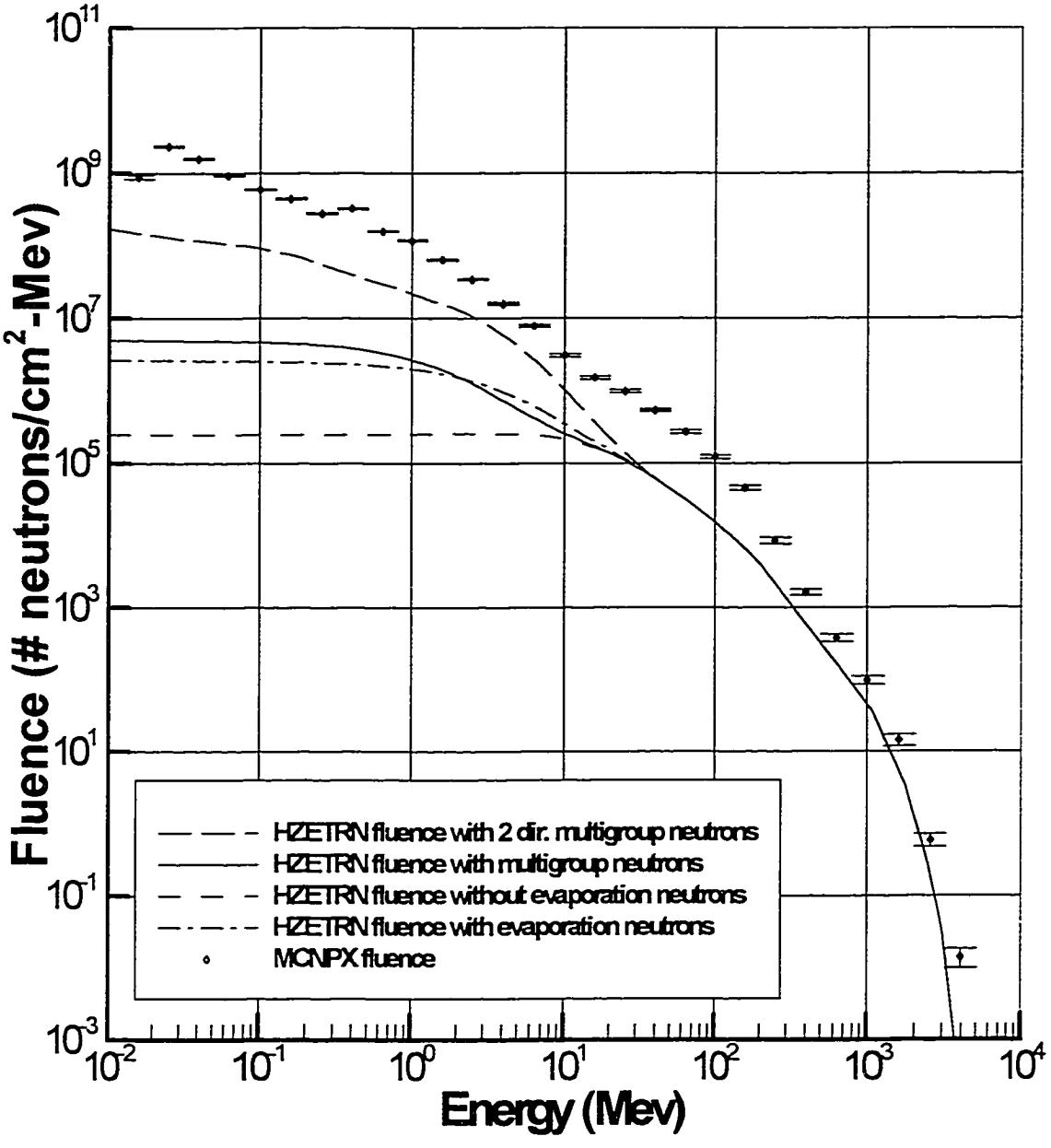

Fig. 18. Energy spectra of neutron fluence at 1 gm/cm^2 depth in the shield of a 100 gm/cm^2 aluminum shield with a target of 100 gm/cm^2 of water behind it.

Reproduced with permission of the copyright owner. Further reproduction prohibited without permission.

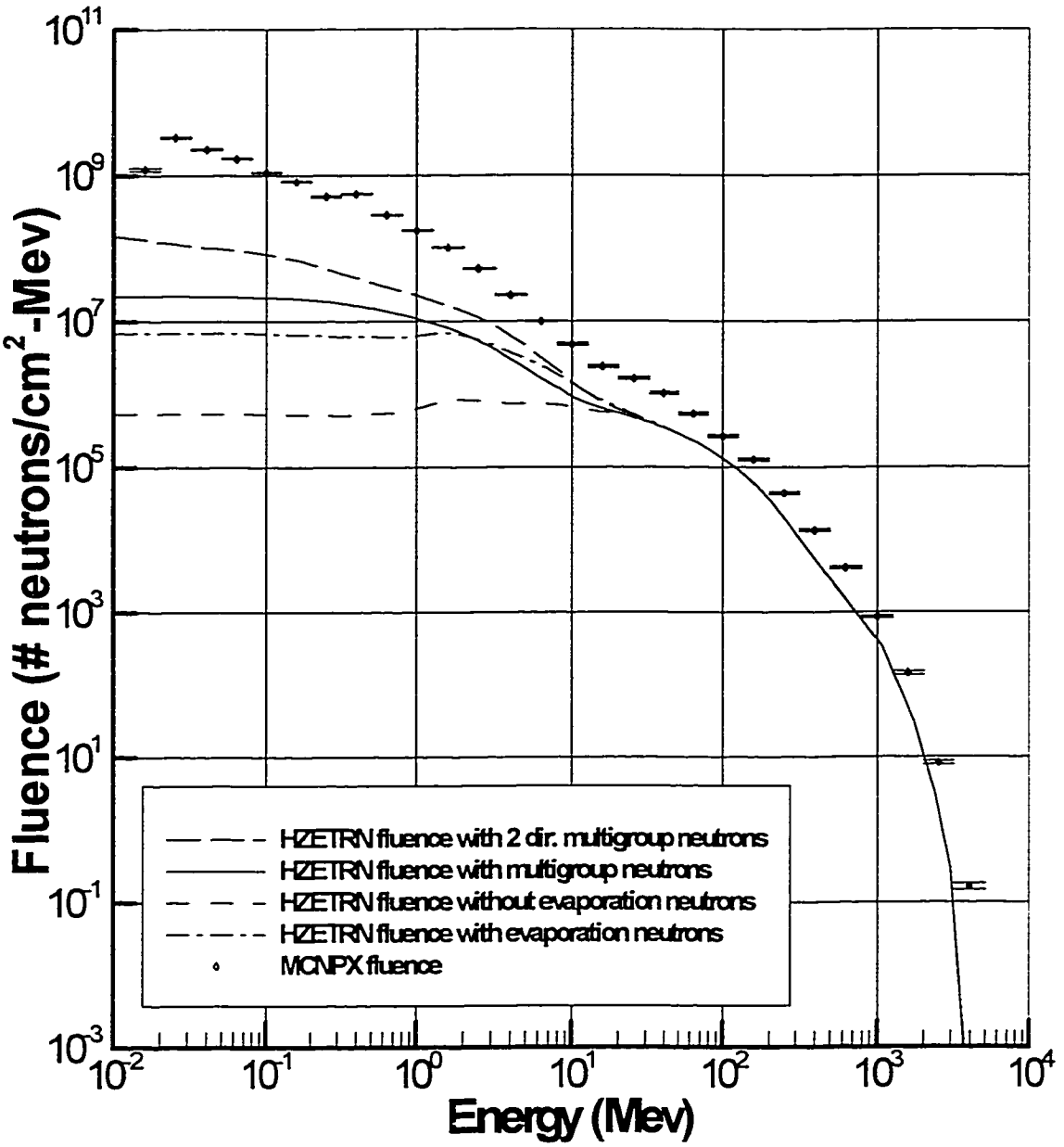

Fig. 19. Energy spectra of neutron fluence at 10 gm/cm^2 depth in the shield of a 100 gm/cm^2 aluminum shield with a target of 100 gm/cm^2 of water behind it.

Reproduced with permission of the copyright owner. Further reproduction prohibited without permission.

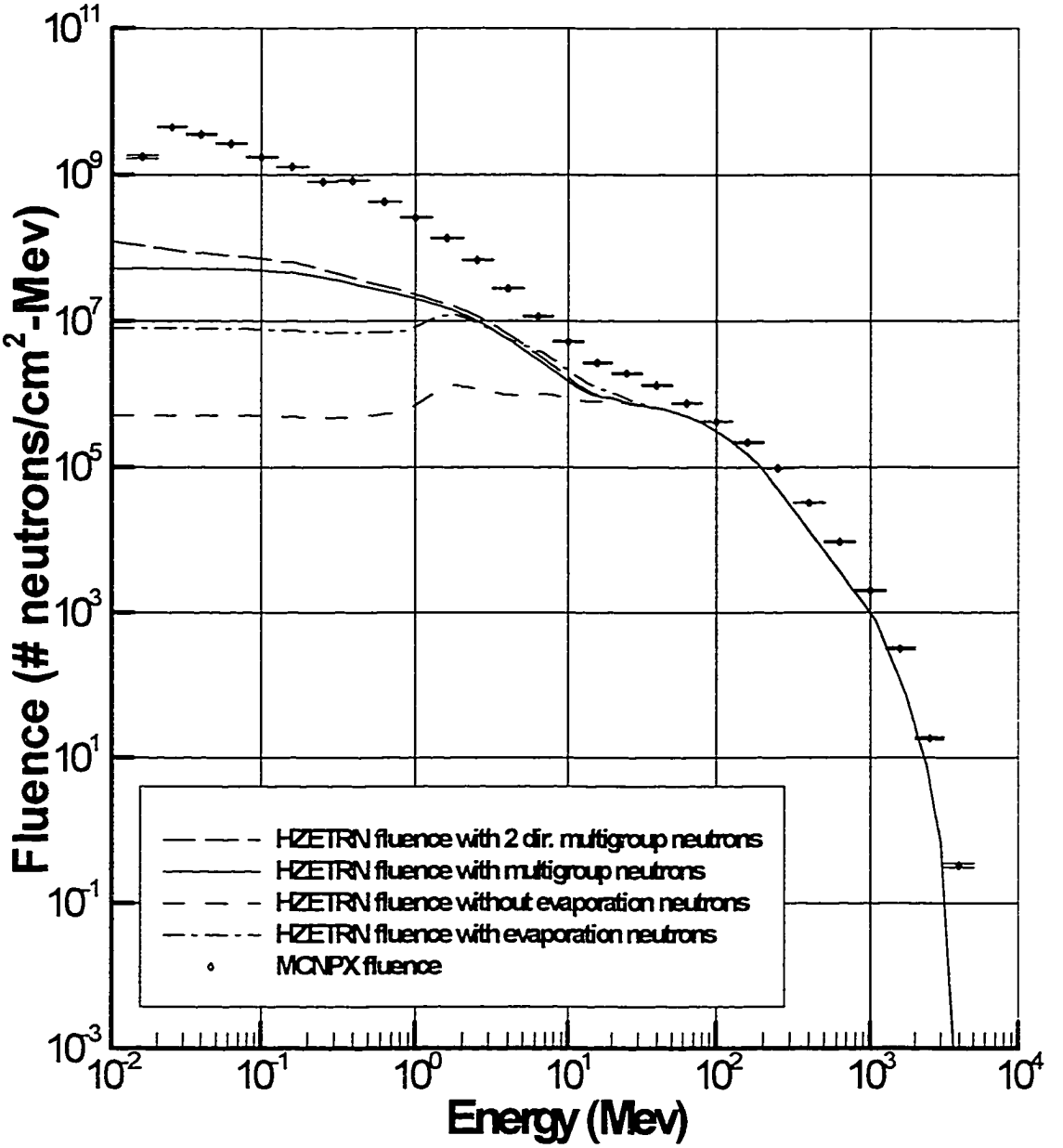

Fig. 20. Energy spectra of neutron fluence at 30 gm/cm^2 depth in the shield of a 100 gm/cm^2 aluminum shield with a target of 100 gm/cm^2 of water behind it.

Reproduced with permission of the copyright owner. Further reproduction prohibited without permission.

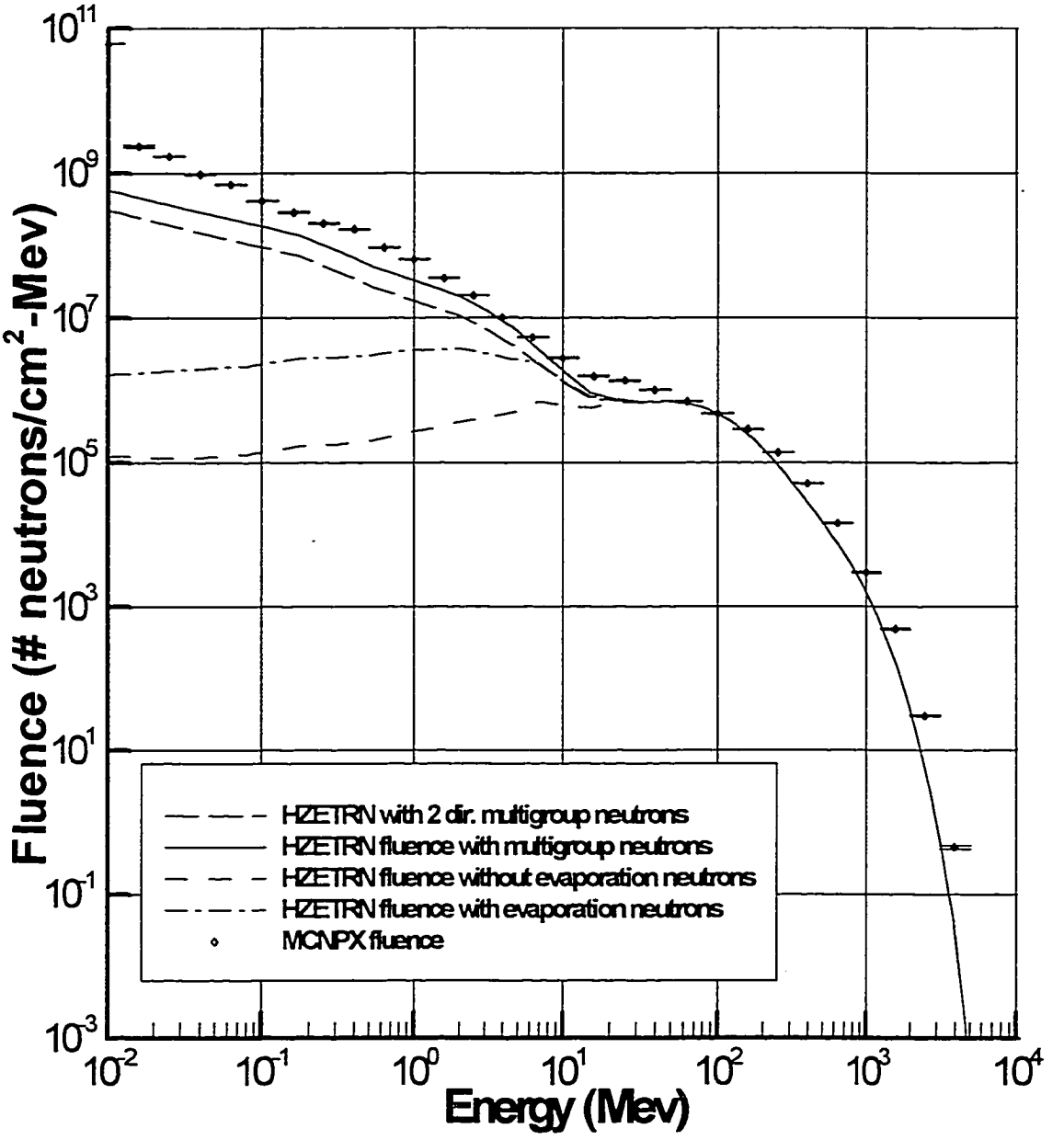

Fig. 21. Energy spectra of neutron fluence at 1 gm/cm^2 depth in the target of a 100 gm/cm^2 aluminum shield with a target of 100 gm/cm^2 of water behind it.

Reproduced with permission of the copyright owner. Further reproduction prohibited without permission.

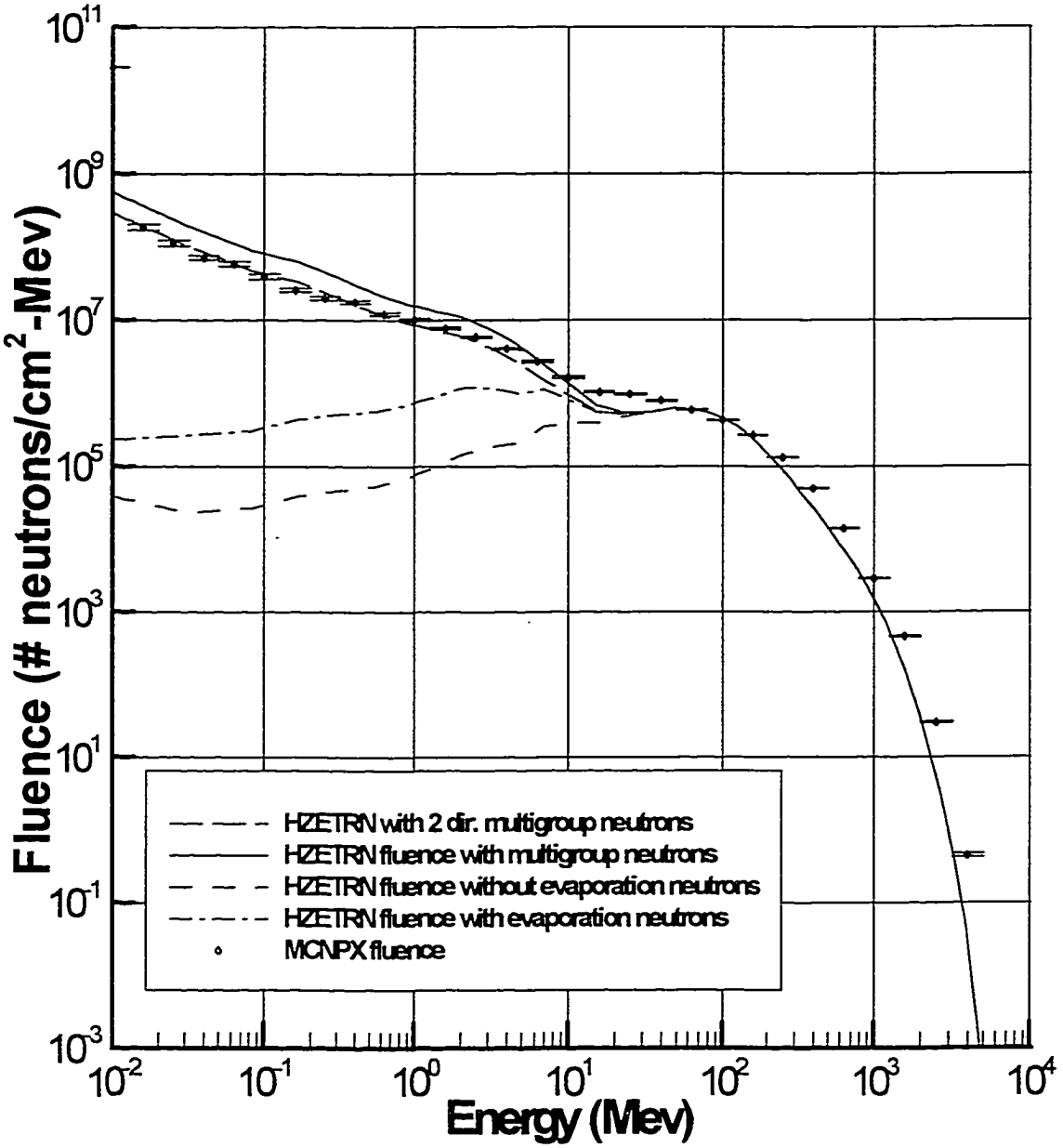

Fig. 22. Energy spectra of neutron fluence at 10 gm/cm^2 depth in the target of a 100 gm/cm^2 aluminum shield with a target of 100 gm/cm^2 of water behind it.

Reproduced with permission of the copyright owner. Further reproduction prohibited without permission.

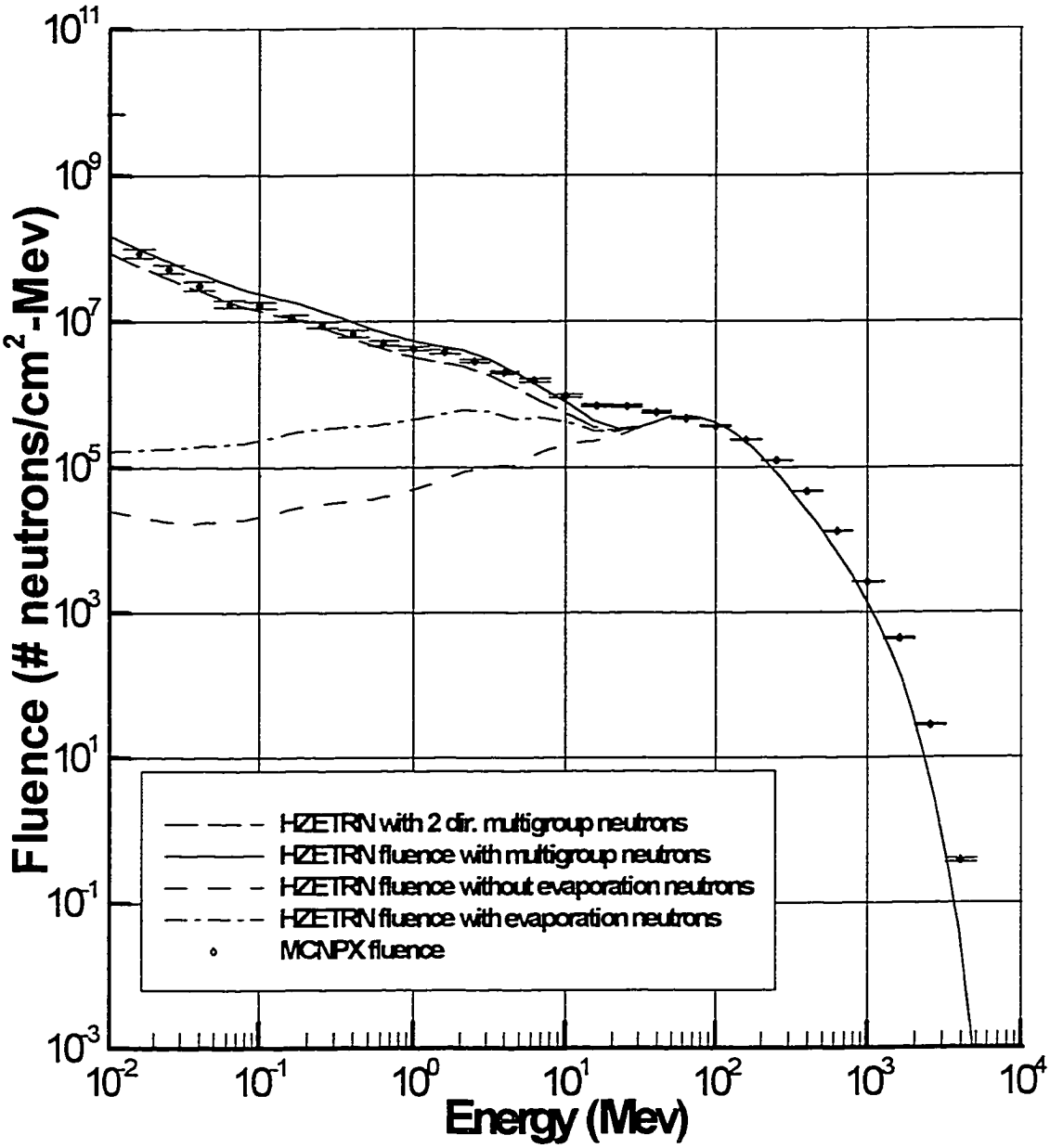

Fig. 23. Energy spectra of neutron fluence at 30 gm/cm^2 depth in the target a 100 gm/cm^2 of aluminum shield with a target of 100 gm/cm^2 of water behind it.

Reproduced with permission of the copyright owner. Further reproduction prohibited without permission.

Figures 18 – 23 show that the two direction multigroup method accurately approximates the transport of evaporation neutrons. The neutron fluences produced by this method are close to those produced by the Monte Carlo method. These figures also show that the one direction multigroup method accurately approximates the low energy neutron fluence for large depths but underestimates the fluence at small depths. The fluences predicted by the one direction multigroup method at small depths are, however, better than those predicted by the old HZETRN method.

The HZETRN program with the two direction NPRP subroutine was also used to calculate the energy spectrum of the neutron fluence in a $25 g/cm^2$ shield of CO_2 with a $100 g/cm^2$ target of regolith[33]. The environment of the February 23, 1956 solar particle event was used for this run. The energy spectrum of the neutron fluence at the boundary between the shield and the target is shown in Figure 24. These shield and target materials were chosen because the atmosphere on mars is mostly CO_2 and the ground is mostly regolith. The energy spectrum of the neutron fluence shown in Figure 24, then, is a good estimate for the energy spectrum of the neutron fluence on the ground on Mars if another large solar flare occurred. With a robotic mission to Mars planned for 2003, this information could be valuable in estimating the radiation environment on the Martian surface.

Figure 24 shows that the fluence calculated using the 2 direction multigroup method is about twice as large as the fluence calculated using the 1 direction multigroup method at low energies. The 1 direction method only calculates those neutrons transported to the surface from higher altitudes. The 2 direction

Reproduced with permission of the copyright owner. Further reproduction prohibited without permission.

method, on the other hand, also includes neutrons created in the Martian ground and transported upward. This demonstrates the importance of the 2 direction method.

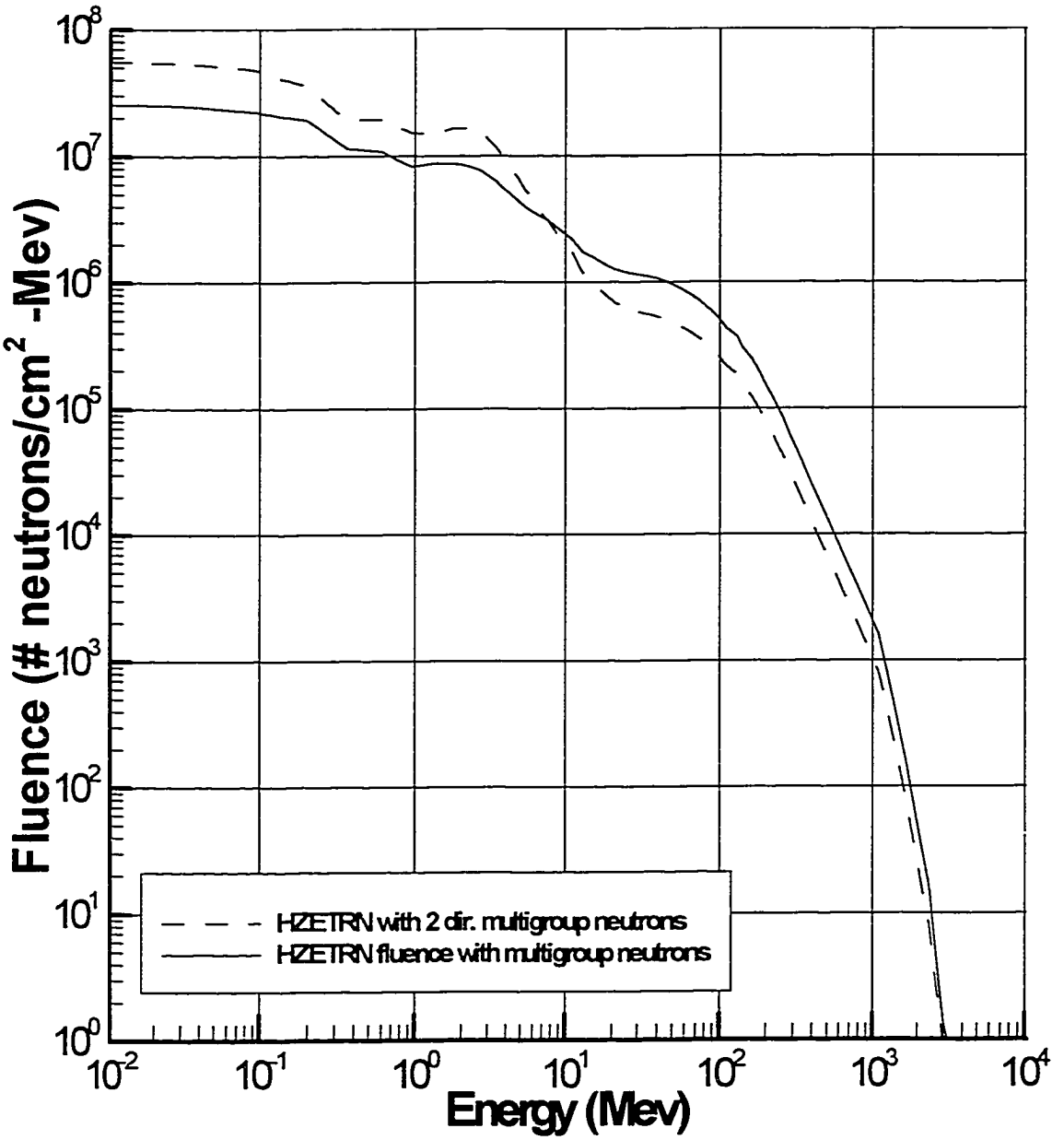

Fig. 24. Energy spectrum of neutron fluence at 25 gm/cm^2 depth in CO_2 with 100 gm/cm^2 of regolith behind it

Reproduced with permission of the copyright owner. Further reproduction prohibited without permission.

CHAPTER VII

RESULTS AND CONCLUSIONS

A one dimensional integro-differential equation was derived to model the elastic scattering of low energy neutrons in a target material. This transport equation utilized the assumption that all scattered neutrons move in the same direction as the primary neutrons. Evaporation neutrons produced when charged particles or higher energy neutrons collide with atomic nuclei are treated as a source term in this equation.

A multigroup method was created to solve this low energy neutron transport equation. This was done by partitioning the energy range into a finite grid and defining an integral fluence for each energy interval. In this way, the transport equation was transformed into a solvable system of differential equations.

This multigroup method was first applied to a test problem in which both the neutron scattering function and the source term were approximated by analytical functions. In this test problem, the dependence of the source term on the depth in the material was removed. This made it possible to solve the transport equation numerically and recursively for small depths. Neutron fluences calculated with the multigroup method in three materials, lithium, aluminum, and lead, compared well with fluences calculated using the other two methods.

Next the multigroup method of calculating low energy neutron transport

Reproduced with permission of the copyright owner. Further reproduction prohibited without permission.

was added to the HZETRN particle transport code. The multigroup method was found to be ideal for this purpose. It is efficient in terms of computer time and it uses the straight ahead approximation used by the main program so the low energy neutron fluences can easily be combined with the higher energy neutrons.

The multigroup method was also expanded to calculate neutron transport in materials with more than one type of atom. This method was applied to a water target and compared well with Monte Carlo results at larger depths where the flux is in near equilibrium with the sources. This comparison, however, also showed that the multigroup method underestimates low energy neutron fluence at small depths in the material. The hypothesis was formed that this was happening because the multigroup method did not account for evaporation neutrons that scattered backward from larger depths in the material. For this reason, a new two direction multigroup method was derived in which half of the source term was transported forward through the material and half was transported backward through the material. Results from this two direction multigroup method compared well with Monte Carlo results even at small depths.

The multigroup method was also applied to an aluminum shield with a water target behind it. These results also compared well with Monte Carlo results but once again the two direction method was needed to calculate fluence at small depths.

Lastly, the multigroup method was applied to a shield of CO_2 with a target of regolith behind it used to model the Mars environment. It was found that the low energy neutron flux on the Martian surface will be due to the albedo from

Reproduced with permission of the copyright owner. Further reproduction prohibited without permission.

the regolith as well as neutrons transported down through the atmosphere. One focus of the Mars 2003 mission is to test these code predictions.

Reproduced with permission of the copyright owner. Further reproduction prohibited without permission.

REFERENCES

1. G. I. BELL and S. GLASSTONE, *Nuclear Reactor Theory*, Van Nostrand Reinhold, New York (1970).

2. J. K. SHULTIS and R. E. FAW, *Radiation Shielding*, Prentice-Hall, Upper Saddle River, New Jersey (1996).

3. W. ZAIHUA, "An Approximate Solution to the Neutron Transport Equation," *Transport Theory and Statistical Physics*, **26**, 263-270 (1997).

4. J. J. DUDERSTADT and L. J. HAMILTON, *Nuclear Reactor Analysis*, J. Wiley and Sons, New York (1976).

5. J. W. WILSON, L. W. TOWNSEND, W. SCHIMMERLING, G. S. KHANDELWAL, F. KHAN, J. E. NEALY, F. A. CUCINOTTA, L. C. SIMONSEN, J. L. SHINN, and J. W. NORBURY, "Transport Methods and Interactions for Space Radiations," NASA RP-1257, National Aeronautics and Space Administration (1991).

6. P. FREIER, E. J. LOFGREN, E. P. NEY, and F. OPPENHIEMER, "The Heavy Component of Primary Cosmic Rays," *Phys. Rev.*, **74**, 1818-1827 (1948).

7. H.ARMSTRONG, H. HABER, and H. STRUGHOLD, "Aero Medical Problems Space Travel-Planning Meeting, School of Aviation Medicine," *J. Aviation Med.*, **20**, 383-417 (1949).

8. H. J. SCHAEFER, "Evaluation of Present-Day Knowledge of Cosmic Radiation at Extreme Altitude in Terms of Hazard to Health," *J. Aviation Med.*, **21**, 375-394 (1950).

9. J. G. JACOBS, ed., "Proceedings of Conference on Radiation Problems in Manned Space Flight," NASA TN D-588, National Aeronautics and Space Administration (1960).

10. S. L. LAMKIN, "A Theory for High-Energy Nucleon Transport in One Dimension," Master's Thesis, Old Dominion University, Norfolk, Virginia (1974).

11. J. W. WILSON and S. L. LAMKIN, "Perturbation Theory for Charged-Particle Transport in One Dimension," *Nuclear Science and Engineering*, **57**, 292-299 (1975).

Reproduced with permission of the copyright owner. Further reproduction prohibited without permission.

12. J. W. WILSON, L. W. TOWNSEND, J. E. NEALY, S. Y. CHUN, B. S. HONG, W. W. BUCK, S. L. LAMKIN, B. D. GANAPOL, F. KHAN, and F. A. CUCINOTTA, "BRYNTRN: A Baryon Transport Model," NASA TP 2887, National Aeronautics and Space Administration (1989).

13. J. L. SHINN, J. W. WILSON, M. WEYLAND, and F. A. CUCINOTTA, "Improvements in Computational Accuracy of BRYNTRN (A Baryon Transport Code)," NASA TP 3093, National Aeronautics and Space Administration (1991).

14. J. W. WILSON, "Analysis of the Theory of High-Energy Ion Transport," NASA TN D-8381, National Aeronautics and Space Administration (1977).

15. J. W. WILSON, "Depth-Dose Relations for Heavy Ion Beams," *Virginia Journal of Science*, **28**, 136-138 (1977).

16. J. W. WILSON, Heavy Ion Transport in the Straight Ahead Approximation," NASA TP 2178, National Aeronautics and Space Administration (1983).

17. J. W. WILSON, S. Y. CHUN, F. F. BADAVI, L. W. TOWNSEND, and S. L. LAMKIN, "HZETRN: A Heavy Ion/Nucleon Transport Code for Space Radiations," NASA TP 3146, National Aeronautics and Space Administration (1991).

18. J. W. WILSON, F. F. BADAVI, F. A. CUCINOTTA, J. L. SHINN, G. D. BADHWAR, R. SILBERBERG, C. H. TSAO, L. W. TOWNSEND, and R. K. TRIPATHI, "HZETRN: Description of a Free-Space Ion and Nucleon Transport and Shielding Computer Program," NASA TP 3495, National Aeronautics and Space Administration (1995).

19. J. W. WILSON, L. W. TOWNSEND, S. L. LAMKIN, and B. D. GANAPOL, "A Closed Form Solution to HZE Propagation," *Radiation Research*, **122**, 223-228 (1990).

20. J. W. WILSON, R. C. COSTEN, J. L. SHINN, and F. F. BADAVI, "Green's Function Methods in Heavy Ion Shielding," NASA TP 3311, National Aeronautics and Space Administration (1993).

21. J. W. WILSON, F. F. BADAVI, J. L. SHINN, and R. C. COSTEN, "Approximate Green's Function Methods for HZE Transport in Multilayered Materials," NASA TM 4519, National Aeronautics and Space Administration (1993).

22. F. A. CUCINOTTA, J. W. WILSON, and F. F. BADAVI, "Extension of the BRYNTRN Code to Monoenergetic Light Ion Beams," NASA TP 3472, National Aeronautics and Space Administration (1994).

Reproduced with permission of the copyright owner. Further reproduction prohibited without permission.

23. J. L. SHINN, J. W. WILSON, W. SCHIMMERLING, M. R. SHAVERS, J. MILLER, E. V. BENTON, A. L. FRANK, and F. F. BADAVI, "A Green's Function Method for Heavy Ion Beam Transport," *Radiation and Environmental Biophysics*, **34**, 155-159 (1995).

24. S. Y. CHUN, G. S. KHANDELWAL, and J. W. WILSON, "A Green's Function Method for High Charge and Energy Ion Transport," *Nuclear Science and Engineering*, **122**, 267-275 (1996).

25. J. W. WILSON, F. A. CUCINOTTA, H. TAI, J. L. SHINN, S. Y. CHUNN, R. K. TRIPATHI, and L. SIHVER, "Transport of Light Ions in Matter," *Advances in Space Research*, **21**, 1763-1771 (1998).

26. J. L. SHINN, J. W. WILSON, M. A. LONE, P. Y. WONG, and R. C. COSTEN, "Preliminary Estimates of Nucleon Fluxes in a Water Target Exposed to Solar-Flare Protons: BRYNTRN Versus Monte Carlo Code," NASA TM 4565, National Aeronautics and Space Administration (1994).

27. R. C. SINGLETERRY, "Neutron Transport Associated with the Galactic Cosmic Ray Cascade," PhD Thesis, University of Arizona, Tucson, Arizona (1993).

28. D. KINCAID and W. CHENEY, *Numerical Analysis*, Brooks/Cole, Belmont, California (1991).

29. B. A. MAGURNO, R. R. KINSEY, and F. M. SCHEFFEL, "Guidebook for the ENDF/B-V Nuclear Data Files," NP-2510, Research Project 975-1, BNL-NCS-31451, ENDF-328, Brookhaven National Laboraty (1982).

30. C. A. HALL and T. A. PORSCHING, *Numerical Analysis of Partial Differential Equations*, Prentice Hall, Englewood Cliffs, New Jersey (1990).

31. G. DAHLQUIST and A. BJORCK, *Numerical Methods*, Prentice Hall, Englewood Cliffs, New Jersey (1974).

32. H. G. HUGHES, R. E. PRAEL, and R. E. LITTLE, "MCNPX-The LAHET/MCNP code merger," LA-UR-97-4891, Los Alamos National Laboratory (1997).

33. L. C. SIMONSEN, J. E. NEALY, L. W. TOWNSEND, and J. W. WILSON, "Space Radiation Shielding for a Martian Habitat," SAE TP 901348 (1990).

34. S. L. LAMKIN, "High Energy Nucleon Transport in One Dimension", PhD Thesis, Old Dominion University, Norfolk, Virginia (1994).

Reproduced with permission of the copyright owner. Further reproduction prohibited without permission.

APPENDIX A

DERIVATION OF THE BOLTZMANN TRANSPORT EQUATION

Shultis and Faw[2], Duderstadt and Hamilton[4], and Bell and Glasstone[1] all contain derivations of the Boltzmann transport equation for neutrons, and Stanley Lamkin's master's thesis[10] contains an easy to follow derivation of the simplified one dimensional Boltzmann equation with the straight ahead approximation for neutrons and charged particles. The derivation described here, however, is most similar to the one described in Lamkin's doctoral dissertation[34]. The full Boltzmann transport equation is derived for neutral particles and charged particles.

An attempt to create a transport equation is an attempt to describe the position and motion of every energetic particle in a medium at a given time. Here, the position of a particle will be given by the vector $\vec{x} = x\vec{i} + y\vec{j} + z\vec{k}$ and its velocity by the vector $\vec{V} = V_x\vec{i} + V_y\vec{j} + V_z\vec{k}$. Note that the velocity can be written in terms of its magnitude, v, and its direction, $\vec{\Omega}$. In this case, $\vec{V} = v\vec{\Omega}$. Also note that the kinetic energy of a particle is related to the magnitude of its velocity by the equation $E = \frac{1}{2}mv^2$, where m is the particle's mass. Therefore, the velocity of a particle can be determined if its energy and direction are known.

The direction $\vec{\Omega}$ can be described in terms of θ and ψ, as shown in Figure 25.

Reproduced with permission of the copyright owner. Further reproduction prohibited without permission.

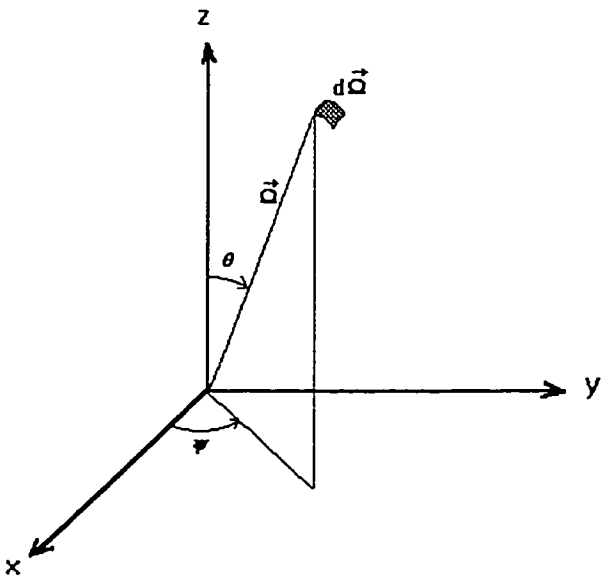

Fig. 25. Solid angle about position $\vec{x}$.

Here, $d\vec{\Omega} = d\vec{\Omega}(\theta, \psi) = \sin\theta \, d\theta \, d\psi$ is a solid angle measured in steradians beginning at direction Ω.

Let $N_j(\vec{x}, E, \vec{\Omega}, t)$ be the total number of type j particles at position $\vec{x}$ with energy E and direction $\vec{\Omega}$ at time t per unit volume per unit energy per steradian. Then $N_j(\vec{x}, E, \vec{\Omega}, t) \, d\vec{x} \, dE \, d\vec{\Omega}$ is the total number of particles in volume element $d\vec{x} = dx \, dy \, dz$ with energy between E and $E + dE$ that have direction in solid angle $d\vec{\Omega}$ at time t. This number is not conserved, but the total number of type j particles in volume element $d\vec{x}$ that have a direction in $d\vec{\Omega}$ with energy greater than E,

$$\Psi_j(\vec{x}, E, \vec{\Omega}, t) \, d\vec{x} \, d\vec{\Omega} = \int_E^\infty dE_s \; N_j(\vec{x}, E_s, \vec{\Omega}, t) \, d\vec{x} \, d\vec{\Omega}, \qquad (A1.1)$$

is conserved.

Reproduced with permission of the copyright owner. Further reproduction prohibited without permission.

The Boltzmann equation can, therefore, be derived by evaluating the rate of change of the number of particles in a volume element $d\vec{x}$ with direction in solid angle $d\vec{\Omega}$ having energy greater than E. This rate of change is equivalent to the difference of the number of particles gained and the number of particles lost,

$$\frac{d}{dt}\Psi_j(\vec{x}, E, \vec{\Omega}, t)\, d\vec{x}\, d\vec{\Omega} = \text{gains} - \text{losses}. \qquad (A1.2)$$

The gains are due to sources and to those particles brought into the volume element $d\vec{x}$ and the solid angle $d\vec{\Omega}$ by collision scattering. Let $g_j(\vec{x}, E, \vec{\Omega}, t)$ be the number of type j particles created at position $\vec{x}$ with energy E and direction $\vec{\Omega}$ by some particle source. Then

$$\int_E^\infty dE_s\; g_j(\vec{x}, E_s, \vec{\Omega}, t)\, d\vec{x}\, d\vec{\Omega} \qquad (A1.3)$$

is the number of particles created with energy greater than E in volume element $d\vec{x}$ and solid angle $d\vec{\Omega}$. Let $\Sigma_{jk}(E, E', \vec{\Omega}, \vec{\Omega}')$ be the probability that a type j particle is produced with energy E and direction $\vec{\Omega}$ when a type k particle with energy E' and direction $\vec{\Omega}'$ collides with an atom, and let $m_{jk}(E, \vec{\Omega})$ be the multiplicity of type j particles produced in the same collision. Note that $m_{jk}(E, \vec{\Omega}) = 1$ for elastic scattering. Then the total scattering function $f_{jk}(E, E', \vec{\Omega}, \vec{\Omega}')$ is given by

$$f_{jk}(E, E', \vec{\Omega}, \vec{\Omega}') = m_{jk}(E, \vec{\Omega})\, \Sigma_{jk}(E, E', \vec{\Omega}, \vec{\Omega}'). \qquad (A1.4)$$

Next, define

$$\phi_j(\vec{x}, E, \vec{\Omega}, t) = v\, N_j(\vec{x}, E, \vec{\Omega}, t) \qquad (A1.5)$$

to be the number of type j particles with energy E and direction $\vec{\Omega}$ at time t per unit area per unit energy per steradian passing through position $\vec{x}$ per second.

Reproduced with permission of the copyright owner. Further reproduction prohibited without permission.

This is called the particle fluence. The total number of type j particles brought into the volume element $d\vec{x}$ and the solid angle $d\vec{\Omega}$ with energy greater then E is

$$\sum_{k\geq j}\int_E^\infty dE_s \int_{E_s}^\infty dE' \int d\vec{\Omega}' f_{jk}(E_s, E', \vec{\Omega}, \vec{\Omega}')\phi_k(\vec{x}, E', \vec{\Omega}', t)d\vec{x}\, d\vec{\Omega}. \quad (A1.6)$$

Note that the integral $\int d\vec{\Omega}'$ is taken over all angles. Also note that conservation of energy prevents a nuclear collision from producing particles with greater energy than the original particle. For this reason, the integral $\int_{E_s}^\infty dE'$, for energy of the particle before the collision, is taken from E_s to ∞ instead of 0 to ∞.

The losses are caused by particles leaving the volume element or the solid angle or dropping below energy E due to scattering. These losses are given by

$$\int_E^\infty dE_s\ \sigma_j(E_s)\phi_j(\vec{x}, E, \vec{\Omega}, t)d\vec{x}\, d\vec{\Omega} \quad (A1.7)$$

where $\sigma_j(E)$ is the nuclear cross-section.

Therefore, the total change to the number of particles in volume element $d\vec{x}$ and solid angle $d\vec{\Omega}$ with energy greater than E at time t is

$$\begin{aligned}
&\frac{d}{dt}\Psi_j(\vec{x}, E, \vec{\Omega}, t)\, d\vec{x}\, d\vec{\Omega} \\
&\quad = \sum_{k\geq j}\int_E^\infty dE_s \int_{E_s}^\infty dE' \int d\vec{\Omega}' f_{jk}(E_s, E', \vec{\Omega}, \vec{\Omega}')\phi_k(\vec{x}, E', \vec{\Omega}', t)d\vec{x}\, d\vec{\Omega} \\
&\quad - \int_E^\infty dE_s\ \sigma_j(E_s)\phi_j(\vec{x}, E, \vec{\Omega}, t)d\vec{x}\, d\vec{\Omega} \\
&\quad + \int_E^\infty dE_s\ g_j(\vec{x}, E_s, \vec{\Omega}, t)\, d\vec{x}\, d\vec{\Omega}. \quad (A1.8)
\end{aligned}$$

The rate of change $\frac{d\Psi_j}{dt}$ can also be expanded to get

$$\begin{aligned}
\frac{d\Psi_j}{dt} &= \frac{\partial\Psi_j}{\partial t} + \frac{\partial\Psi_j}{\partial x}\frac{dx}{dt} + \frac{\partial\Psi_j}{\partial y}\frac{dy}{dt} + \frac{\partial\Psi_j}{\partial z}\frac{dz}{dt} \\
&\quad + \frac{\partial\Psi_j}{\partial E}\frac{dE}{dt} + \frac{\partial\Psi_j}{\partial\theta}\frac{d\theta}{dt} + \frac{\partial\Psi_j}{\partial\psi}\frac{d\psi}{dt}. \quad (A1.9)
\end{aligned}$$

Reproduced with permission of the copyright owner. Further reproduction prohibited without permission.

Now, let $\frac{dE}{dt} = \frac{\partial E}{\partial t} + \frac{\partial E}{\partial l}\frac{dl}{dt}$, where $l = \sqrt{x^2+y^2+z^2}$ is the path length. Note that $\frac{dl}{dt} = v$ and $\frac{\partial E}{\partial t} = 0$. Also, recall that $\frac{dE}{dl} = -S_j(E)$, where $S_j(E)$ is the linear stopping power. This is the energy lost per unit path length due to ionization. It is treated as a continuous function because the ionizing events are so close together. Also, note that the angular velocity terms $\frac{d\theta}{dt}$ and $\frac{d\psi}{dt}$ are 0 for most materials. An exception to this would be a material with a magnetic field that pulled charged ions from their normal straight ahead path. Here, they are assumed to be zero. Therefore, equation (A1.9) becomes

$$\frac{d\Psi_j}{dt} = \frac{\partial \Psi_j}{\partial t} + \vec{V}\cdot\nabla_{\vec{x}}\Psi_j - vS_j(E)\frac{\partial \Psi_j}{\partial E}. \qquad (A1.10)$$

Using equation (A1.1), equation (A1.10) becomes

$$\frac{d\Psi_j}{dt} = \frac{\partial}{\partial t}\int_E^\infty N_j(\vec{x},E_s,\vec{\Omega},t)\,dE_s + \vec{V}\cdot\nabla_{\vec{x}}\int_E^\infty N_j(\vec{x},E_s,\vec{\Omega},t)\,dE_s$$
$$- vS_j(E)\frac{\partial}{\partial E}\int_E^\infty N_j(\vec{x},E_s,\vec{\Omega},t)\,dE_s \qquad (A1.11)$$

or equivalently

$$\frac{d\Psi_j}{dt} = \frac{1}{v}\frac{\partial}{\partial t}\int_E^\infty \phi_j(\vec{x},E_s,\vec{\Omega},t)\,dE_s + \vec{\Omega}\cdot\nabla_{\vec{x}}\int_E^\infty \phi_j(\vec{x},E_s,\vec{\Omega},t)\,dE_s$$
$$- S_j(E)\frac{\partial}{\partial E}\int_E^\infty \phi_j(\vec{x},E_s,\vec{\Omega},t)\,dE_s. \qquad (A1.12)$$

Note that $\lim_{E\to\infty}\phi_j(\vec{x},E,\vec{\Omega},t) = 0$. Therefore,

$$\frac{\partial}{\partial E}\int_E^\infty \phi_j(\vec{x},E_s,\vec{\Omega},t)\,dE_s = -\phi_j(\vec{x},E,\vec{\Omega},t). \qquad (A1.13)$$

For this reason, equation (A1.12) takes the form

$$\frac{d\Psi_j}{dt} = \frac{1}{v}\frac{\partial}{\partial t}\int_E^\infty \phi_j(\vec{x},E_s,\vec{\Omega},t)\,dE_s + \vec{\Omega}\cdot\nabla_{\vec{x}}\int_E^\infty \phi_j(\vec{x},E_s,\vec{\Omega},t)\,dE_s$$
$$+ S_j(E)\phi_j(\vec{x},E,\vec{\Omega},t). \qquad (A1.14)$$

Reproduced with permission of the copyright owner. Further reproduction prohibited without permission.

Substituting equation (A1.8) into equation (A1.14) produces the equation

$$\sum_{k\geq j}\int_E^\infty dE_s \int_{E_s}^\infty dE' \int d\vec{\Omega}' f_{jk}(E_s, E', \vec{\Omega}, \vec{\Omega}')\phi_k(\vec{x}, E', \vec{\Omega}', t)$$
$$- \int_E^\infty dE_s\, \sigma_j(E_s)\phi_j(\vec{x}, E, \vec{\Omega}, t) + \int_E^\infty dE_s\, g_j(\vec{x}, E_s, \vec{\Omega}, t)$$
$$= \frac{1}{v}\frac{\partial}{\partial t}\int_E^\infty \phi_j(\vec{x}, E_s, \vec{\Omega}, t)\, dE_s + \vec{\Omega}\cdot\nabla_{\vec{x}}\int_E^\infty \phi_j(\vec{x}, E_s, \vec{\Omega}, t)\, dE_s$$
$$+ S_j(E)\phi_j(\vec{x}, E, \vec{\Omega}, t). \qquad (A1.15)$$

If the partial derivative of every term of this equation is taken, equation (A1.15) becomes

$$\frac{1}{v}\frac{\partial}{\partial t}\phi_j(\vec{x}, E, \vec{\Omega}, t) + \vec{\Omega}\cdot\nabla_{\vec{x}}\phi_j(\vec{x}, E, \vec{\Omega}, t) - \frac{\partial}{\partial E}\left[S_j(E)\phi_j(\vec{x}, E, \vec{\Omega}, t)\right]$$
$$+ \sigma_j(E)\phi_j(\vec{x}, E, \vec{\Omega}, t)$$
$$= \sum_{k\geq j}\int_E^\infty dE' \int d\vec{\Omega}' f_{jk}(E, E', \vec{\Omega}, \vec{\Omega}')\phi_k(\vec{x}, E', \vec{\Omega}', t)$$
$$+ g_j(\vec{x}, E, \vec{\Omega}, t). \qquad (A1.16)$$

This is the full Boltzmann transport equation.

If a steady-state distribution is assumed, $\frac{\partial\phi_j}{\partial t} = 0$, the Boltzmann transport equation takes the form

$$\vec{\Omega}\cdot\nabla\phi_j(\vec{x}, E, \vec{\Omega}) - \frac{\partial}{\partial E}\left[S_j(E)\phi_j(\vec{x}, E, \vec{\Omega})\right] + \sigma_j(E)\phi_j(\vec{x}, E, \vec{\Omega})$$
$$= \sum_{k\geq j}\int_E^\infty dE' \int d\vec{\Omega}' f_{jk}(E, E', \vec{\Omega}, \vec{\Omega}')\phi_k(\vec{x}, E', \vec{\Omega}')$$
$$+ g_j(\vec{x}, E, \vec{\Omega}). \qquad (2.1)$$

The source term is usually assumed to be zero when dealing with space

Reproduced with permission of the copyright owner. Further reproduction prohibited without permission.

radiation. In this case, equation (2.1) becomes

$$\vec{\Omega}\cdot\nabla\phi_j(\vec{x},E,\vec{\Omega})-\frac{\partial}{\partial E}\left[S_j(E)\phi_j(\vec{x},E,\vec{\Omega})\right]+\sigma_j(E)\phi_j(\vec{x},E,\vec{\Omega})$$
$$=\sum_{k\geq j}\int_E^\infty dE'\int d\vec{\Omega}' f_{jk}(E,E',\vec{\Omega},\vec{\Omega}')\phi_k(\vec{x},E',\vec{\Omega}'). \qquad (A1.17)$$

For neutrons, $j=1$ in the HZETRN program, the stopping power is zero, $S_1(E)=0$, because no energy is lost due to ionization. The neutron transport equation, therefore, becomes

$$\vec{\Omega}\cdot\nabla\phi_1(\vec{x},E,\vec{\Omega})+\sigma_1(E)\phi_1(\vec{x},E,\vec{\Omega})$$
$$=\sum_{k\geq 1}\int_E^\infty dE'\int d\vec{\Omega}' f_{1k}(E,E',\vec{\Omega},\vec{\Omega}')\phi_1(\vec{x},E',\vec{\Omega}')$$
$$+g_1(\vec{x},E,\vec{\Omega}). \qquad (2.3)$$

If a straight ahead approximation is made, the Boltzmann equation becomes

$$\frac{\partial}{\partial x}\phi_j(x,E)-\frac{\partial}{\partial E}\left[S_j(E)\phi_j(x,E)\right]+\sigma_j(E)\phi_j(x,E)$$
$$=\sum_{k\geq j}\int_E^\infty f_{jk}(E,E')\phi_k(x,E')dE'+g_j(x,E). \qquad (2.2)$$

Here, the assumption is made that all secondaries move in the same direction as the primaries, in this case, the x direction. While this assumption is only an approximation, it has been found to be reasonably accurate for the transport of high energy nucleons and is used in the HZETRN program.

Reproduced with permission of the copyright owner. Further reproduction prohibited without permission.

APPENDIX B

CHOOSING AN ENERGY GRID

The way the energy grid, $E_1, E_2, E_3, ..., E_N, E_{N+1}$, is chosen for the multi-group method affects the accuracy of the results. For a given interval, $[E_i, E_{i+1}]$, there are three possibilities. In Case I, $E_{i+1} < E_i/\alpha$, in Case II, $E_{i+1} > E_i/\alpha$, and in Case III, $Ei + 1 = E_i/\alpha$. The way in which the order of integration is switched in expression (3.6),

$$\int_{E_i}^{E_{i+1}} \int_{E}^{E/\alpha} f(E, E')\phi(x, E')dE'dE, \tag{3.6}$$

depends on which case applies.

For Case I, switching the order of integration in expression (3.6) leads to the expression

$$\begin{aligned} &\int_{E_i}^{E_{i+1}} \int_{E_i}^{E'} f(E, E')\phi(x, E')dEdE' \\ &+ \int_{E_{i+1}}^{E_i/\alpha} \int_{E_i}^{E_{i+1}} f(E, E')\phi(x, E')dEdE' \\ &+ \int_{E_i/\alpha}^{E_{i+1}/\alpha} \int_{\alpha E'}^{E_{i+1}} f(E, E')\phi(x, E')dEdE'. \end{aligned} \tag{A2.1}$$

See Figure 26.

Reproduced with permission of the copyright owner. Further reproduction prohibited without permission.

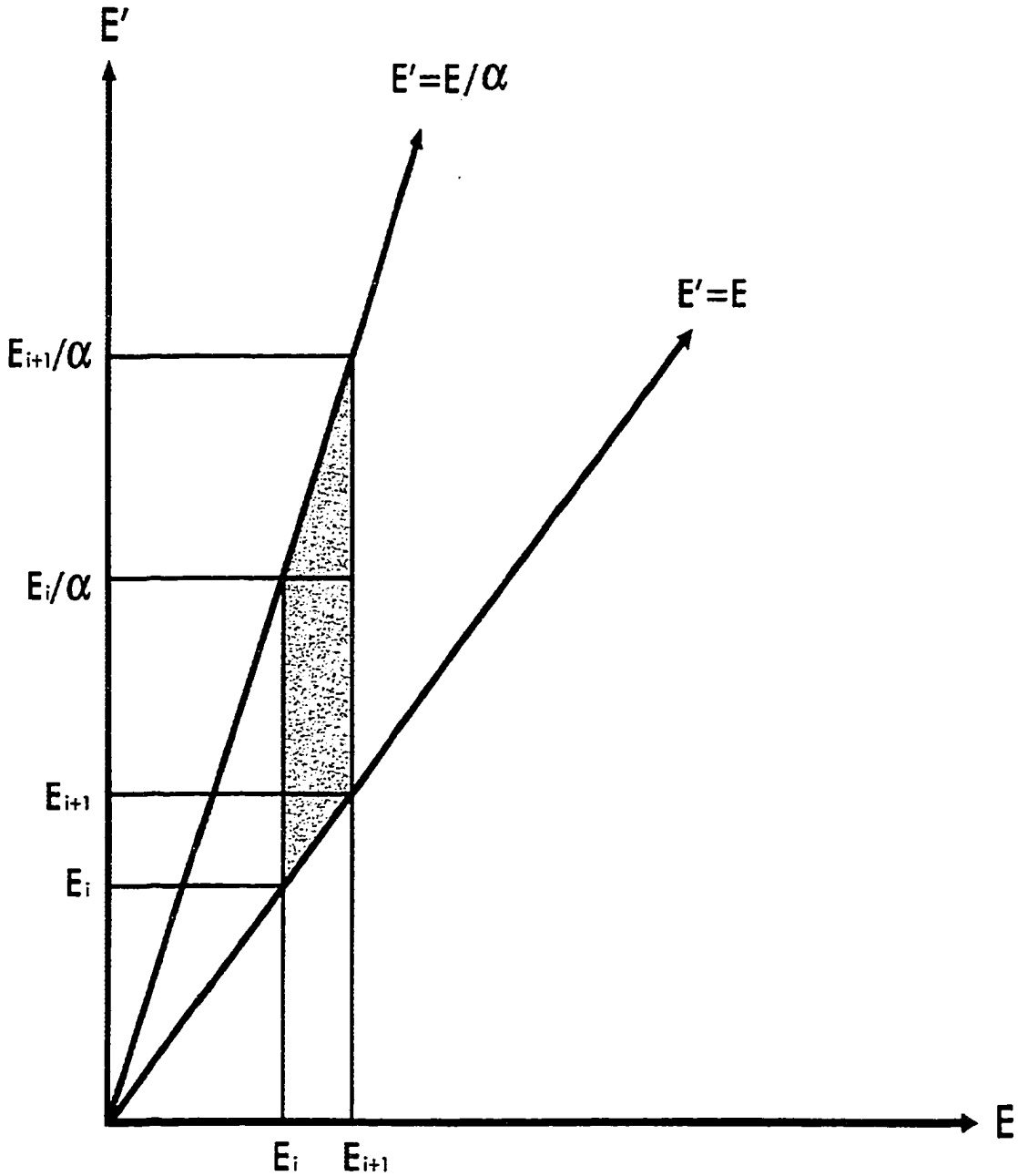

Fig. 26. Multigroup energy partition when $E_{i+1} < E_i/\alpha$.

This expression can then be rewritten in terms of a number of smaller integrals by including every point of the energy grid as shown in Figure 27.

Reproduced with permission of the copyright owner. Further reproduction prohibited without permission.

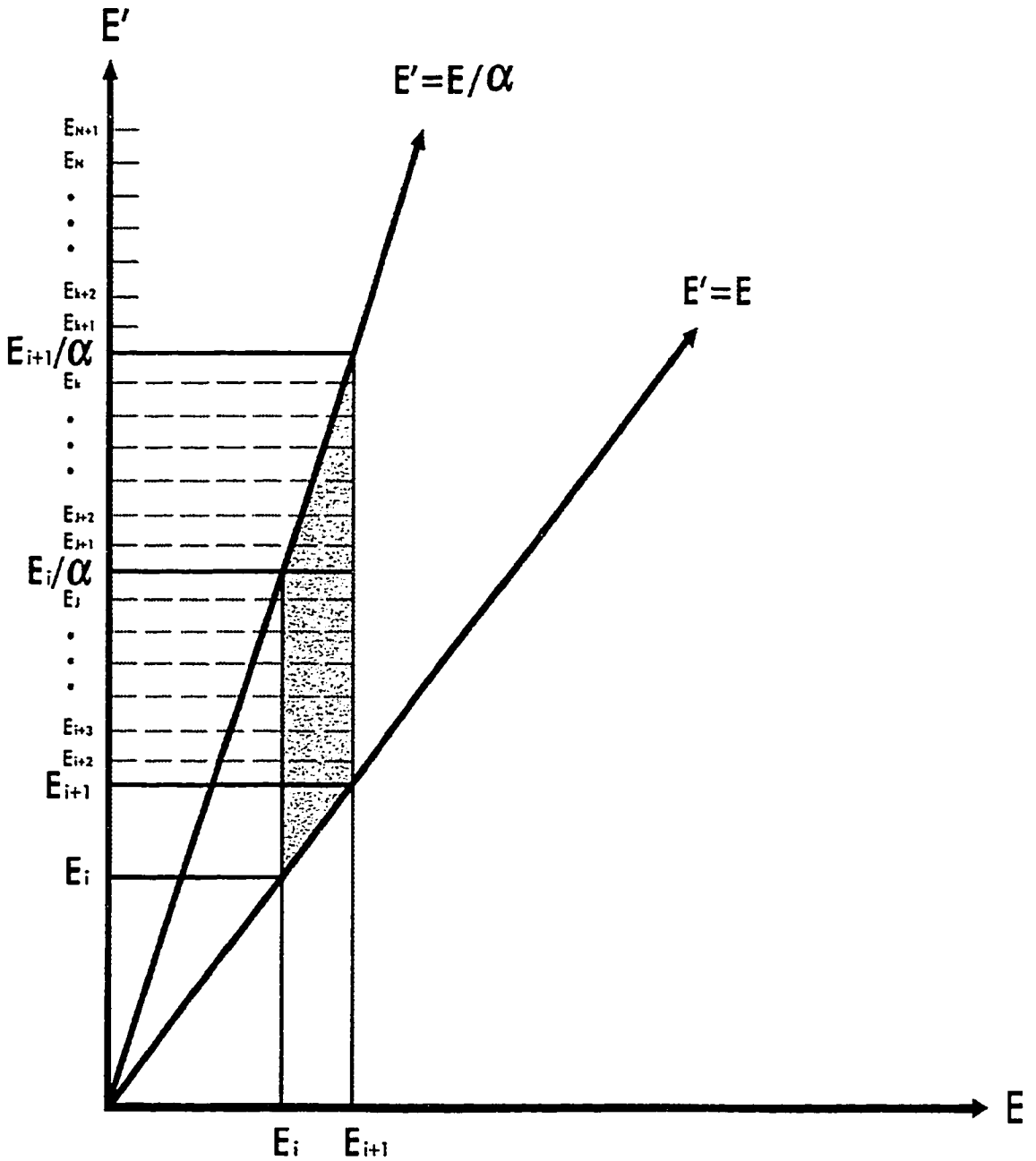

Fig. 27. Detailed multigroup energy partition when $E_{i+1} < E_i/\alpha$.

Reproduced with permission of the copyright owner. Further reproduction prohibited without permission.

In this case, the above expression takes the form

$$\begin{aligned}
&\int_{E_i}^{E_{i+1}} \int_{E_i}^{E'} f(E,E')\phi(x,E')dEdE' \\
&+ \sum_{m=i+1}^{j-1} \int_{E_m}^{E_{m+1}} \int_{E_i}^{E_{i+1}} f(E,E')\phi(x,E')dEdE' \\
&+ \int_{E_j}^{\frac{E_i}{\alpha}} \int_{E_i}^{E_{i+1}} f(E,E')\phi(x,E')dEdE' \\
&+ \int_{E_i/\alpha}^{E_{j+1}} \int_{\alpha E'}^{E_{i+1}} f(E,E')\phi(x,E')dEdE' \\
&+ \sum_{m=j+1}^{k-1} \int_{E_m}^{E_{m+1}} \int_{\alpha E'}^{E_{i+1}} f(E,E')\phi(x,E')dEdE' \\
&+ \int_{E_k}^{E_{i+1}/\alpha} \int_{\alpha E'}^{E_{i+1}} f(E,E')\phi(x,E')dEdE'. \qquad (A2.2)
\end{aligned}$$

Note that E_j is the largest point on the energy grid that is less than E_i/α and E_k is the largest point in the energy grid that is less than E_{i+1}/α.

A first attempt to write this expression in terms of $\Phi_m(x)$ for the values given by $m = i, i+1, i+2, ..., k$ yields

$$\begin{aligned}
&\left[\int_{E_i}^{E_i^{(1)}} f(E,E_i^{(1)})dE\right]\Phi_i(x) \\
&+ \sum_{m=i+1}^{j-1} \left[\int_{E_i}^{E_{i+1}} f(E,E_m^{(1)})dE\right]\Phi_m(x) \\
&+ \int_{E_j}^{E_i/\alpha} \int_{E_i}^{E_{i+1}} f(E,E')\phi(x,E')dEdE' \\
&+ \int_{\frac{E_i}{\alpha}}^{E_{j+1}} \int_{\alpha E'}^{E_{i+1}} f(E,E')\phi(x,E')dEdE' \\
&+ \sum_{m=j+1}^{k-1} \left[\int_{\alpha E_m^{(1)}}^{E_{i+1}} f(E,E_m^*)dE\right]\Phi_m(x) \\
&+ \int_{E_k}^{E_{i+1}/\alpha} \int_{\alpha E'}^{E_{i+1}} f(E,E')\phi(x,E')dEdE', \qquad (A2.3)
\end{aligned}$$

Reproduced with permission of the copyright owner. Further reproduction prohibited without permission.

where a mean value theorem is once again used with $E_m^{(1)} = E_m + \theta_m^*(E_{m+1} - E_m)$ and θ_m^* chosen so that $0 < \theta_m^* < 1$.

In order to write

$$\int_{E_j}^{E_i/\alpha} \int_{E_i}^{E_{i+1}} f(E, E')\phi(x, E')dEdE' \tag{A2.4}$$

in terms of $\Phi_j(x)$, another approximation must be made. This term is a fraction of the expression

$$\int_{E_j}^{E_{j+1}} \int_{E_i}^{E_{i+1}} f(E, E')\phi(x, E')dEdE'. \tag{A2.5}$$

Therefore,

$$\int_{E_j}^{E_i/\alpha} \int_{E_i}^{E_{i+1}} f(E, E')\phi(x, E')dEdE' = \overline{\eta_1} \int_{E_j}^{E_{j+1}} \int_{E_i}^{E_{i+1}} f(E, E')\phi(x, E')dEdE' \tag{A2.6}$$

for some $\overline{\eta_1}$ such that $0 < \overline{\eta_1} < 1$. Since $\overline{\eta_1}$ is not known, an η_1^* is chosen to approximate $\overline{\eta_1}$. The quantity $\eta_1^* = \frac{E_i/\alpha - E_j}{E_{j+1} - E_j}$ is a logical choice. Then

$$\int_{E_j}^{E_i/\alpha} \int_{E_i}^{E_{i+1}} f(E, E')\phi(x, E')dEdE' = \eta_1^* \int_{E_j}^{E_{j+1}} \int_{E_i}^{E_{i+1}} f(E, E')\phi(x, E')dEdE' \tag{A2.7}$$

and using the same mean value theorem this becomes

$$\int_{E_j}^{E_i/\alpha} \int_{E_i}^{E_{i+1}} f(E, E')\phi(x, E')dEdE' = \eta_1^* \left[\int_{E_i}^{E_{i+1}} f(E, E_j^{(2)})\phi(x, E')dE \right] \Phi_j(x) \tag{A2.8}$$

where $E_j^{(2)} = E_j + \theta_j^{(2)}(\frac{E_i}{\alpha} - E_j)$ for some $\theta_j^{(2)}$ chosen so that $0 < \theta_j^{(2)} < 1$.

Similarly,

$$\int_{E_i/\alpha}^{E_{j+1}} \int_{\alpha E'}^{E_{i+1}} f(E, E')\phi(x, E')dEdE' = \eta_2^* \left[\int_{\alpha E_j^{(3)}}^{E_{i+1}} f(E, E_j^{(3)})\phi(x, E')dE \right] \Phi_j(x) \tag{A2.9}$$

Reproduced with permission of the copyright owner. Further reproduction prohibited without permission.

where $\eta_2^* = 1 - \eta_1^*$ and $E_j^{(3)} = \frac{E_i}{\alpha} + \theta_j^{(3)}(E_{j+1} - \frac{E_i}{\alpha})$ for some $\theta_j^{(3)}$ chosen so that $0 < \theta_j^{(3)} < 1$ and

$$\int_{E_k}^{E_{i+1}/\alpha} \int_{\alpha E'}^{E_{i+1}} f(E, E')\phi(x, E')dEdE' = \eta_3^* \left[\int_{\alpha E_j^{(4)}}^{E_{i+1}} f(E, E_j^{(4)})\phi(x, E')dE \right] \Phi_k(x) \tag{A2.10}$$

where $\eta_3^* = \frac{E_{i+1}/\alpha - E_k}{E_{k+1} - E_k}$ and $E_j^{(4)} = E_k + \theta_j^{(4)}(\frac{E_{i+1}}{\alpha} - E_k)$ for some $\theta_j^{(4)}$ chosen so that $0 < \theta_j^{(4)} < 1$.

Now expression (A2.3) takes the form

$$\begin{aligned}
&\left[\int_{E_i}^{E_i^{(1)}} f(E, E_i^{(1)})dE \right] \Phi_i(x) \\
&+ \sum_{m=i+1}^{j-1} \left[\int_{E_i}^{E_{i+1}} f(E, E_m^{(1)})dE \right] \Phi_m(x) \\
&+ \left\{ \eta_1^* \left[\int_{E_i}^{E_{i+1}} f(E, E_j^{(2)})\phi(x, E')dE \right] + \eta_2^* \left[\int_{\alpha E_j^{(3)}}^{E_{i+1}} f(E, E_j^{(3)})\phi(x, E')dE \right] \right\} \Phi_j(x) \\
&+ \sum_{m=j+1}^{k-1} \left[\int_{\alpha E_m^{(1)}}^{E_{i+1}} f(E, E_m^{(1)})dE \right] \Phi_m(x) \\
&+ \eta_3^* \left[\int_{\alpha E_j^{(4)}}^{E_{i+1}} f(E, E_j^{(4)})\phi(x, E')dE \right] \Phi_k(x).
\end{aligned} \tag{A2.11}$$

Note that if $k > N$, this expression will be truncated to include only values of $\Phi_m(x)$ where $m \leq N$.

In Case II, the energy grid is set in such a way that on the interval $[E_i, E_{i+1}]$, $E_{i+1} > \frac{E_i}{\alpha}$ as in Figure 28.

Reproduced with permission of the copyright owner. Further reproduction prohibited without permission.

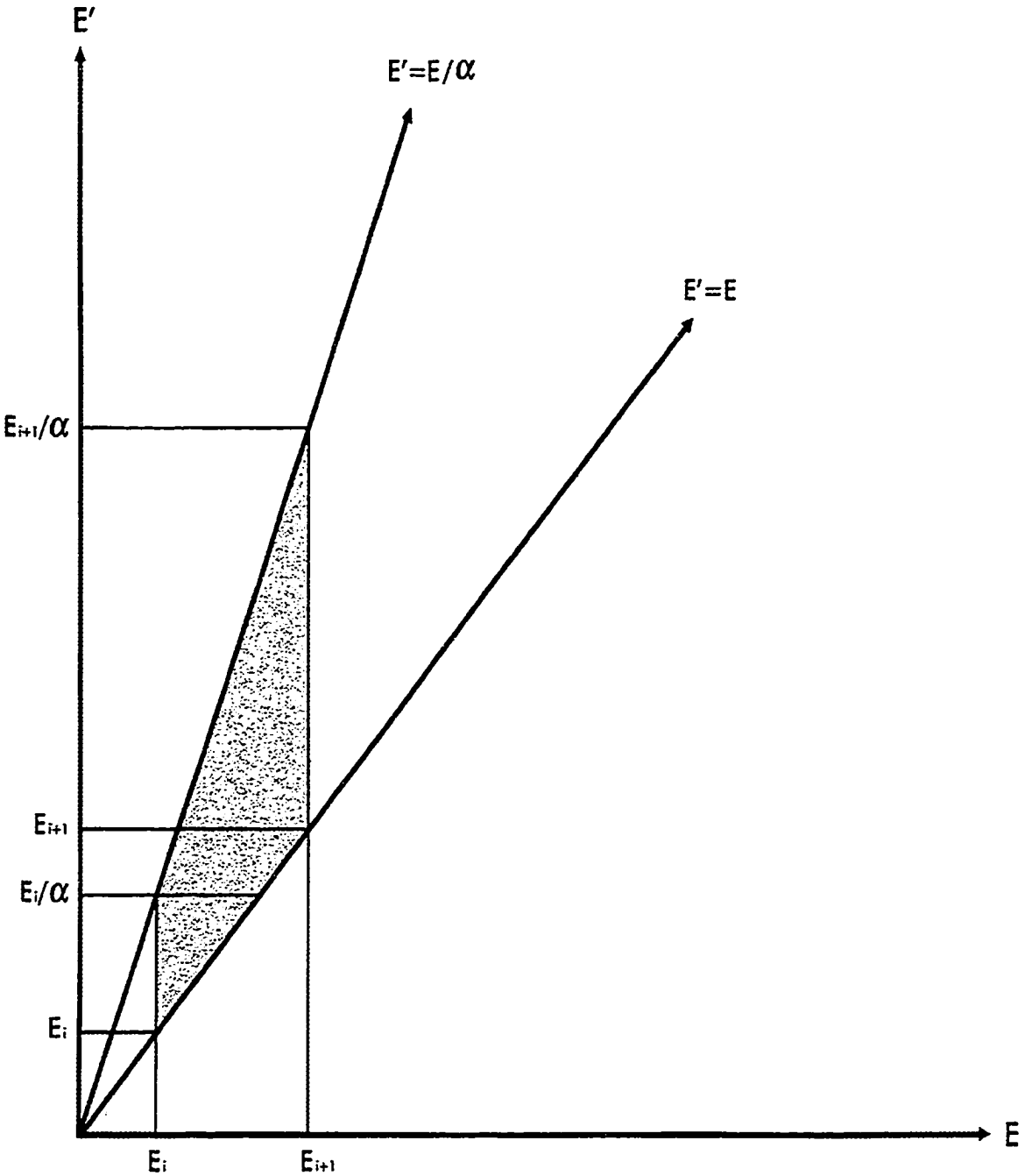

Fig. 28. Multigroup energy partition when $E_{i+1} > E_i/\alpha$.

Reproduced with permission of the copyright owner. Further reproduction prohibited without permission.

In this case, switching the order of integration in expression (3.6) leads to the expression

$$\int_{E_i}^{E_i/\alpha}\int_{E_i}^{E'} f(E,E')\phi(x,E')dEdE' + \int_{E_i/\alpha}^{E_{i+1}}\int_{\alpha E'}^{E'} f(E,E')\phi(x,E')dEdE' + \int_{E_{i+1}}^{E_{i+1}/\alpha}\int_{\alpha E'}^{E_{i+1}} f(E,E')\phi(x,E')dEdE'. \quad (A2.12)$$

If all of the energy grid points are used, as in Figure 29,

Reproduced with permission of the copyright owner. Further reproduction prohibited without permission.

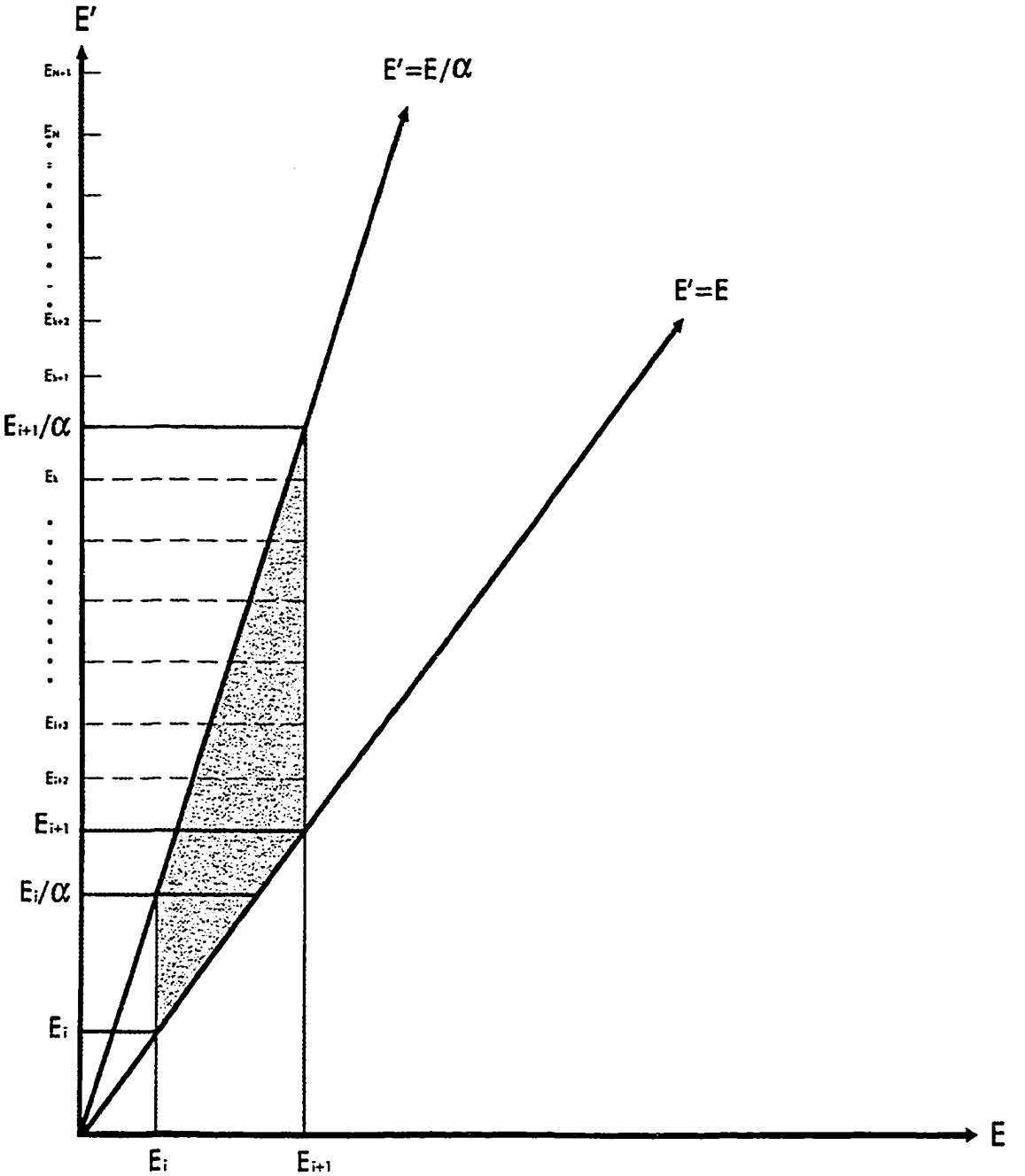

Fig. 29. Detailed multigroup energy partition when $E_{i+1} > E_i/\alpha$.

Reproduced with permission of the copyright owner. Further reproduction prohibited without permission.

this expression becomes

$$\int_{E_i}^{E_i/\alpha}\int_{E_i}^{E'} f(E,E')\phi(x,E')dEdE'$$
$$+\int_{E_i/\alpha}^{E_{i+1}}\int_{\alpha E'}^{E'} f(E,E')\phi(x,E')dEdE'$$
$$+\sum_{m=i+1}^{k-1}\int_{E_m}^{E_{m+1}}\int_{\alpha E'}^{E_{i+1}} f(E,E')\phi(x,E')dEdE'$$
$$+\int_{E_k}^{E_{i+1}/\alpha}\int_{\alpha E'}^{E_{i+1}} f(E,E')\phi(x,E')dEdE'. \qquad (A2.13)$$

As in the first case, some approximations must be made in order to write this expression in terms of Φ_m for $m = i, i+1, i+2, ..., k$. In this case, the above expression can be approximated by

$$\left\{\eta_1^*\left[\int_{E_i}^{E_i^{(2)}} f(E,E_i^{(2)})dE\right]+\eta_2^*\left[\int_{\alpha E_i^{(3)}}^{E_i^{(3)}} f(E,E_i^{(3)})dE\right]\right\}\Phi_i(x)$$
$$+\sum_{m=i+1}^{k-1}\left[\int_{\alpha E_m^*}^{E_{i+1}} f(E,E_m^{(1)})dE\right]\Phi_m(x)$$
$$+\eta_3^*\left[\int_{\alpha E_k^{(4)}}^{E_{i+1}} f(E,E_k^{(4)})dE\right]\Phi_k(x). \qquad (A2.14)$$

Reproduced with permission of the copyright owner. Further reproduction prohibited without permission.

where

$$\eta_1^* = \frac{E_i/\alpha - E_i}{E_{i+1} - E_i},$$

$$\eta_2^* = 1 - \eta_1^*,$$

$$\eta_3^* = \frac{\frac{E_{i+1}}{\alpha} - E_k}{E_{k+1} - E_k},$$

$$E_i^{(2)} = E_i + \theta_i^{(2)}(\frac{E_i}{\alpha} - E_i),$$

$$E_i^{(3)} = \frac{E_i}{\alpha} + \theta_i^{(30}(E_{i+1} - \frac{E_i}{\alpha}),$$

$$E_m^{(1)} = E_m + \theta_m^{(1)}(E_{m+1} - E_m),$$

and

$$E_k^{(4)} = E_k + \theta_k^{(4)}(\frac{E_{i+1}}{\alpha} - E_k)$$

with $0 < \theta_i^{(2)}, \theta_i^{(3)}, \theta_m^*, \theta_k^{(4)} < 1$.

In Case III, $E_{i+1} = E_i/\alpha$ on interval $[E_i, E_{i+1}]$ as shown in Figure 30.

Reproduced with permission of the copyright owner. Further reproduction prohibited without permission.

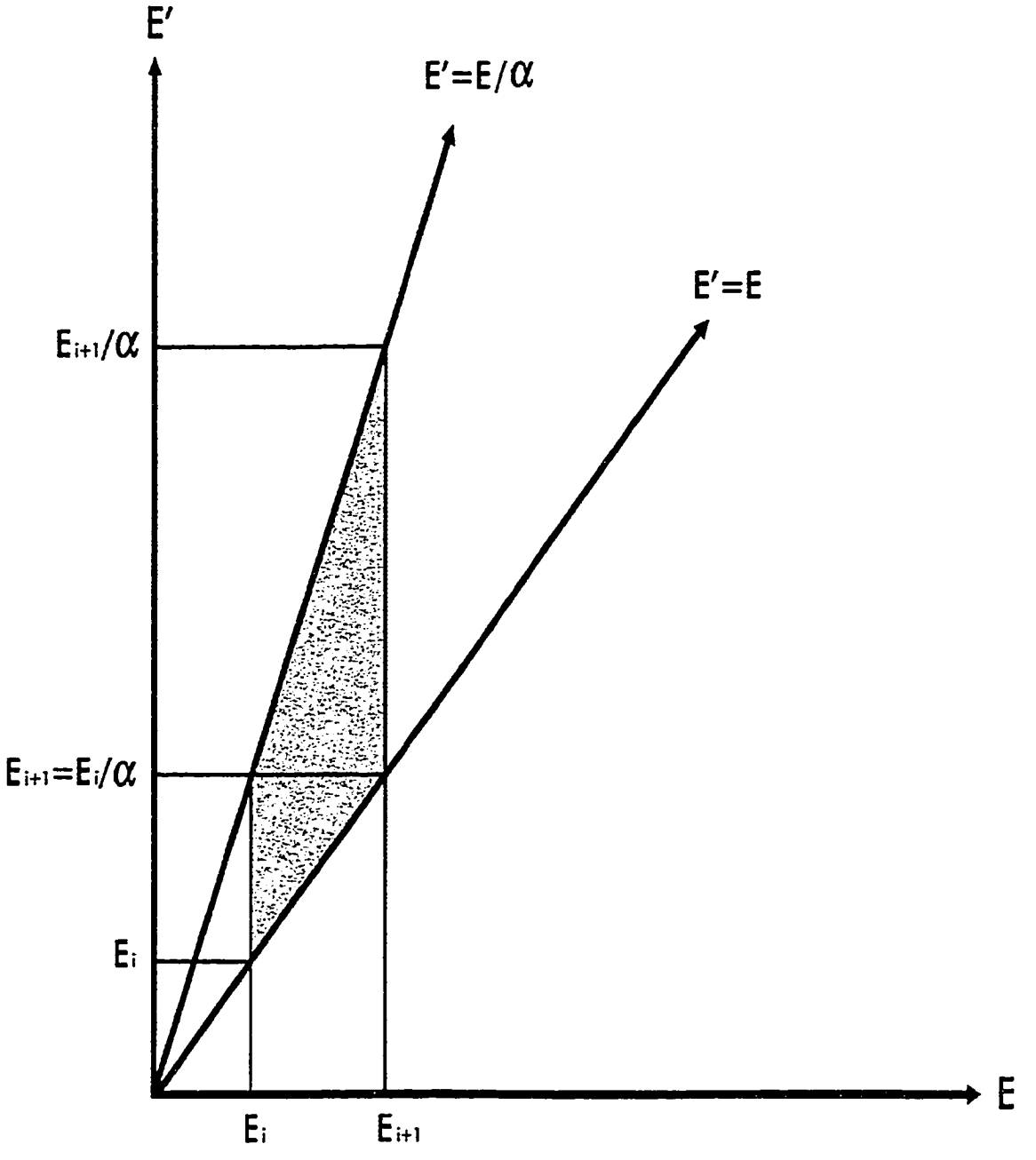

Fig. 30. Multigroup energy partition when $E_{i+1} = E_i/\alpha$.

Reproduced with permission of the copyright owner. Further reproduction prohibited without permission.

In this case, switching the order of integration in expression (3.6) gives

$$\int_{E_i}^{E_{i+1}} \int_{E_i}^{E'} f(E,E')\phi(x,E')dEdE' + \int_{E_{i+1}}^{E_{i+1}/\alpha} \int_{\alpha E'}^{E_{i+1}} f(E,E')\phi(x,E')dEdE'. \qquad (A2.15)$$

This expression can easily be written in terms $\Phi_i(x)$ and $\Phi_{i+1}(x)$

$$\left[\int_{E_i}^{E_i^*} f(E,E_i^*)dE\right] \Phi_i(x) + \left[\int_{\alpha E_i^*}^{E_{i+1}} f(E,E_i^*)dE\right] \Phi_{i+1}(x), \qquad (A2.16)$$

by once again using a mean value theorem with $E_i^* = E_i + \theta_i^*(E_{i+1} - E_i)$ where θ_i^* is chosen so that $0 \leq \theta_i^* \leq 1$.

All three cases required the use of a mean value theorem. The error created by using a mean value theorem decreases with the size of the interval. This would favor using Case I. However, in both Case I and Case III, additional approximations were made creating additional errors. This implies that Case II was the best in terms of error as well as simplicity of calculation. Therefore, the energy grid should be set so that $E_{i+1} = E/\alpha$ for all i.

All three cases were tried on the simplified problem described in Chapter 3, and the error resulting from Case I or Case II type energy grids was found to be within acceptable limits. The error resulting from a Case III type energy grid, however, was much larger.

Reproduced with permission of the copyright owner. Further reproduction prohibited without permission.

VITA

Martha Sue Clowdsley was born on February 16, 1968 in Portsmouth, Virginia. She graduated from the University of Notre Dame in Notre Dame, IN with a B.S. in Mechanical Engineering in May 1990. She received a M.S. in Computational and Applied Mathematics from Old Dominion University in May 1995. She continued her studies at Old Dominion University, Department of Mathematics and Statistics, BAL 500, Hampton Boulevard, Norfolk, Virginia, 23529-0077, and received a PhD in Computational and Applied Mathematics in May 1999.

Reproduced with permission of the copyright owner. Further reproduction prohibited without permission.

IMAGE EVALUATION TEST TARGET (QA-3)

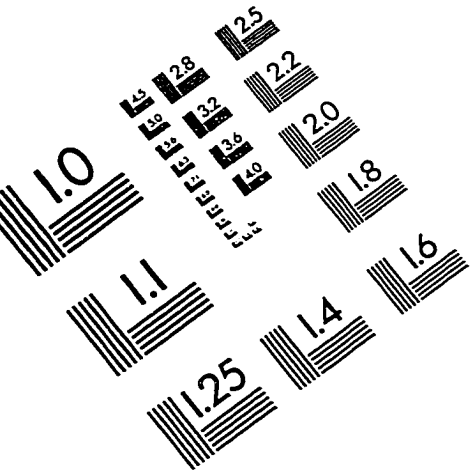

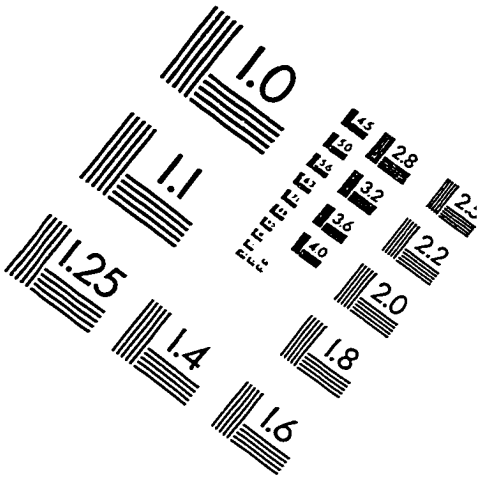

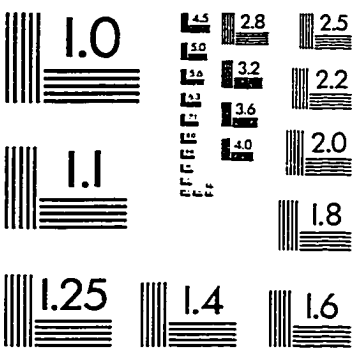

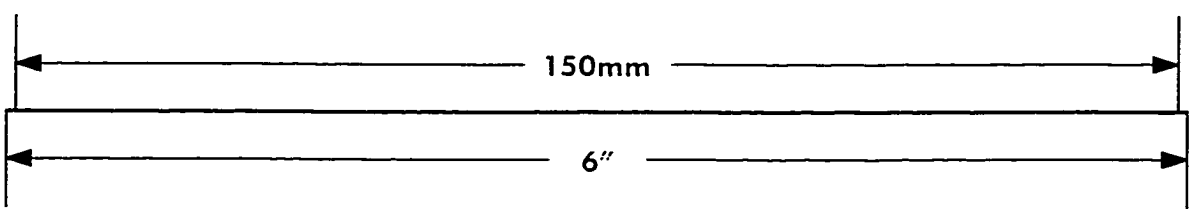

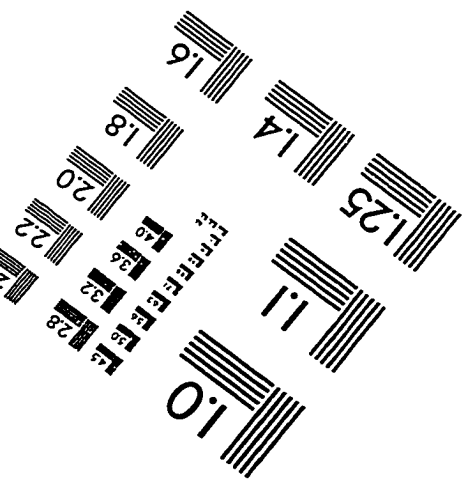

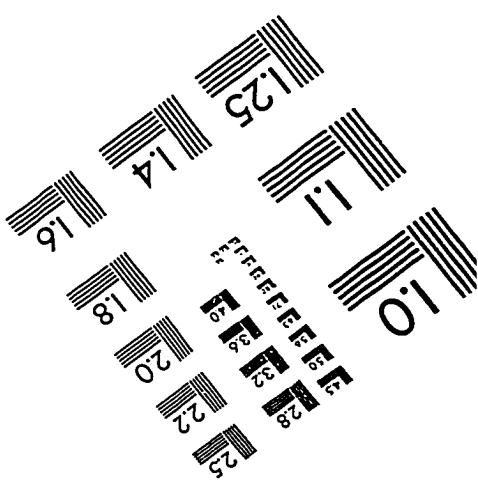

APPLIED IMAGE, Inc
1653 East Main Street
Rochester, NY 14609 USA
Phone: 716/482-0300
Fax: 716/288-5989

© 1993, Applied Image, Inc., All Rights Reserved

Reproduced with permission of the copyright owner. Further reproduction prohibited without permission.